



University  
of Glasgow

<https://theses.gla.ac.uk/>

Theses Digitisation:

<https://www.gla.ac.uk/myglasgow/research/enlighten/theses/digitisation/>

This is a digitised version of the original print thesis.

Copyright and moral rights for this work are retained by the author

A copy can be downloaded for personal non-commercial research or study, without prior permission or charge

This work cannot be reproduced or quoted extensively from without first obtaining permission in writing from the author

The content must not be changed in any way or sold commercially in any format or medium without the formal permission of the author

When referring to this work, full bibliographic details including the author, title, awarding institution and date of the thesis must be given

Enlighten: Theses

<https://theses.gla.ac.uk/>  
[research-enlighten@glasgow.ac.uk](mailto:research-enlighten@glasgow.ac.uk)

**FUSION BONDING OF REINFORCED THERMOPLASTIC**

by

I.J. McGregor, B.Sc.

Dissertation submitted to the Faculty of Engineering,  
University of Glasgow, for the degree of Doctor of Philosophy.

November, 1987.

© I.J. McGregor, 1987.

ProQuest Number: 10948177

All rights reserved

INFORMATION TO ALL USERS

The quality of this reproduction is dependent upon the quality of the copy submitted.

In the unlikely event that the author did not send a complete manuscript and there are missing pages, these will be noted. Also, if material had to be removed, a note will indicate the deletion.



ProQuest 10948177

Published by ProQuest LLC (2018). Copyright of the Dissertation is held by the Author.

All rights reserved.

This work is protected against unauthorized copying under Title 17, United States Code  
Microform Edition © ProQuest LLC.

ProQuest LLC.  
789 East Eisenhower Parkway  
P.O. Box 1346  
Ann Arbor, MI 48106 – 1346

## LIST OF CONTENTS

ACKNOWLEDGEMENTS		i
SUMMARY		ii
LIST OF SYMBOLS		iv
CHAPTER 1	INTRODUCTION	1
CHAPTER 2	FUSION BONDING OF APC-2	
	2.1 Introduction	7
	2.2 Manufacture and Testing of Specimens	9
	2.3 Results and Discussion	16
	2.4 Conclusions	30
CHAPTER 3	THICK ADHEREND TESTING OF PEEK	
	3.1 Introduction	32
	3.2 Experiment	35
	3.3 Results and Discussion	47
	3.4 Conclusions	53
CHAPTER 4	THEORETICAL PREDICTION OF THE STRENGTH OF FUSION JOINTS	
	4.1 Introduction	54
	4.2 Theoretical Analysis	58
	4.3 Results and Discussion	82
	4.4 Conclusions	92

CHAPTER 5	SPOT WELDING OF APC-2	
5.1	Introduction	94
5.2	Experiment	97
5.3	Results and Discussion	102
5.4	Conclusions	115
CHAPTER 6	CONCLUSIONS	117
REFERENCES		121
APPENDIX A		126
APPENDIX B		132
FIGURES, TABLES		

## ACKNOWLEDGEMENTS

The author would like to thank Mr. T.H. Cain, Department of Aeronautics and Fluid Mechanics, Glasgow University for his guidance and encouragement throughout this project. Thanks are also due to Mr. A. Duthie, Westland Helicopters PLC for his supervision and supply of basic materials, Professor B.E. Richards for his support, Mr. W. Hillier for the manufacture of laminates and helpful comments, Mr. D. Whitelaw for his extensive work in the preparation of experimental equipment, Mr. G. Wright for his excellent assistance during the development of the spot welding technique and Dr. J. Barnes, ICI, for helpful discussion and information.

The author acknowledges the considerable financial support of his parents and family throughout this work and the encouragement of his wife Janice.

The project was funded by the Science and Engineering Research Council as a CASE award, with Westland Helicopters PLC as external collaborating body.

## SUMMARY

A laboratory technique developed to produce fusion joints under carefully controlled conditions is described. The technique was used to manufacture single-lap specimens from the reinforced thermoplastic APC-2, and the influence of processing temperature and surface degreasing on joint strength is presented. The influence of laminate type, testing rate, bondline thickness and overlap length on joint strength were investigated, and the results from these tests are presented.

In order to enable mathematical modelling of fusion joints to be carried out, the shear stress-strain curve of the reinforced thermoplastic matrix, PEEK, was measured using the thick adherend specimen. This curve is presented along with an analysis of the thick adherend specimen failure surface using scanning electron microscopy. The influence of matrix viscosity on control of bondline thickness is also discussed.

The mathematical model of Hart-Smith was used to predict joint strength. His theoretical analysis for the prediction of adherend failure was modified to consider the strain distribution in the composite adherends rather than stress distribution, and the derivation of this is presented. A bi-elastic model for the prediction of adhesive shear failure was developed, and a comparison is made with the results from Hart-Smith's elastic-plastic analysis.

From the theoretical analyses, failure curves are presented for the three dominant failure modes of single-lap joints. These are plotted as failure load/width against overlap length, and a comparison is made with the experimental results for the influence of overlap length and bondline thickness on joint strength for several laminates. The influence of adherend thickness on predicted joint strength is also considered.

Finally, the work conducted into the development of a practical technique for producing fusion joints in APC-2 is presented. The technique uses a direct heating method to heat the bondline through the thickness of the composite, and, therefore, a discussion is conducted into the effect of processing on the adherend material as well as the influence of processing parameters on joint strength.



## LIST OF SYMBOLS

$A, B, C$	Constants
$A_c$	Area under shear stress-strain curve
$a$	Distance between extensometer measurement points across bondline
$c$	half length of overlap
$c_{cr}$	Half the maximum overlap length for which strain distribution confined to region 2 of bi-elastic representation at failure
$D$	Flexural rigidity of adherend
$d$	Length of elastic zone in adhesive bond
$d_1$	Half length of overlap where strain distribution confined to region 1 of bi-elastic representation
$E$	Extensional modulus of adherend
$E_c, E_c'$	Adhesive peel (transverse tension) modulus
$E_f$	Flexural modulus of adherend
$E_n$	Transverse modulus of adherend
$E_{c, bi}$	Adhesive Young's modulus corrected to account for bi-axial state of stress in joint
$G$	Adhesive shear modulus (elastic-plastic representation)
$G_1, G_2$	Adhesive shear modulus (bi-elastic representation)
$K$	Mathematical coefficient
$k$	Bending moment coefficient
$k_b$	Bending stiffness parameter

$l$	Overlap length
$l_{cr}$	Maximum overlap for joint to be fully plastic in shear at failure
$M$	Bending moment in adherend per unit width
$M_o$	Bending moment in adherend per unit width at end of overlap
$P$	Load per unit width applied to joint
$r_x$	Radius of curvature (x direction)
$s$	Co-ordinate aligned along load path
$s_1, s_2$	Co-ordinates aligned along load path for bi-elastic analysis
$T$	Tension force per unit width in adherend
$t$	Adherend thickness
$u$	Axial displacement in adherend adjacent to bondline
$u_c$	Adhesive deformation in thick adherend specimen
$u_d$	Metal deformation measured on thick adherend dummy specimen
$u_m$	Metal deformation corrected to account for bondline present in bonded specimen
$u_s$	Measured deformation of bonded thick adherend specimen
$V$	Transverse shear force on adherend per unit width
$w$	Transverse displacement of adherend
$x$	Axial co-ordinate aligned along load path

$(x_b, y_b)$	Co-ordinates of intersection point of bi-elastic shear stress-strain curve representation
$(x_e, y_e)$	Co-ordinates of intersection point of elastic-plastic shear stress-strain curve representation
$(x_f, y_f)$	Co-ordinates of ultimate shear stress and strain for adhesive
$\gamma$	Adhesive shear strain
$\gamma_e$	Elastic adhesive shear strain (elastic-plastic representation)
$\gamma_p$	Plastic adhesive shear strain (elastic-plastic representation)
$\gamma_{ult}$	Ultimate shear strain of adhesive
$\gamma_{1L}$	Limit strain in region 1 of bi-elastic representation
$\gamma_{2L} = \gamma_{ult}$	Limit strain in region 2 of bi-elastic representation
$\epsilon_{av} = \sigma_{av}/E$	Average adherend strain
$\epsilon_{x,max}$	Maximum adherend strain (x direction)
$\epsilon_{x,bending}$	Adherend strain due to bending (x direction)
$\epsilon_{x,tension}$	Adherend strain due to tension (x direction)
$\zeta$	Axial co-ordinate
$n$	Bondline thickness
$\lambda, \lambda'$	Exponents of elastic shear stress distribution
$\lambda_1, \lambda_1', \lambda_2, \lambda_2'$	Exponents of shear stress distribution in bi-elastic analysis
$\xi$	Exponent of bending stress distribution in adherend

$\sigma_c$	Peel stress in adhesive
$\sigma_{av} = P/t$	Average adherend stress
$\sigma_{max}$	Maximum adherend stress
$\sigma_{c,max}$	Maximum adhesive peel stress
$\tau$	Adhesive shear stress
$\tau_p$	Plastic adhesive shear stress (elastic-plastic representation)
$\nu$	Poisson's ratio of adherends
$\nu_c$	Poisson's ratio of adhesive
$x$	Peel stress distribution exponent

#### SUBSCRIPTS

$c$	Adhesive
$n$	Property normal to plane of adherends

## CHAPTER 1

### INTRODUCTION

The advantages of using reinforced plastics in structures where weight is of prime importance has been long realised. The material offers the engineer the possibility of designing large structures with considerable weight savings over structures utilising traditional materials. The weight savings, however, are not only a result of the high strength and stiffness to weight ratio of the composites. The ability of the material to be manufactured to provide the majority of its strength and stiffness in a specific direction, enables it to be employed more efficiently.

With the introduction of reinforced plastics into advanced experimental structures, it has been quickly realised that a considerable change in approach to both design and manufacture of structures is required, in order to take full advantage of the new material. Although several large aerospace industries have initiated research programmes to establish expertise into designing and fabricating with composites, there is a requirement for detailed experimental and theoretical research into several areas of particular interest. One of these areas is the joining of fibre reinforced plastics.

Generally, structures are joined by either mechanical fastening or adhesive bonding. The fibrous nature of fibre reinforced plastics

results in very large stress concentrations being created when mechanical fasteners, such as bolts and rivets, are used to join them. The ultimate strength of this type of joint is limited by the bearing strength of the laminate. In particular, the cutting of the hole in the laminate produces discontinuous fibres, which produce high stress concentrations between the bolt and the laminate. Failure often results in "brooming" of the discontinuous fibres. However, one advantage of mechanical fastening over adhesive bonding, is the ability of the joint to be dismantled. It is for this reason, that a practical structure will always contain a mixture of both mechanical and adhesive joints. Several investigators have looked carefully at bolted joints in composites, and some of these are listed as References 1 to 3. Reference 4 gives a useful survey of the most significant work in this field.

It is generally accepted, however, that adhesive bonding is the preferred method of joining reinforced plastics. Although stress concentrations are still present in the joint, these are generally less significant than those in mechanically fastened joints. It is possible, therefore, to achieve a joint strength very close to that of the basic laminate strength. However, the preparation and subsequent fabrication of adhesive joints, requires a great deal of care in order to obtain repeatable joint strengths. It is a consequence of this, that manufacturers often use extremely high factors of safety. This, combined with the rather long curing times of the traditional adhesive bond, tends to make the adhesive bond less attractive than would otherwise be the case.

The introduction of fibre reinforced thermoplastic composites, however, provides an opportunity for the development of a new and exciting type of adhesive joint.

The majority of research conducted into fibre reinforced plastics, has concerned thermosetting plastics. During laminate manufacture of these materials, the matrix undergoes an irreversible cure, very often requiring long processing times. Since the matrix of these materials cannot be remelted, shaping of the laminates must take place during initial laminate manufacture.

During processing of thermoplastics, however, the material merely undergoes a change from a solid to a molten phase, and can be remelted at any time by simply heating above the melting temperature of the material. This means that flat pre-consolidated laminates can be rapidly formed into shape by simply heating them until molten, and then pressing the molten material into a cold tool of the required shape. The result is a large reduction in the processing time compared to reinforced thermosetting plastics. In Reference 5, Hillier discusses the fabrication technology currently being developed by Westland Helicopters. This technology was used in the manufacture of the components for the Research and Demonstrator programme described by Duthie in Reference 6.

The thermoplastic nature of reinforced thermoplastics, provides the opportunity to join them by fusing them together. By the application of heat and pressure, the thermoplastic matrix flows between the two adherends to form a "fusion joint". This enables

bonds to be formed between the components very quickly and with the minimum of preparation. A major part of this work has been to prove the feasibility of this type of joint, and to identify the important parameters influencing joint strength.

There are some obvious advantages of this "fusion joint" over traditional adhesive bonding. Since the matrix of the composite is the "adhesive", preparation of the joint can be greatly reduced. The matrix forming the joint can be bled out of the composite during the bonding process, effectively welding the composite together. Alternatively, excess matrix can be introduced into the joint region in the form of a film, or from matrix which has been previously consolidated onto the laminate.

The proving and demonstration of "fusion bonding", requires a great deal of experimental research and development. Chapter 2 describes in detail, the experimental equipment and procedure developed to prove the feasibility of "fusion bonding". However, this approach alone does not provide the full information necessary to encourage confidence in this type of joint. It has been recognised from an early stage in research into adhesive bonding, that a complete understanding of the problem can only be obtained through a combination of both experimental and theoretical research. Very few investigators have conducted their research with both an experimental and theoretical study; most preferring to study using one approach or the other. The main reason for this, is probably due to the need to have the adhesive material properties to enable comparison of the results.



As early as 1964, Kutscha (Reference 7) pointed out that the problem of most concern in adhesive bonding research, was the lack of reliable and accurate adhesive material properties to use with the many theoretical analyses being developed. This is still a problem today, and since the "adhesive" material properties for the thermoplastic matrix used in this research were not known, it was necessary to measure those properties required to enable theoretical modelling of the joint to be carried out. The majority of mathematical models require the adhesive shear stress-strain curve, and Chapter 3 describes the work conducted in order to measure this curve for the particular thermoplastic matrix used in this investigation.

The reinforced thermoplastic used throughout this research was APC-2, manufactured by Imperial Chemical Industries (ICI). The composite uses Hercules AS-4 carbon fibres to reinforce ICI's thermoplastic matrix Polyetheretherketone (PEEK). ICI has specially developed the fibre surface to ensure optimum bonding between the fibres and the partially crystalline matrix. This material is claimed to have several advantages over traditional reinforced thermosetting plastics, including improved environmental and chemical resistance, and improved impact performance.

Many mathematical models have been developed to obtain the stress distribution in adhesive bonded joints. Many of these models assume linear elastic material properties for the adhesive. Consequently, poor correlation is found between predicted results and the

experimental results, especially when the adhesive exhibits significant plasticity. One of the first models to take into account the non-linear behaviour of the adhesive in shear, was the theoretical work of Hart-Smith (Reference 8). In Chapter 4, a detailed discussion is made of this analysis, and the material properties obtained in Chapter 3, are used to compare the results from this model with the experimental results.

Although one of the main aims of this study was to prove the feasibility of "fusion bonding", the development of practical techniques to produce reliable joints is required, before "fusion bonding" can be accepted as an alternative means to the joining of reinforced thermoplastics. With this in mind, it was attempted to develop a simple practical technique to produce "spot welds" in APC-2. Chapter 5 describes the development of this technique, and compares the results to the standard set in Chapter 2.

FUSION BONDING OF APC-2

2.1 Introduction

Fusion bonding is a new type of adhesive joint, particular to reinforced thermoplastics. One of the first tasks of the work, was to demonstrate the feasibility of such a joint. In order to do this, a technique had to be developed to produce fusion bonds in APC-2 under carefully controlled conditions. Although great interest lies in the development of practical techniques for producing these joints, it was felt that the development of a laboratory technique, would provide the best opportunity for obtaining and controlling the processing parameters necessary to form such a joint.

The types of technique initially considered were based on the existing processing techniques used in the manufacture of the basic laminates. The techniques which received most consideration were the use of a hot press, or the use of a high temperature oven combined with a vacuum bag. It was recognised at an early stage, that careful control of temperature and consolidation pressure were the most important factors to obtain reliable results. Therefore, it was decided that the use of a high temperature oven in combination with a vacuum bag, would provide the best opportunity for achieving the control required.

This Chapter describes in detail the development of this technique, and presents the results of tests to determine the influence of processing and testing variables on the joint strength of single-lap specimens. The influence of processing temperature, surface cleaning and testing rate is presented, as well as the influence of overlap length, bondline thickness and laminate lay-up.

Examination of the joint cross-section was conducted in order to evaluate the quality of joint obtained. This, combined with optical and scanning electron microscopic examination of the failure surfaces, provided valuable information as to the possible modes of failure of the specimens.

It was hoped that the strength of joint obtained from this work would set a standard of joint strength, against which the results from more practical techniques could be compared.

## 2.2 Manufacture and Testing of Specimens

### 2.2.1 Experimental Equipment

Careful control of temperature and good vacuum, were recognised as being the most important factors for obtaining reliable results. The equipment used for controlling these factors is described below and is shown in Figure 2.1.

#### 2.2.1.1 High Temperature Oven

The use of a high temperature oven made it possible to have a uniform temperature over the specimen, combined with very good temperature control. A temperature controller was developed which kept the oven temperature to within  $\pm 1^{\circ}\text{C}$  of the set point during processing. An Omron digital temperature controller, (Model E5C4), was used in combination with a "burst fire" power controller, to provide very well controlled processing temperatures.

A type K metal sheathed thermocouple was placed inside the vacuum bag to measure the specimen temperature. This was placed as close as possible to the area of the specimen to be bonded. During processing, sufficient time was given to ensure thermal equilibrium had been achieved over this area, in order that a representative reading of specimen temperature was being recorded. A digital thermocouple thermometer was used to provide automatic cold junction compensation and a digital readout of the specimen temperature. This was linked into a pen recorder to give a permanent record of the

specimen temperature at each stage of processing.

From Figure 2.1, it can be seen that an extraction system was incorporated into the arrangement. The extractor consisted of five small diameter brass tubes which extracted the smoke and gases given off by the A800 sealant. This was found to be necessary, since the gases tended to ignite if confined in an unventilated oven. The tubes were carefully designed and positioned in order to extract the gases as uniformly as possible.

#### 2.2.1.2 Vacuum Bag

The vacuum bag used was similar to that employed in the fabrication of the basic laminates, and is shown in Figure 2.2. A800 sealant and Kapton film were the two materials which formed the basis of the bag. It was found that the 0.025mm thick Kapton film held the shape of the bag better than the thicker films which are available. A great deal of operator skill had to be developed, in order to make a vacuum bag which was airtight throughout the specimen processing.

Initially it was found difficult to obtain a uniform vacuum over the full length of the vacuum bag. Glass cloth is normally incorporated into a vacuum bag in order to produce a uniform vacuum during the manufacture of laminates. However, this was found to be ineffective in the development of this technique, and a uniform vacuum was only achieved after the introduction of a small brass bleeder pipe which ran the length of the bag. This bleeder pipe had many small holes drilled along its length, and this ensured that any

gases drawn into the bag were quickly drawn through the bag into the rotary vacuum pump. The vacuum was measured using a Pirani vacuum gauge, and during processing the vacuum varied between 0.2mmHg and 0.7mmHg. It is believed this variation was due to the outgassing of the A800 sealant.

In order to produce standard size specimens, a small steel "picture frame" was introduced into the vacuum bag. Since the whole of the specimen was melted during processing, the picture frame provided lateral support, and helped to maintain surface quality. The picture frame also helped to prevent resin being squeezed out of the joint region.

To provide support for the top adherend of the single-lap specimen, a packing piece was incorporated into the lay-up inside the picture frame, as shown in Figure 2.2. The packing piece was made 0.15mm thinner than the composite, to ensure good contact between the surfaces to be bonded. 0.1mm thick stainless steel foil helped to maintain, and in some cases improve, the surface finish of the specimen. This was important to prevent premature adherend failure during testing.

#### 2.2.2 Specimen Preparation

The specimens were produced from pre-fabricated 8 ply laminates manufactured by Westland Helicopters PLC. Vacuum bag consolidated laminates were preferred to press consolidated laminates, because of their superior fibre orientation, although they generally had a

poorer surface finish. Particularly bad fibre orientation was found in press consolidated laminates, and specimens manufactured from these laminates failed prematurely from adherend splitting.

Strips of the composite were cut from the parent laminate with a diamond tipped circular saw, and then reduced in width on a sanding machine so that a good fit between composite and "picture frame" was achieved. The fitting between composite and frame was important, since this had an effect on the surface finish of the specimen. Particularly bad surface finish was obtained in those areas of the specimen where there was a poor fit between composite and frame.

The only surface preparation made prior to bonding, was solvent degreasing of the adherends and any PEEK film being introduced into the joint. An alternative surface preparation of the adherends would have been surface abrasion to remove any contaminants on the adherend surface. However, since the majority of the vacuum consolidated laminates had areas of poor consolidation, there was a danger of damaging the fibres during abrasion. Consequently, only surface degreasing of the composite was investigated, and this is discussed in detail later.

The influence of excess resin on the joint strength was also examined. Specimens were made either with or without introducing excess PEEK into the joint region. The effect of this is discussed later, and the results are presented to show the effect of both type and thickness of PEEK film used.



After processing, the specimens were reduced to the dimensions given in Figure 2.3. This gave a specimen whose general dimensions and, more importantly, overlap area could be accurately measured. Before testing, aluminium end plates were bonded onto the specimen to prevent premature failure in the machine grips.

### 2.2.3 Heating Cycle

An investigation of the influence of processing temperature on joint strength was conducted. For each ultimate temperature, the same general heating cycle was employed. Figure 2.4 shows a plot of the heating cycle for a specimen processed at 380°C. The time taken for the specimen to reach 380°C from room temperature was approximately 30 minutes. The specimen was then kept at its processing temperature for a further five minutes to ensure thermal equilibrium, before being removed from the oven and air cooled. Once the specimen had cooled to below 150°C, the vacuum was released. Cooling time from 380°C to 150°C was approximately 6 minutes, giving an average cooling rate over this period of 38°C/min.

The degree of crystallinity of PEEK is controlled by the rate of cooling of the material. Optimum performance of APC-2 laminates is only achieved by cooling at the correct rate, so that optimum crystallinity is achieved in the PEEK matrix. The cooling rate for optimum crystallinity is in the range 10°C - 700°C/min. When PEEK is reprocessed, the degree of crystallinity is only dependent on the subsequent rate of cooling and not on the degree of crystallinity before processing. The cooling cycle of this work produced a cooling

rate within the recommended range.

It was found necessary to set the oven temperature approximately 5°C above the required processing temperature in order to achieve reasonable heating times. Figure 2.5, shows the variation of oven temperature with distance from the centre of the joint. The maximum length of joint tested was 40mm, and Figure 2.5 shows that there is almost no variation of oven temperature over this overlap length. For the remainder of the specimen length, there is a very small variation of temperature, with oven temperatures well above the PEEK melting point.

#### 2.2.4 Specimen Testing

The specimens were tested in tension on a 250kN Instron tensile testing machine, using jaw grips to hold the specimen. The specimens had to be deformed slightly prior to loading because of the inability of these grips to account for the unsymmetrical nature of single-lap joints. However, this was not felt to be of significance for the thin 8 ply laminates. With thicker laminates, however, grips similar to those designed for the thick adherend specimens in Chapter 3, would have to be used.

By placing a displacement transducer across the joint, a plot of load against deformation was obtained. A typical plot is shown in Figure 2.6. This merely gave an indication of the general response of the joint to loading. An investigation of the variation of joint strength with crosshead speed was also made and is discussed later.

Microscopic examination of the specimens was undertaken. Several specimens were sectioned at various positions in the overlap. These were then polished using standard polishing techniques. The sections were examined using an optical microscope, to measure the bondline thickness, and provide information on the degree of wetting achieved between resin and fibre. The failure surfaces of the specimens were examined using a scanning electron microscope (SEM). Before examination, gold was vacuum-evaporated onto the fracture surfaces. Valuable information was obtained on the possible failure modes of the specimens from this examination.

## 2.3 Results and Discussion

### 2.3.1 Processing Temperature

Several practical methods of producing fusion joints have been proposed. Most of these techniques confine the heating to those surfaces of the adherends to be bonded, and to any PEEK films introduced into the joint. One possibility in employing these techniques, is that it may be possible to melt the PEEK film and produce a satisfactory joint at much lower temperatures than 380°C (the usual temperature for laminate manufacture). This would not only mean shorter processing times, but also reduce the amount of distortion in the thermoplastic adherends. It was decided, therefore, to look at the variation of joint strength with processing temperature using the experimental arrangement developed. The three temperatures which were examined were 340°C, 360°C and 380°C, and the results of the tests are shown in Figure 2.7.

It can be seen that at 340°C very little bonding took place. All of the specimens were made by introducing one layer of 0.1mm thick 450 Grade PEEK film. After processing at 340°C, the general appearance of the PEEK film was that it had softened but not fully melted. This result is consistent with the data given by ICI, which gives the melting temperature of PEEK as 343°C. Since PEEK is a partially crystalline material, it should be necessary to melt the material before bonding is achieved, and this is confirmed by the observed result. Some materials which are amorphous in nature, however, can be fused together at temperatures lower than their

melting temperature. These materials would obviously be able to take advantage of the points mentioned above.

Processing at 360°C, produced extremely random joint strengths. Increasing this temperature by only 20°C, however, resulted in very strong joints with very little scatter of results. The conclusion from this is, as initially anticipated, that joint strength is very sensitive to processing temperature. The implication is that successful practical techniques must be able to accurately control processing temperature. In fact, it has been found that the failing in the majority of unsuccessful practical techniques, has been the inability to accurately control the processing temperature. It was partly for this reason that the development of the practical technique described in Chapter 5 was undertaken.

The results suggest that 360°C is an intermediate bonding temperature, with 380°C as the optimum temperature. 370°C is probably the lowest temperature that will produce reliable joint strength.

### 2.3.2 Surface Cleaning

With all types of adhesive bonding, it is essential that the surfaces to be bonded are properly prepared in order to remove any contaminants which would adversely affect joint strength. Often with reinforced plastics, the surface preparation involves solvent degrease, followed by abrasion. With abrasion techniques, however, there is the possibility of damaging the fibres in the surface layer

of the composite, giving rise to the possibility of premature failure of the adherends during loading. In order to avoid this, great care has to be taken when using abrasion techniques, and this results in an increase in the time taken to prepare the joint prior to bonding. For this reason, it was hoped that for fusion bonding, only simple degreasing of the surfaces would be sufficient to produce a high standard of joint strength. Therefore, a limited study was conducted, to look at the effect of degreasing the joint area prior to bonding, with two different commonly used solvents. Table 2.1 compares the strengths of specimens degreased with acetone to those degreased with trichloroethane.

It can be seen immediately that acetone produced the specimens with the greatest strength, and this was eventually the solvent used in the preparation of all future specimens. After processing of the specimens cleaned with trichloroethane, it was observed that some marking of the adherends had taken place in those areas where trichloroethane had been applied during preparation of the joint region. The appearance of these areas suggested that the composite was "dry" of PEEK. During testing of the specimens cleaned with trichloroethane, it was found that the load did not rise steadily with constant crosshead speed, and that a rising and falling of the load occurred. After failure of the specimens, surface examination revealed a "honeycomb" type failure surface, markedly different from the specimens cleaned with acetone.

Figure 2.8(a) shows the failure surface of a typical specimen cleaned with trichloroethane, while Figure 2.8(b), shows a SEM

micrograph of the failure surface. Figure 2.8(a) shows that the failure surface was random in nature, and from Figure 2.8(b), it can be seen that large bubble craters were present.

After discussions with ICI, (Reference 9), a general explanation was formed which may explain the effect of the trichloroethane on the joint. PEEK is a partially crystalline material, and this partly accounts for its excellent chemical and environmental resistance. However, it is known that the amorphous part of PEEK demonstrates the tendency to absorb small amounts of chlorinated solvents. Therefore, it is possible that during the application of trichloroethane to the surface of the APC-2, a small amount of the solvent was absorbed by the amorphous part of the PEEK present, and that this was then released during heating of the material. This would lead to the formation of voids and gaseous inclusions in the bondline, giving rise to the "honeycomb" failure surface as seen in Figure 2.8. Since the failure surface showed random formation of voids, this would be equivalent to an overall reduction in bonded area, and would explain the consistently reduced strength of  $40\text{N/mm}^2$ . ICI now recommends against using chlorinated solvents with PEEK and APC-2.

For the purposes of this investigation, it was demonstrated that simple degreasing alone was sufficient to produce a high standard of joint strength. However, a more detailed study will have to be conducted to investigate more fully the effect of surface pretreatment on joint strength.

### 2.3.3 Rate of Testing

The viscoelastic nature of PEEK required that careful consideration was made of the rate of testing. Figure 2.9 shows the results of tests conducted for crosshead speeds of 0.2mm/min, 0.5mm/min and 2mm/min. It can be seen there was generally very little variation of strength with crosshead speed. However, at the fastest speed, slightly higher strengths were observed, but with an associated increase in the scatter.

From these results it was decided to test the majority of unidirectional specimens at 0.5mm/min, since this gave a compromise between the time taken to run a test and scatter of the results. For the tests on the more practical laminate lay-ups, where  $\pm 45^\circ$  layers were incorporated, the rate of testing was increased to 2mm/min. This ensured that although these laminates had a reduced stiffness compared to unidirectional laminates, the time taken to failure was similar.

Figure 2.6 shows a typical plot of load against displacement for a 20mm overlap specimen with  $0^\circ$ , 8 ply adherends. Most of the curve is linear with some levelling of the load prior to failure. This was very similar to the plots for laminates which contained some  $0^\circ$  plies together with some angled plies. Only those laminates which did not contain  $0^\circ$  plies in their lay-up, showed a non-linear load-displacement curve.



#### 2.3.4 Influence of Excess PEEK

One of the potential advantages of fusion bonding over traditional adhesive bonding, is the possibility of a reduction in the preparation of the joint. For this reason, it was initially hoped that it would be possible to form a bond by utilising the surface layer of PEEK on the parent laminate. In this case, the surface layer of PEEK would be squeezed out of the laminate, and used to form the bondline. Figure 2.10 and Table 2.2 gives the results of tests to determine the influence on the joint strength of excess PEEK introduced into the bondline.

Three different types of specimen were produced. Figure 2.10 compares the strengths obtained for specimens produced without introducing PEEK film into the bondline, specimens produced using 450 Grade film and specimens produced using Stabar film. It can be seen that specimens produced without any excess PEEK film showed a considerably lower joint strength as compared to those which included PEEK film.

The influence of bondline thickness on joint strength is looked at carefully in Chapter 4. It is possible here, however, to provide an explanation as to the increase in scatter of the specimens produced without any excess PEEK. Since, from Figure 2.10, it is possible to determine that bondline thickness plays an important role in the resulting joint strength, it can be deduced that a process which produces an inconsistent bondline thickness will also produce specimens with an inconsistent joint strength. Therefore, since the

amount of PEEK present in the surface of a parent laminate will be variable, it could be expected that specimens produced using this surface layer for the bondline would exhibit an inconsistent joint strength. This is reflected in the results.

The 450 Grade film used was manufactured by an extrusion process from 450 Grade PEEK. This grade of PEEK is normally used for injection moulding. The thickness of the film was 0.1mm. The joint strength obtained using this film was consistently  $61\text{N/mm}^2$ , as compared to between 36 and  $47\text{N/mm}^2$  for specimens without any excess PEEK film. Figure 2.11 and Figure 2.12 show pictures of the cross-sections of specimens produced with and without excess PEEK. From Figure 2.11(a), it can be seen that a consistently uniform bondline thickness was obtained with the 450 Grade film. This was measured to be close to 0.1mm thick over the full width of the specimen. Figure 2.12(a) shows the cross-section of a specimen produced without any PEEK film. Although a very fine line of PEEK can be observed in the middle of the joint, this line was not continuous over the whole width of the specimen, and similar lines of PEEK were observed in other areas of the cross-section, well away from the middle of the joint. Figure 2.12(b) shows that in the thicker areas, this bondline thickness was approximately twice the fibre diameter, equivalent to a bondline thickness of 0.016mm. In general, however, these specimens showed an inconsistent bondline thickness over the full width of the specimen.

It was attempted to incorporate two layers of 450 Grade film into the joint in order to obtain a thicker bondline with this material.

However, difficulty was experienced in obtaining repeatable joint strengths when processing at 380°C. Increasing the temperature to 390°C improved the scatter of the results, and an average strength just greater than that for one layer of PEEK film was observed.

Stabar film is the commercially available form of PEEK sold by ICI. The particular film type used was K200, and this number is given to PEEK film which has been cooled rapidly to form the PEEK in its amorphous state. It was found that joints produced using the Stabar film showed a slight increase in the joint strength over those using the 450 Grade film. Increasing the thickness of the film also increased the joint strength. However, there were found to be significant differences in the way in which 450 Grade and Stabar film behaved during processing. In general Stabar film tended to flow more freely during processing, and this resulted in a reduction of the bondline thickness from the original 0.1mm film thickness to around 0.075mm. 450 Grade film, however, did not seem to flow to the same extent, and hence the bondline after processing was almost the same as the original PEEK film thickness. Figure 2.11(b) shows a close up of the bondline of a specimen produced using one layer of 0.1mm thick 450 Grade film. Although the PEEK did not flow as freely as Stabar film, it flows sufficiently to fill the uneven contours of the laminate to form a continuous, void free, bondline between the two adherends. The PEEK film readily coats the surface fibres of the adherends, and some of these fibres migrate into the bondline from the adherend. It was found that the fibre migration of the adherends bonded with Stabar film was substantially greater than for 450 Grade film. The effect of fibre migration into the bondline is not really

known, and this is an area for future research.

After discussions with ICI, it was discovered that Stabar film has a lower molecular weight than 450 Grade film. This results in the Stabar film having a lower viscosity than the 450 Grade, giving rise to the different processing behaviour of the two films. This may also explain the increased joint strength observed for specimens produced using Stabar film, despite a reduced bondline thickness. The average joint strength for Stabar was  $64.5\text{N/mm}^2$  compared to  $61.0\text{N/mm}^2$  for 450 Grade film. The lower molecular weight Stabar film may have been more like the PEEK in the APC-2 material, resulting in improved fusion of the film and the adherend.

There are some important practical implications of the influence of film viscosity on the control of bondline thickness. Since bondline thickness plays an important role in determining the joint strength, the ability to produce repeatable joint strengths depends on the ability to produce repeatable bondline thicknesses. This will be very important in the development of practical techniques, and a film which tends to flow less during processing, permitting easier control of bondline thickness, will be particularly attractive.

#### 2.3.5 Influence of Adherend Type and Overlap Length

The strength of joints does not only depend on the surface preparation, type of adhesive and bondline thickness, but also on the adherend type and joint geometry. Most of the initial research was conducted using unidirectional laminates. This choice of laminate

permitted testing of specimens over a wide range of overlap lengths, with adherend failure being restricted to those specimens with a very large overlap length. The influence of other laminate types was also investigated, and in Chapter 4 the results of this as well as the influence of overlap length, are compared to theoretical results.

Figure 2.13 shows the results of tests to determine the influence of laminate type on joint strength. All the specimens were made with 20mm overlaps and one layer of 0.1mm Stabar film in the bondline. The Table in Figure 2.13 gives the results and indicates the type of failure for each joint. Since in fusion bonding the adhesive is the same as the matrix in the composite, it is difficult to distinguish between adhesive failure of the bondline and cohesive failure of the film forming the bondline. For this reason, the failure is referred to as either bondline failure, where the failure is seen to be restricted to the bondline, or adherend failure, where the failure has occurred in the adherend. Adherend failure could be easily distinguished from bondline failure, due to the presence of a broad band of exposed fibres in the joint region which had been pulled from one of the adherends.

From Figure 2.13, it is seen that failure occurred in the bondline only for the unidirectional laminate, and for the other laminates the failure occurred in the adherend. In some of these laminates, the failure occurred well away from the joint region. This indicates that for laminates containing some angled plies, an overlap of 20mm is long enough to have the joint strength limited by the adherend strength, rather than the bond strength.

In order to look at the variation of joint strength with overlap length, tests were conducted on both a unidirectional laminate and the more practical laminate  $(0,0,+45,-45)_S$ . Figures 2.14 and 2.15 and Tables 2.3 and 2.4 give the results of these tests. Both laminates showed a similar trend, with a linear relationship between failure load/width and overlap length for the initial overlap lengths tested. The specimens with overlaps in this range, for both laminate types, showed bondline failure of the joint, with an average shear stress at failure of  $60\text{N/mm}^2$  and above. With larger overlap lengths, (40mm for unidirectional laminate and 20 mm for  $(0,0,+45,-45)_S$  laminate), the specimens deviated from this linear relationship, and showed a drop of average shear stress at failure to around  $50\text{N/mm}^2$ .

At larger overlap lengths, the strength of the specimen is limited by the strength of the adherend, and consequently there is a drop in the shear stress at failure and a levelling of the load/width with respect to overlap length. A detailed discussion of these results, together with a comparison with the theoretical results, is given in Chapter 4.

#### 2.3.6 Failure Surface Examination

Figure 2.16 presents photographs of the failure surfaces of some of the unidirectional specimens. The failure surfaces of those specimens produced using 450 Grade film for the bondline, were much easier to examine with the naked eye since the film remained visible. The failure surfaces of the specimens produced using Stabar

film were very difficult to examine since the Stabar film seemed to remain transparent after processing.

Figure 2.16(a) shows the failure surface of a 20mm overlap specimen produced using 450 Grade film. It can be seen that the failure surface is random in appearance, with patches of the film torn from the adherend. This type of failure surface could be described as showing adhesive failure.

Figure 2.16(b) shows the failure surface of a 40mm overlap unidirectional specimen. It can be seen that a broad band of fibres is present on the surface of the film, and these have been torn from the other adherend. This type of failure surface is typical of adherend failure. The combination of both tension and bending stresses in the outermost fibres of the adherend exceeds a critical value and failure then occurs.

Figure 2.16(c) shows the failure surface for a 20mm overlap specimen typical of those produced without any PEEK film introduced into the bondline. The strange white patches were present on all of these specimens, and only occurred at the end of the overlap. In some of the specimens, the patches were not uniform across the width but could be highly irregular in shape. Although these white areas were not as prominent on specimens produced with excess PEEK, similar areas were observed.

Figure 2.16(d), shows the failure surface of a 20mm overlap specimen produced using two layers of 450 Grade PEEK film. The

failure surface is similar to that in Figure 2.16(a), but with the additional feature of one film being torn from the other. This indicates that the two films were not completely fused together to form one thick bondline, and would suggest that thick bondlines should be formed from thick PEEK films.

Examination of the joint failure surfaces was carried out using a scanning electron microscope. The sketch in Figure 2.17(a) shows the three main areas examined in the following discussion. Figure 2.17(b) shows a micrograph of the failure surface of a 20mm overlap unidirectional specimen, 1mm from the outer edge of the overlap, (Area 1 in Figure 2.17(a)). The fibres can be easily seen running up towards the top of the micrograph, with PEEK matrix pulled up between the fibres. The fibres look very clean of matrix, and this suggests that failure has initiated very close to the fibre matrix interface. On very close examination of the fibre surface, patches of PEEK film can be observed and it is, therefore, difficult to decide whether failure has occurred between the fibre and matrix, or in a very thin layer close to the fibre surface. The general conclusion which can be drawn from this picture, however, is that this region is under high normal stress at failure; apparent from the way in which the matrix is pulled up and between the fibres. It is difficult to decide whether failure has resulted from these high normal stresses, or from the presence of the high shear stresses in this region of the joint.

Figure 2.18, shows micrographs of the failure surface of a unidirectional specimen in Areas 2 and 3 of Figure 2.17(a). In



Figure 2.18(a), the matrix appears broken and very rough in appearance. In Figure 2.18(b), however, the matrix appears very smooth. In both of these pictures, very few fibres are seen in comparison to the picture of Figure 2.17(b). This change of failure surface, from very rough at the edge of the joint, changing to a smoother surface towards the middle of the joint, was apparent on all the specimens examined with the scanning electron microscope. It is felt that this is a result of a change in the rate of fracture during failure of the joint. At slow rates of fracture, PEEK exhibits very ductile behaviour, and at high rates of fracture, very brittle behaviour. As the joint failed, the rate of crack propagation would speed up as the crack travelled towards the middle of the joint, and this could give rise to the failure surface observed above.

When the white regions of Figure 2.16(c) were examined with the scanning electron microscope, they appeared to be the same as the failure surfaces shown in Figure 2.18(a). It appears, therefore, that the broken matrix in these white regions tends to reflect the light, making them easily observed with the naked eye. Generally, the white regions on specimens produced without any PEEK film, were much larger than those in specimens produced with a PEEK film.

## 2.4 Conclusions

It has been demonstrated that the use of a high temperature oven combined with vacuum bag, provided favourable conditions for the manufacture of fusion joints. The following conclusions were drawn from the work:

- (1) The strength of the bond was found to be very sensitive to processing temperature. Processing at 380°C gave the strongest joints with very little scatter of results.
- (2) Surface cleaning with acetone was sufficient to produce a high standard of joint strength. The use of trichloroethane for solvent degreasing of the specimen, was found to give reduced bond strengths with associated degradation of the material after processing. This was a result of the tendency for PEEK to absorb chlorinated solvents, and it is recommended not to use these solvents with PEEK or APC-2.
- (3) Very little change in joint strength was observed with change in crosshead speed during testing. However, at the higher speeds, there was a slight increase in the joint strength, but with an associated higher scatter of results.
- (4) The inclusion of an 0.1mm thick film of PEEK increased the strength of joints and reduced the scatter of results, compared to specimens formed without any excess PEEK. It

was found that an increase in bondline thickness gave an increase in joint strength. Film viscosity was found important in the control of bondline thickness. A bondline produced from high viscosity material was found easier to control.

(5) In laminates containing angled plies, a 20mm overlap fusion joint was sufficient to produce failure in the adherend. The failure was only seen to be confined to the bondline for unidirectional material. For practical purposes, there was initially found to be a linear relationship between load/width at failure and overlap length for the two types of laminate considered. For longer overlap lengths, the results deviated from this trend, and this coincided with a change from failure in the bondline to failure in the adherend.

(6) Failure surface analysis revealed a reduction in the surface roughness of the joint, running from the joint ends towards the middle of the overlap. This was felt to be due to a change in the rate of fracture during failure of the joint. It was concluded that the very broken appearance of the failure surface at the end of the joint, was due to the presence of very high peel stresses prior to failure.

THICK ADHEREND TESTING OF PEEK

3.1 Introduction

As early as 1964, Kutscha (Reference 7) pointed out that the problems of most concern regarding adhesive bonding analysis was a general lack of good data on the properties of adhesives to use in the numerous theoretical analyses being developed. Since then much work has been carried out on developing suitable specimens for obtaining the necessary material properties. It has been shown that bulk or free film material properties are not representative of the adhesive when bonded to adherends. The in-plane support provided to the adhesive by the adherend requires that measurement of the material properties be carried out when the adhesive is bonded to adherends. This presents problems, since the resulting thickness of material available for experimental measurement is extremely small.

One of the most important material properties required by the majority of mathematical models, is the shear stress-strain curve of the adhesive. The two main techniques used to obtain this curve, are the thick adherend test and the "napkin ring" torsion test. Although the "napkin ring" torsion test measures the material properties of the adhesive in uniform shear, the difficulty in the manufacture of the specimen tends to encourage widespread use of the thick adherend specimen. In Reference 10, Renton published the results of a poll of

fifteen investigators who had a working knowledge of test specimens for obtaining adhesive material properties. The results from this poll, indicated that the thick adherend specimen was the preferred method for obtaining the shear properties of the adhesive. Renton also presented work on obtaining the optimum geometry for the thick adherend shear specimen. Many investigators, however, develop their own thick adherend specimen to suit the dimensions of their manufacturing facilities.

In Reference 11, Althof reported the findings of a major research program, using the thick adherend specimen to determine the effect of environment on the elastic-plastic properties of adhesives. His experimental approach establishes a good guide as to the use of the thick adherend specimen for measurement of adhesive shear properties. In his work, he used 6mm thick aluminium adherends to form a specimen with a 5mm overlap length. The specimen was loaded steadily to failure in around 30 seconds in gimbal mountings, to ensure moment free application of load. A finite element method was used to calculate that the ratio of maximum shear stress at the ends of the overlap to the mean shear stress of the specimen, was only 1.115. This allowed the assumption of uniform shear stress distribution along the overlap length. For the measurement of the bondline displacement, Althof used a displacement transducer similar to that extensively studied by Krieger in Reference 12.

Kreiger attempted to demonstrate the accuracy of his displacement transducer, designated KGR-1, by conducting experimental and theoretical analyses. In his report, he describes the KGR-1

extensometer, and identifies six major sources of error from the thick adherend specimen. The most serious errors arise from false signals from imperfect specimens and from metal deformations in perfect specimens. By careful manufacture of specimens, errors from imperfect specimen geometry and imperfect bondline can be eliminated. The use of two extensometers, one to either side of the specimen, can help to detect imperfect specimens.

In order to account for metal deformation in specimens, Krieger demonstrated the use of a solid dummy specimen, which had the overall dimensions of the bonded specimen. By measuring the metal deformation of this specimen during load, it was possible to correct the recording from bonded specimens. In particular, he pointed out the importance of the correct positioning of the pick-up points on the adherend, to limit the error from bending deformation of the adherend. His suggested pattern for the pick-up points was used in this work, and is shown in Figure 3.1.

In this work, the thick adherend specimen used by Althof was used to obtain the shear stress-strain curve of PEEK. In order to obtain the displacements of the specimen during loading, an existing extensometer used for tension tests was modified, based on the work of Krieger. The work provided a stress-strain curve for PEEK which could be used to model fusion joints in shear.

### 3.2 Experiment

The manufacture and testing of thick adherend specimens, has to be very carefully conducted in order to obtain accurate material properties. During the manufacture of the specimen, attention must be paid to obtaining a void free bondline with uniform bondline thickness. Accuracy is required in the machining of dimensions, and quality control checks must be carried out to ensure consistent results. This type of approach should be taken for all experimental work involving the use of test specimens, but in the case of thick adherend specimens special attention to detail is required because of the large errors which can result from small variations in specimen manufacture and testing. The following sections describe in detail, the manufacture and testing techniques used in this research.

#### 3.2.1 Specimen Manufacture

Figure 3.1 shows the overall dimensions of the thick adherend specimen used in this work. The aluminium alloy BS2L93 was used as the adherends. Since the original plate had a slight curvature, it was found best to leave the original plate thickness of 6.17mm as the adherend thickness. This enabled the profiles of the individual adherends to be matched before processing, and ensured uniform contact along the length of the specimen. After processing, the adherends were found to have straightened, and the resulting specimen was without any curvature.

The adherends were cut from the original plate with a length of 140mm

and a width of 16mm. The width was very accurately machined in order to ensure a good fit between specimen and vacuum plate sides. For the thick adherend specimen, a special vacuum plate was manufactured, and a detail drawing is given in Appendix A. A good fit was required in order to limit the amount of relative side movement between the two adherends, but enough space had to be provided to allow for the different thermal expansions of the steel vacuum plate and the aluminium adherends. If the fit had been too tight, the top aluminium adherend may have jammed during processing, resulting in poor consolidation of the specimen.

Since no information was available on the best surface preparation of the aluminium for bonding with PEEK, it was decided to use the same preparation as for epoxy adhesives, given in Reference 13. The adherends were degreased with acetone, and then etched in a solution of concentrated sulphuric acid and sodium dichromate at 65°C, before being rinsed in water and dried in hot air. The PEEK film was degreased with acetone prior to processing.

In order to control bondline thickness, 0.1mm thick control wires were introduced into the bondline as shown in Figure 3.1. Special end stops were used in the vacuum plate to prevent undue longitudinal movement of the adherends during processing. The rest of the vacuum bag was made up similar to that shown in Figure 2.2, with a bleeder pipe again being used to ensure good vacuum over the full length of the specimen.



The experimental arrangement shown in Figure 2.1, was used to process the specimens at a temperature of 380°C. The specimens were held at this temperature for ten minutes before being removed from the oven and air cooled. The average cooling rate between 380°C and 200°C was 73.2°C/min. The specimen was not removed from the vacuum plate until a temperature of around 70°C had been achieved.

After processing, the specimens were reduced in width to the dimension shown in Figure 3.1. This ensured that a good bondline was present across the whole of the specimen width. The holes were then drilled and finally the notches machined. The most important dimension on the specimen was the relative positioning of the notches to ensure consistent overlap length. The depth of the notches was also important, since they had to be deep enough to cut through the bondline, but not so deep as to effectively reduce the strength of the specimen section. The most effective method for making the notches was found to be horizontal milling. An 0.81mm thick blade was used to machine the notches, and good control of depth and position of the notches was achieved.

The extensometer developed to measure the displacements of the specimen during test, used three steel points which dug into the specimen at the locations shown in Figure 3.1. Three small depressions were made in the adherends at these positions with the aid of a very fine drill. The positioning of the points was based on the work of Krieger in Reference 12. Only one extensometer was used in this work, and this is described in detail in Section 3.2.4. It was found necessary to use small abrasive pads on the specimen to

hold the extensometer clamps in position during testing. These were stuck onto the specimen as shown in Figure 3.1.

### 3.2.2 Other Methods of Specimen Manufacture

The specimen manufacture described in Section 3.2.1, was developed after other techniques had been tried and later abandoned. A great deal of time was spent on the development of the special vacuum plate described above, since vacuum during processing was found to be very important in obtaining consistently strong joints. Initially, a vacuum bag similar to that in Figure 2.2 was made for the thick adherend specimen. However, since the thick adherend specimen was six times the thickness of the APC-2 specimens, extreme difficulty was found in obtaining an air tight bag using a flat vacuum plate. The vacuum plate shown in Appendix A, was developed to allow the thick adherend specimen to be placed into a deep recess in the plate. The plastic film forming the top of the bag could then be used to form a flat cover over the specimen, and this enabled an excellent vacuum bag to be formed.

Since the material properties from the thick adherend specimens were to be used to model joints using APC-2 adherends, concern was expressed as to how representative the material properties would be from thick adherend specimens using aluminium adherends. For this reason, it was attempted to develop a specimen which used an APC-2 surface as the bonded surface. However, rather than using APC-2 to form the whole of the thick adherend specimen, it was attempted to fabricate a specimen by bonding thick aluminium pieces to an 8 ply

unidirectional APC-2 specimen. The APC-2 specimen was processed as described in Chapter 2, with a 0.1mm thick layer of 450 Grade PEEK film. Thick aluminium pieces were then bonded to the specimen to give an overall thickness of 12mm. The aluminium was prepared using a chromic acid etch, and the APC-2 adherends prepared by degreasing followed by surface abrasion. The aluminium was then bonded to the APC-2 using the two part epoxy adhesive Araldite 2005. Problems were found in obtaining sufficient bond strength between the aluminium and the APC-2, and failure of this specimen resulted from debonding between the aluminium and the APC-2. For this reason, and concern over the ability of this specimen to produce a reasonably uniform stress distribution in the joint region, the specimen was abandoned in favour of the specimen described in Section 3.2.1.

A particular problem which arose during the development of the above specimen, highlighted an area which will be very important when APC-2 is bonded to other materials at high temperatures. The aluminium was originally bonded to the APC-2 at around 80°C, and after cooling of the specimen it was found that severe warping of the specimen had taken place. This was a result of the different thermal expansions of the aluminium and the APC-2. If fusion bonding is used to bond APC-2 to a material with a different coefficient of thermal expansion, consideration will have to be given to the effect of the high processing temperatures producing thermal stresses in the joint.

### 3.2.3 Development of loading Equipment

The method of loading of the thick adherend specimen is extremely

important in order to ensure reliable results. The preferred method of loading, is by using loading blocks to ensure the load is applied in a moment free manner. Figure 3.2 shows the thick adherend specimen and the type of loading blocks developed. In Appendix A, a detailed drawing is given for these blocks showing the main dimensions, and Figure 3.3 shows a picture of the loading blocks positioned in the testing machine. A steel pin was used to load the specimen through its end, and PTFE spacers were used to ensure accurate alignment of the specimen in the blocks. All points of the loading assembly were lubricated to ensure friction was kept to a minimum.

The loading blocks consisted of an inner and outer block, and were based on the gimbal mountings used by Althof in Reference 11. These were machined from AISI 4140 alloy steel, hardened and tempered to an ultimate tensile strength of 850MPa. The inner loading block was designed for an ultimate load of 15kN. It was intended that the outer loading block could be used with a different inner block, in order to load bonded APC-2 to APC-2 specimens, such as those in Chapter 2. Since these specimens could potentially carry very high loads, the outer block was designed to an ultimate load of 52.5kN. Although an inner block to take the APC-2 specimens was never actually made, this may be done at a future stage, since most mathematical models assume moment free application of load for the joints. Although, in this work, the APC-2 specimens were loaded in grips that could have introduced some moment at the end of the specimen, this was not regarded as important for very thin adherends. For thicker adherends, moment free application of load

would be very important, and the loading blocks described above would have to be used.

#### 3.2.4 Development of Extensometer

In order to obtain the displacements of the specimen during loading, an existing Instron extensometer, used for tension tests, was modified to measure the shear displacement in the bondline. This Instron extensometer was a 10mm gauge length extensometer with a maximum displacement of 1.0mm. The modifications took the form of developing attachments to locate the extensometer at three points on the thick adherend specimen. Figure 3.4(a), shows the correct arrangement of the pick-up points on the specimen, as given by Krieger in Reference 12. This particular pattern tends to limit the error from bending deformations of the adherend. In Appendix A, a detailed drawing is given of the attachments developed.

Since only one extensometer was being used, extensometer supports had to be developed to hold the instrument on the specimen during testing. These are shown in Figure 3.4(b), and a detailed drawing is given in Appendix A. Any relative movement between the supports and the attachments during loading, would introduce additional errors. Therefore, small patches of abrasive paper were stuck onto the specimen at the positions where the supports contacted the specimen. This ensured that the support and the extensometer attachment, for each half of the specimen, moved as one unit. If no abrasive pad had been used, slipping of the support relative to the adherend surface may have caused rotation of the extensometer,

introducing associated error.

### 3.2.5 Extensometer Calibration Frame

Calibration of the extensometer is extremely important in order to accurately measure the displacements of the specimen under test. However, the very small displacements and the precise geometry of the thick adherend specimen, requires the construction of very accurate and geometrically representative calibration equipment. The extensometer must be calibrated on a frame, where the extensometer can be attached as it will be during actual testing of a specimen. Figure 3.5 shows a photograph of the extensometer mounted on the calibration frame developed in this work. A steel frame was used to mount a large diameter micrometer barrel, which controlled the relative displacement of two aluminium pieces, simulating the movement of a specimen under test. The scale on the micrometer allowed displacements to be measured to within 0.001mm.

In order to simulate the PEEK bondline in the real specimen, a layer of 0.1mm thick Stabar film was placed between the two aluminium pieces of the calibration frame. Small pads of the abrasive paper were also positioned on the aluminium, and the extensometer was mounted on the frame in exactly the same manner as on the real specimens. The extensometer was then calibrated to give an electrical output to a pen recorder corresponding to the displacement of the micrometer barrel. It was found extremely difficult to obtain consistent accuracy over the full range of the displacements required. Table 3.1 gives the errors from the extensometer when

calibrated to 0.2mm full scale displacement. The correlation between displacement on micrometer and recorded displacement was considered at 5%, 25%, 50%, 75% and 100% of the full scale displacement. The errors given in Table 3.1 are in terms of the difference between recorded displacement and micrometer displacement. It can be seen that when first calibrated, the recorded displacements are within 6% of the micrometer displacements, except over the first 0.01mm of displacement.

It was felt necessary, to check the effect on the measured displacement of the extensometer being moved from the calibration frame to the specimen. This was performed by simply calibrating the extensometer, then removing and replacing the extensometer on the calibration frame, and, finally, rechecking the recorded displacements. Table 3.1 shows that after repositioning, the measured displacements are within 12% of the micrometer displacements. This suggests that during testing of a specimen, the measured displacement can be expected to be within 12% of the actual displacement, except within the first 0.01mm. The implications of these results, on the accuracy of the measured curve, is discussed in Section 3.3.1.

#### 3.2.6 Thick Adherend Metal Correction

During testing of the thick adherend specimens, a certain amount of deformation takes place in the metal adherends and this is recorded by the displacement transducer. In order to account for the metal deformation, a one piece specimen was made with the same

overall dimensions as the final bonded specimens. This specimen did not contain a bondline. Therefore, by measuring the metal deformation taking place during loading of this specimen, the total deformation recorded for the actual bonded specimens could be corrected to give the bondline displacements only. The distance between the pick up points of the extensometer are the same on both specimens, and this requires that an allowance is made for the smaller amount of metal present between the points in the bonded specimen. The way in which this is calculated is given in Reference 12 and in Appendix B.

A linear relationship between deformation and load was obtained from the metal correction specimen. This relationship is given below as equation 3.1, where  $u_d$  is the metal deformation in meters, and  $F$  is the applied load in Newtons

$$u_d = 3.0 \times 10^{-9} F \quad 0 \leq F \leq 6000N \quad (3.1)$$

The bondline displacement,  $u_c$ , is given by equation 3.2, where  $u_s$  is the measured displacement during test, and  $u_m$  is the metal deformation given in equation 3.1 corrected for the inclusion of the bondline in the actual bonded specimen

$$u_c = u_s - u_m \quad (3.2)$$

The details of this calculation are given in Appendix B.



### 3.2.7 Specimen Testing

The ability to obtain a good recording of displacement of the specimen during test, was found to be very dependent on the care taken to set up the test prior to loading. The following testing technique was developed through testing of several specimens.

Before putting the specimen into the loading blocks, all pins were lubricated in order to ensure free rotation of the specimen and, therefore, provide true loading alignment. This was found to be important in order to ensure accurate displacement measurement.

The extensometer was initially calibrated on the calibration frame, described in Section 3.2.5, before being positioned on the specimen. It was found particularly important to slightly pre-load the specimen and reset the extensometer to zero prior to testing. This ensured a positive measurement of displacement at the start of testing, and effectively eliminated the errors arising from the settling of the loading blocks during the initial loading. The effect of zeroing the extensometer reading prior to testing was easily corrected later, by extrapolating the initial linear portion of the curve back to zero. The loading speed was 2mm/min, and this resulted in failure in around 30 seconds.

In order that the shear strain could be calculated, the bondline thickness for each specimen had to be measured. Although bondline control wires were used to try and produce a consistently uniform bondline thickness of 0.1mm, it was found that the specimens produced

from Stabar film had a reduction of bondline thickness to around 0.075mm from the original 0.1mm film thickness. The thickness varied slightly from specimen to specimen, and it was necessary, therefore, to measure the bondline thickness for each specimen.

It was found that external examination of the bondline at the edges of the specimen, provided inaccurate information regarding the bondline thickness over the majority of the specimen cross-section. Therefore, a specimen was made and the bondline thickness measured at the middle of the overlap section, and also at 10mm from the middle section. This was done by sectioning the specimen at these positions and measuring by using a special eye piece on an optical microscope. The average bondline thickness measured at both positions of the specimen agreed to within 3%. It was, therefore, decided to use this technique to measure the bondline thickness for all specimens. After testing, each specimen was sectioned 10mm from the middle section and the bondline thickness measured. The specimens produced using 0.1mm thick 450 Grade film, were found to consistently produce a bondline thickness of 0.1mm. This was a result of this material flowing very little during processing.

### 3.3 Results and Discussion

#### 3.3.1 Shear Stress-Strain Curves

Figure 3.6 shows the results of two thick adherend specimens tested to failure as described in section 3.2.7. The specimens were made using 0.1mm thick 450 Grade film. These results give the maximum and minimum values of failure stress for all the specimens tested, including those values obtained using Stabar film. It can be seen that the curves are very non-linear, with a very large plastic region, and relatively small elastic region.

The maximum shear stress at failure was recorded as  $72.27\text{N/mm}^2$ , and the minimum  $66.07\text{N/mm}^2$ . The curves represent the limits of the scatter of the results. The curves have failure strains of 1.92 and 2.10, and generally the results from other specimens gave values in this region. It must be appreciated that due to experimental error, the curve with the highest failure stress does not necessarily have the highest failure strain.

For the calculations in Chapter 4, the curve with the lowest failure stress was used. This ensured that a conservative estimate of joint strength was made. The shear stress was calculated by dividing the measured load by the overlap area. The shear strain was calculated by dividing  $u_c$ , from equation 3.2, by the measured bondline thickness. The results were then plotted as shear stress against shear strain.

In Section 3.2, it was mentioned that the specimens produced using Stabar film, rather than 450 Grade film, had a significant reduction in bondline thickness. However, it was also found that the specimens produced using Stabar film had a good deal of void content in the bondline, unlike the 450 Grade films, where voids were almost non-existent. It was felt that this was due to the much greater flow of the Stabar film during processing, and that with better control of bondline thickness, this could be overcome.

Figure 3.7, shows a comparison between a curve obtained for 450 Grade film, without any voids in the bondline, and a curve for Stabar film, with 17% of the bonded area covered with voids. The Stabar film shows a negative shear strain with respect to shear stress, over the initial portion of the curve. This is due to the voids in the bondline offsetting the loading alignment, and results in the extensometer measuring a smaller displacement in the bondline than should be the case for the applied load.

Krieger identified this problem as a possible source of error in Reference 12. The small diagram in Figure 3.7, demonstrates the effects the voids have on the loading alignment and the measured displacement. When the measured displacement is corrected for metal deformation, as in equation 3.2, the resulting displacement is negative, and hence the calculated shear strain is negative.

In assessing the results, the accuracy of the measurements must be considered. In Section 3.2.5, the accuracy of the extensometer as measured using the calibration frame was discussed. In general, the

extensometer was less accurate in the first part of the measurement range. This would correspond to the elastic region of the shear stress-strain curve, and, therefore, the extensometer developed was not sensitive enough to give reliable information about the shear modulus of PEEK. In this work, the important requirement was to obtain the overall shape of the curve, together with accurate measurement of the failure strain. Although accurate information regarding the shear modulus of the material would have been desirable, it was not necessary in order to model the joint using the theory described in Chapter 4. A more sensitive extensometer would have to be used in order to accurately measure the shear modulus.

### 3.3.2 Failure Surface Examination

For accurate measurement of the shear properties of an adhesive, the failure mode of the specimen should be cohesive within the adhesive. If the failure results from adhesive failure between the adhesive and the adherend, then the measured failure stress and strain are a measure of the bond strength between the two materials, rather than a measurement of the properties of the adhesive. In this work, it was found extremely difficult to obtain cohesive failure in the PEEK film across the full width of the thick adherend specimen.

With 450 Grade film, the failure was adhesive failure between the film and the surface of the aluminium adherend. There was never any indication of cohesive failure in the film. Similarly, in the APC-2 bonded specimens, 450 Grade and Stabar film showed adhesive failure at the ends of the overlap. The value of the measured curve,

therefore, can only be assessed in terms of how good a correlation exists between theoretical and experimental results when the curve is used in a given mathematical model. It will be shown in Chapter 4, that the results obtained, when using the curve in the theoretical work of Hart-Smith, gave very good correlation with the experimental results.

The specimens produced using Stabar film, did show areas of cohesive failure in the film. Figure 3.8(a), shows a picture of the failure surface of a specimen produced with 0.1mm thick Stabar film. Although large void regions can be easily identified from this picture, the voids were not easily observed when a cross-section of the bondline was examined with an optical microscope. After failure of the specimen, however, the voids were easily identified as regions of reflective resin. Between the voids, there was a region of cohesive failure in the PEEK, seen as ridges of PEEK running between the two void areas.

To the left of the picture in Figure 3.8(a), adhesive failure between the PEEK and the aluminium adherend is seen. This region is located at the end of the overlap at the point of maximum stress shown in Figure 3.8(b). The pattern of adhesive failure at the inner edge of the overlap, with cohesive failure of the PEEK in the middle area changing to adhesive failure between the PEEK and the opposite adherend at the outer edge of the overlap, was the same on all the specimens tested. In Reference 14, Ojalvo and Eidinoff analysed the effect of bondline thickness on the elastic stresses of single-lap adhesive joints. Their results showed, that a significant variation

of stress existed through the thickness of the bondline, with the maximum stresses occurring at the positions shown in Figure 3.8(b). In their paper, they presented some experimental evidence which supported the proposed failure hypothesis of failure initiating at the points of maximum stress, and then propagating along the adhesive-adherend interface, before passing through the bondline at the central area of the overlap. Although the thick adherend specimen has much larger dimensions than those considered by Ojalvo, and the stresses at failure are in the plastic region of the PEEK shear stress-strain curve, the observed results tend to provide additional evidence for this failure sequence.

Figures 3.9 and 3.10, show SEM micrographs of some of the features found on the failure surfaces of the thick adherend specimens produced with 0.1mm thick Stabar film. Figure 3.9(a), shows a close-up of the void and the cohesive regions of the failure surface. The void surface was extremely smooth, and consisted of a very thin layer of PEEK bonded to the adherend surface and increasing in thickness towards the boundary between the void and the cohesive failure surface. Figure 3.9(b), shows that the thickness of this layer is only around 0.04mm thick, with a very smooth surface finish. To the bottom of this picture, the aluminium adherend surface can be seen, with most of the PEEK debonded from the surface.

In Figure 3.10(a), the cohesive failure surface can be seen. After discussions with ICI, (Reference 15), it was felt that these ridges of PEEK may have been formed in a similar manner to the hackle formation seen on epoxy fracture surfaces. These hackles were first

reported by Chamis and Sinclair, (Reference 16), who named them lacerations. In Reference 17, Johannesson, et al., described the role which the stress system played in the formation of hackles. The hypothesis proposes that the principal stresses open up microcracks in the matrix perpendicular to the direction of the principal stress. Generally, the size of the hackles in epoxy, are on a much smaller scale than those shown in Figure 3.10(a).

In Figure 3.10(b), a sketch shows the possible way in which the "macrohackles" of Figure 3.10(a) may have been formed. It is assumed that the thick adherend specimen loads the bondline in pure shear, and this is equivalent to the direct stress system shown. Under the action of these principal stresses, it is assumed that microcracks open in the PEEK, forming the basis of the hackles. Failure would result from microcracks linking the opened cracks together, and forming the features shown in Figure 3.10(a). The void regions in the bondline would cause stress concentrations at their boundary, and the failure would propagate across the overlap between the voids. It is emphasised that this is only a tentative explanation for the formation of the observed features, and much work will have to be carried out in order to confirm whether or not this is the case.



### 3.4 Conclusions

The measurement of the shear stress-strain curve was found to involve considerable development of both equipment and testing technique. Both 450 Grade and Stabar film were tested, and it was found that film viscosity had a considerable effect on ease of processing, but little effect on the resulting curve. The main conclusions were as follows:

- (1) PEEK was found to have a very non-linear curve, with a large plastic region and a relatively small elastic region.
- (2) The measured failure stress of PEEK was between  $66\text{N/mm}^2$  and  $72\text{N/mm}^2$ , with a failure strain between 1.9 and 2.1m/m.
- (3) Stabar film was found to be less viscous than 450 Grade film, and this resulted in problems in controlling bondline thickness during processing. It was found difficult to obtain a void-free bondline with Stabar film. Failure of the specimen resulted from mixed adhesive and cohesive failure with Stabar film, and adhesive failure with 450 Grade film.
- (4) The modified Instron extensometer provided satisfactory measurement over the full range of specimen displacements. However, this extensometer was not sufficiently sensitive to give reliable information regarding the shear modulus of PEEK.

THEORETICAL PREDICTION OF THE STRENGTH OF FUSION JOINTS

4.1 Introduction

Many theoretical analyses of single-lap joints have been developed over the years, and range from the very simple to the very complex. In 1964, Kutscha, (Reference 7), gave an excellent review of the work completed to that date. It is generally considered that the earliest paper on the theoretical analysis of lap joints was by Volkersen in 1938 (Reference 18). Typical of many of the analyses to follow, an elastic stress distribution in the joint was considered with adherends in which only differential straining took place. It wasn't until 1944, that the effect of adherend bending on the adhesive stress distribution in single-lap joints was taken into account. This analysis was presented by Goland and Reissner in Reference 19, where, again, the stress distribution was considered only for elastic deformation of the adhesive. By 1972, however, interest had been shown in the influence of non-linear response of the adhesive on the stress distribution. Dickson, Hsu and McKinney (Reference 20), presented work on the development of a linear analysis for bonded joints in laminated composites. They extended the analysis to include non-linear adhesive stress-strain behaviour by using a "plastic zone" approach, together with a perfectly elastic-plastic effective stress-strain curve. From their analysis, they were also able to take into account transverse shear and

thickness normal deformations, (normal deformations across the thickness), of the adherends. They found that although composites generally have a much lower transverse shear modulus compared to axial Young's modulus, the effect of interlaminar shear deformation on the stress distribution is very small. However, it was shown that thickness normal deformations do have a significant effect on the adhesive shear distribution.

In 1972, Grimes et al., (Reference 21), published work on a discrete element method and a continuum elasticity method to predict stress distributions in single, double and step lap joints. They included non-linear behaviour of both adherends and adhesive, and used a Ramberg-Osgood representation of the adhesive normal and shear properties.

In 1973, Hart-Smith, (Reference 8), presented work on the analysis of single-lap joints. A continuum model was developed in which the adherends were considered elastic, and the adhesive properties were approximated by an elastic-plastic representation in shear, and by assuming perfectly elastic behaviour in transverse tension. The model was based on an extension of the Volkersen analysis, and included an important correction of the bending parameter first developed by Goland and Reissner (Reference 19), to give a more realistic approximation of the stress distribution in the adherends at the end of the joint. The object of the work was to provide a simple design technique which included only the major joint parameters known to be important in the analysis of single-lap joints.

1973 also saw the start of a series of publications by Renton and Vinson, (References 22 to 24), on analytical techniques for single-lap joints under static and dynamic loads. The analysis considered only elastic deformation of the adhesive, but included the effects of transverse shear and normal strain. Experimental measurement by Sharpe and Muha, (Reference 25), showed that the Renton-Vinson closed form analysis gave the best agreement with their results out of over twenty models examined.

Several literature surveys have been completed in recent years, and Oplinger, (Reference 26), and Vinson and Sierakowski, (Reference 4), present excellent discussions on most of the research conducted into adhesive joints to date.

It was hoped as part of this research to show the correlation between fusion bonding and a mathematical model which would provide useful guidelines for the manufacture of these bonds in practical structures. From the work in Chapter 3, it can be seen that the model used would have to include non-linear behaviour of the adhesive in shear to provide the opportunity of achieving good correlation between theory and experiment. From the literature discussed above, it was decided that the analysis of Hart-Smith, (Reference 8), seemed the most suitable, although the limitations of the analysis were recognised. From his work, the three dominant failure modes of single-lap joints were considered, and this allowed the examination of the importance of each mode of failure with respect to several important joint parameters.

The results of the analysis were compared to the experimental results, looking at the influence of adherend type, overlap length and bondline thickness on joint strength. The influence of adherend thickness on predicted joint strength was also considered.

Although Hart-Smith modelled the adhesive shear properties using an elastic-plastic approach, in this work, the shear property curve was also modelled using a bi-elastic approach. The results of the two representations are compared, especially in the overlap length range of practical interest.

## 4.2 Theoretical Analysis

### 4.2.1 Hart-Smith Model

The following gives a brief description and discussion of Hart-Smith's analysis from Reference 8. The three dominant failure modes for single-lap joints are considered; namely, adhesive shear failure, peel failure and adherend failure. Reference 8 should be consulted for the derivation of Hart-Smith's equations.

An inconsistency in the derivation of the equations for shear failure in plane strain is pointed out. A modification is also made to the analysis for adherend failure of composite adherends, by considering the strain distribution in the adherends rather than the stress distribution.

#### 4.2.1.1 Adhesive Shear Failure

In single-lap joints, there are three dominant modes of failure. That which springs most readily to mind when considering single-lap joints, but which can be the least likely, is shear failure of the adhesive. It has been recognised that consideration of adhesive non-linear behaviour in shear is essential in order to produce good correlation with experimental results. Hart-Smith represented the adhesive shear property curve by using an elastic-plastic representation of the curve, as shown in Figure 4.1. The approximate curve is made up of two lines, the first line giving a perfectly elastic representation and terminating at the ultimate shear stress

value of the adhesive. The second line represents the perfectly plastic portion of the curve, where the ultimate shear stress is taken as constant over a range of shear strain values up to the measured ultimate shear strain of the adhesive. The point of intersection of these two lines is determined by ensuring that the area under both the approximate and actual curves is the same. This means that the adhesive shear strain energy at failure is the same for both curves.

Due to the eccentric load path of single-lap joints, considerable bending moments are introduced into the adherends at the ends of the overlap. However, in his analysis, Hart-Smith takes into account the significant bending moment relief associated with the deformation of the structure under load. In the determination of the bending moments at the ends of the overlap, ( $M_0$ ), he assumed that the adhesive was perfectly elastic. It was shown that the resultant equation for  $M_0$  was the same for both perfectly elastic and also perfectly plastic adhesive behaviour, and was, therefore, assumed independent of adhesive characteristic. The equation obtained for  $M_0$  was as follows,

$$M_0 = k P \frac{t}{2} \left( 1 + \frac{n}{t} \right) \quad (4.1)$$

where  $t$  is the adherend thickness,  $n$  is the bondline thickness and  $k$  is the bending moment coefficient given by

$$k = \frac{1}{1 + \xi c + \frac{1}{6} \xi^2 c^2} \quad (4.2)$$

where

$$\xi = \left[ \frac{P}{D} \right]^{\frac{1}{2}} \quad (4.3)$$

P is the applied load on the joint per unit width, D is the flexural rigidity of the adherends and c is half the overlap length. Since composite materials may have a different bending modulus compared to extensional modulus, the two are uncoupled by the use of the parameter  $k_b$ , where

$$k_b = \frac{E_f}{E} \quad (4.4)$$

$E_f$  is the flexural modulus and E is the extensional modulus. Therefore, the equation for the flexural rigidity is given by,

$$D = \frac{k_b E t^3}{12 (1 - \nu^2)} \quad (4.5)$$

Hart-Smith starts his analysis of the joint region by considering equilibrium of adherend elements. Using the stress-strain relations, and accounting for both tensile and bending strain, he is able to derive an equation for the stress distribution in the joint assuming elastic behaviour of the adhesive,



$$\tau = A_2 \cosh (2\lambda's) + B_2 \sinh (2\lambda's) + C_2 \quad (4.6)$$

where  $B_2 = 0$  due to symmetry of the stress distribution. The co-ordinate system is given in Figure 4.2.

The parameter  $\lambda'$  takes the form,

$$(\lambda')^2 = \left[ \frac{1 + 3(1 - \nu^2)/k_b}{4} \right] \lambda^2 \quad (4.7)$$

where

$$\lambda^2 = \frac{2G}{Et\eta} \quad (4.8)$$

It should be pointed out that Hart-Smith made an inconsistency in the derivation of equation 4.6 regarding the assumption of plane strain. When deriving the strain in the adherends immediately adjacent to the adhesive, he assumed the strain due to the tension force,  $T$ , as

$$\frac{du_2}{ds_{\text{tension}}} = \frac{T_2}{Et} \quad (4.9)$$

which is for plane stress.

For plane strain this should have been taken as

$$\frac{du_2}{ds_{\text{tension}}} = \frac{(1 - \nu^2)}{Et} T_2 \quad (4.10)$$

This introduced an error into the calculation of the parameter  $\lambda'$ , which should have been calculated as,

$$(\lambda')^2 = (1 - \nu^2) \left[ \frac{1 + 3/k_b}{4} \right] \lambda^2 \quad (4.11)$$

The inconsistency is also apparent in equation 68 in Reference 8 in the derivation of the elastic-plastic analysis, and this should be corrected accordingly. In practical joints, this should not introduce significant error, and in the case of joints analysed in plane stress, (when the Poisson's ratio is dropped from the equations), no error should be present.

Hart-Smith takes the shear strain as,

$$\gamma = \frac{u_3 - u_2}{n} \quad (4.12)$$

where  $u_2$  and  $u_3$  are the adherend displacements in regions 2 and 3, shown in Figure 4.2.

Since the adhesive is modelled as elastic-plastic, the

stress-strain relation is taken as

$$\left. \begin{array}{ll} \tau = G\gamma & 0 \leq \gamma \leq \gamma_e \\ \tau = \tau_p & \gamma_e \leq \gamma \leq \gamma_{ult} \end{array} \right\} \quad (4.13)$$

$\gamma_e$  is the limit of the elastic region in the approximate adhesive stress-strain curve,  $G$  is the shear modulus and  $\tau_p$  and  $\gamma_{ult}$  are the ultimate shear stress and strain at failure.

At failure of the joint, it is assumed that the joint contains two regions of deformation. In the central core of the overlap, it is assumed that there is a region of elastic deformation over a length  $d$ . At the edges of the joint it is assumed that there are regions of plastic deformation, each of length  $(l - d)/2$ . In the elastic region, the stress distribution is given by equation 4.6. In the plastic region of the joint, the strain distribution is given by

$$\gamma = A_3 \zeta^2 + B_3 \zeta + C_3 \quad (4.14)$$

where the origin of  $\zeta$  is at  $s = d/2$ .

The solution of the problem is obtained by solving for the unknown constants  $A_2, C_2, A_3, B_3, C_3, d$  and the failure load/width  $P$ . This is achieved by using the known boundary conditions of the strain distribution throughout the joint. Failure is considered to occur when  $\gamma = \gamma_e + \gamma_p = \gamma_{ult}$  at the ends of the joint. The value of  $\gamma_{ult}$

is taken from the shear stress-strain curve of the adhesive. The problem then reduces to the simultaneous solution of the following three equations, together with equation 4.2,

$$2 \left[ \frac{\gamma_p}{\gamma_e} \right] = K \left\{ \left[ 2\lambda' \left[ \frac{\ell - d}{2} \right] + \tanh(\lambda'd) \right]^2 - \tanh^2(\lambda'd) \right\} \quad (4.15)$$

$$\left[ 1 + \frac{3k(1 - \nu^2)}{k_b} \left[ 1 + \frac{n}{t} \right] \right] \frac{\tau_{av}}{\tau_p} (\lambda\ell) \lambda \left[ \frac{\ell - d}{2} \right] = 2 \left[ \frac{\gamma_p}{\gamma_e} \right] + K \left[ 2\lambda' \left[ \frac{\ell - d}{2} \right] \right]^2 \quad (4.16)$$

$$\frac{\tau_{av}}{\tau_p} (\lambda'\ell) = 2\lambda' \left[ \frac{\ell - d}{2} \right] + \tanh(\lambda'd) + (1 - K)[\lambda'd - \tanh(\lambda'd)] \quad (4.17)$$

The coefficient K is introduced into the notation in order to make the derivation of the equations simpler.

In this work, the four equations were solved using a computer to obtain the values for the unknowns K, d, k and P, where P is the load/width at failure for the given joint configuration. The NAG Fortran routine C05PBF was used in the solution and this requires the user to supply the Jacobian of the equations. It gives a good rate of convergence to the solution.

The four equations given above, however, are derived assuming that the joint contains both elastic and plastic deformation.

Consequently it was found difficult to obtain a reasonable solution of the equations for joint configurations where the joint was fully plastic at failure. Hart-Smith derived the equation giving the maximum overlap length ( $l_{cr}$ ) for the joint to be fully plastic at failure. This is given by,

$$l_{cr} = \frac{1}{\lambda} \left[ \frac{8 \frac{\gamma_p}{\gamma_e}}{1 + \frac{3k(1 - \nu^2)}{k_b} \left[ 1 + \frac{n}{t} \right]} \right]^{\frac{1}{2}} \quad (4.18)$$

This equation was solved on computer, by using the Newton-Raphson method, to give the critical overlap length.

All joints with an overlap length less than  $l_{cr}$  have a failure load/width given by

$$P = \tau_p l \quad \text{for } l \leq l_{cr} \quad (4.19)$$

For overlaps greater than  $l_{cr}$ ,  $P$  is obtained by solving equations 4.15 to 4.17 and equation 4.2.

If  $P$  is plotted against  $l$ , all overlaps less than  $l_{cr}$  will lie on a straight line, the slope of which will be  $\tau_p$ . This is a consequence of assuming perfectly plastic behaviour in the model of the shear stress-strain curve. Although there is a strain variation in the joint, this equates to uniform shear stress over the overlap

length.

#### 4.2.1.2 Peel Failure

Due to the eccentric load path in single-lap joints, significant peel stresses are present at the ends of the joint. In his analysis, Hart-Smith assumes perfectly elastic behaviour of the adhesive in transverse tension, and gives two reasons to support this. First he states that for composite adherends, the adherend is usually much weaker in transverse tension than the adhesive, and, therefore, failure will occur in the adherend when the adhesive stress reaches the adherend transverse strength. This would mean that the adhesive could not deform plastically at the same peel stress over an area of the overlap, since the joint would fail as soon as the adherend transverse strength was achieved. This, however, assumes that elastic modelling of the stress-strain curve gives a reasonable approximation to the curve. In the case of an adhesive which shows significant non-linear behaviour over a large range of stress values, the author here feels that bi-elastic modelling of the curve may be more appropriate.

Hart-Smith's second argument may have more merit. He suggests that since the adhesive is bonded to adherends which impose stiff in-plane constraint, the long chain adhesive is essentially prevented from yielding and deforming plastically. Certainly it has been appreciated for many years that adherend constraint has a significant effect on the observed material properties of adhesives. It is for this reason that tests to obtain the material properties of adhesives

should be conducted while the adhesive is bonded to adherends.

Hart-Smith takes the normal stress  $\sigma_c$  as

$$\sigma_c = E_c' \frac{(w_3 - w_2)}{n} \quad (4.20)$$

where  $w_2$  and  $w_3$  are the normal displacements of the adherends in regions 2 and 3 of the joint as shown in Figure 4.2.  $E_c'$  is an effective peel modulus for the adhesive which makes allowance for the transverse deformations of the adherend under peel stresses.

Hart-Smith gave the following approximate equation for this effective modulus

$$\frac{1}{E_c'} = \frac{1}{E_c} + \frac{6}{E_n} \quad (4.21)$$

where  $E_c$  is the measured tensile modulus of the adhesive taking account of the effects of in-plane support from the adherends, and  $E_n$  is the transverse modulus of the adherend.

Using equation 4.20 and the equations from equilibrium of adherend elements, Hart-Smith obtained the following equation for the symmetrical distribution of peel stresses in the joint overlap

$$\sigma_c = A \cos(xs) \cosh(xs) + B \sin(xs) \sinh(xs) \quad (4.22)$$

where

$$x^4 = \frac{E_c'}{2nD} \quad (4.23)$$

The origin of the  $s$  coordinate is at the middle of the overlap. The solution of the constants  $A$  and  $B$  can be obtained from the boundary conditions that there is zero resultant transverse force across the bondline, and that the bending moment ( $M_0$ ) is known from equation 4.1.

Of particular interest is the value of the maximum peel stress in the joint. This occurs at the end of the overlap, and is given by

$$\sigma_{c,max} = \sigma_{av} k \left[ 1 + \frac{n}{t} \right] \left[ \frac{3E_c'(1 - \nu^2)t}{2 k_b E n} \right]^{\frac{1}{2}} \quad (4.24)$$

This equation was used to obtain the value for the failure load/width assuming failure occurred when  $\sigma_{c,max}$  equalled the ultimate transverse strength of the adherend. A computer was used to solve 4.24 using the Newton-Raphson method.

#### 4.2.1.3 Adherend Failure

For long overlaps, the load carried by the joint can be sufficient to initiate failure in the adherends. Under the combined action of tensile and bending stresses, the stress in the outermost fibres at the end of the overlap can produce failure in the adherend.



Hart-Smith analysed the adherends as beams in tension and bending, and gave the equation for the maximum stress in the outermost fibres ( $\sigma_{\max}$ ) as

$$\sigma_{\max} = \sigma_{av} \left[ 1 + 3k \left[ 1 + \frac{n}{t} \right] \right] \quad (4.25)$$

This equation, however, is only valid assuming isotropic adherends. The effect of ply stacking sequence on resulting maximum stress must be accounted for by introducing the parameter  $k_b$ .

Equation 4.25 is obtained by the addition of a uniform stress distribution in the adherends, due to the tension force, with a linearly varying stress due to bending. This approach may be acceptable for isotropic adherends, but the author here feels that for composite adherends, consideration of strain distribution would be more appropriate.

It was, therefore, decided to derive an equation describing the strain distribution in the adherend assuming uniform strain due to the tension force  $P$ , and a linearly varying strain due to the bending moment  $M_0$ . The strain due to tension is, therefore, given by

$$\epsilon_{x,tension} = \frac{P}{t} \frac{(1 - \nu^2)}{E} \quad (4.26)$$

The strain distribution due to the bending moment is obtained from

$$\epsilon_{x,\text{bending}} = \frac{z}{r_x} = \frac{z M_o}{D} \quad (4.27)$$

where  $r_x$  is the radius of curvature of the adherend, and  $z$  is the vertical coordinate with its origin at the neutral axis of the adherend.

Adding 4.26 and 4.27, substituting for  $D$  and evaluating at  $z = t/2$  gives,

$$\epsilon_{x,\text{max}} = \frac{(1 - \nu^2)}{Et} \left[ P + \frac{6M_o}{k_b t} \right] \quad (4.28)$$

Substitution of  $M_o$  into 4.28 gives,

$$\epsilon_{x,\text{max}} = \frac{(1 - \nu^2)}{E} \sigma_{av} \left[ 1 + \frac{3k}{k_b} \left[ 1 + \frac{n}{t} \right] \right] \quad (4.29)$$

This equation has been derived assuming plane strain. For plane stress the Poisson's ratio term should be dropped. This equation is similar to Hart-Smith's equation 4.25, but there is an essential difference.  $E$  in equation 4.29 is the Young's modulus for the laminate and is a measure of the ratio of average laminate stress to average laminate strain. Equation 4.29 could, therefore, be written

in the form

$$\epsilon_{x,\max} = (1 - \nu^2) \epsilon_{av} \left[ 1 + \frac{3k}{k_b} \left[ 1 + \frac{n}{t} \right] \right] \quad (4.30)$$

where

$$\epsilon_{av} = \frac{\sigma_{av}}{E} \quad (4.31)$$

In order to calculate the stress in the outermost ply of the adherend,  $\epsilon_{x,\max}$  would have to be multiplied by the Young's modulus for that particular ply.

Equation 4.29 was solved by computer for the value of P at failure, assuming that failure initiated in the outermost ply, and taking the value of  $\epsilon_{x,\max}$  as the ultimate strain of that ply.

#### 4.2.2 Development of Bi-Elastic Analysis for Shear Failure

In Reference 8, Hart-Smith developed a shear stress analysis for single-lap joints based on an elastic-plastic approximation of the shear stress-strain curve. It was shown that the ultimate potential joint strength was dependent on adhesive shear strain energy to failure.

As was discussed in section 4.2.1.1, however, the assumption of a perfectly plastic portion for the stress-strain curve, leads to the result of a uniform stress distribution over the joint overlap

although there is a variation of shear strain. This is especially of interest for those overlap lengths where failure of the joint takes place while the strain distribution is completely confined to the plastic region of the approximate curve. With the elastic-plastic approximation, the shear stress is given as a uniform distribution. In reality, however, there should a variation of shear stress. This could only be predicted by taking better account of the shape of the stress-strain curve. In order to do this, a bi-elastic analysis can be performed. In this analysis, the curve is approximated by two non-horizontal lines, where their intersection is again determined by ensuring equivalent strain energy of the approximate and actual curves. This approximation is shown in Figure 4.3.

Although Hart-Smith performed a bi-elastic analysis of double-lap joints in Reference 27, no analysis was given for single-lap joints. Since the author here wished to look at the effect of more accurate modelling of the shape of the stress-strain curve, a bi-elastic analysis for single-lap joints was developed. Full details of this are given in Appendix B.

The shear stress-strain curve is considered in two regions as shown in Figure 4.3. The stress-strain relation for each region is given by

$$\tau = G_1 \gamma \quad \text{where } 0 \leq \gamma \leq \gamma_{1L} \quad (4.32)$$

$$\tau = G_1 \gamma_{1L} + G_2 (\gamma - \gamma_{1L}) \quad \text{where } \gamma_{1L} \leq \gamma \leq \gamma_{2L} \quad (4.33)$$

The shear strain is taken as,

$$\gamma = \frac{u_3 - u_2}{n} \quad (4.34)$$

where  $u_2$  and  $u_3$  are the displacements of the adherends in sections 1 and 2 of the joint as shown in Figure 4.2.

By differentiating equation 4.34, and considering equilibrium of adherend elements, it is possible to determine that the shear strain distribution in the joint is given by

$$\gamma = A_1 \cosh(2\lambda_1' s_1) + B_1 \sinh(2\lambda_1' s_1) + C_1 \quad 0 \leq \gamma \leq \gamma_{1L} \quad (4.35)$$

$$\gamma = A_2 \cosh(2\lambda_2' s_2) + B_2 \sinh(2\lambda_2' s_2) + C_2 \quad \gamma_{1L} \leq \gamma \leq \gamma_{2L} \quad (4.36)$$

$$\left. \begin{aligned} \lambda_1^2 &= \frac{2G_1}{Etn} & \lambda_2^2 &= \frac{2G_2}{Etn} \\ (\lambda_1')^2 &= \frac{(1 - \nu^2)}{4} \left[ 1 + \frac{3}{k_b} \right] \lambda_1^2 & , & \quad (\lambda_2')^2 = \frac{(1 - \nu^2)}{4} \left[ 1 + \frac{3}{k_b} \right] \lambda_2^2 \end{aligned} \right\} (4.37)$$

$s_1$  and  $s_2$  are taken as the coordinates describing the strain distribution in the joint for  $\gamma$  in equations 4.32 and 4.33 respectively. The origin of  $s_1$  is taken at the centre of the joint and the origin of  $s_2$  is taken at  $s_1 = d_1$ , where  $d_1$  is an unknown term. The solution of the problem, therefore, is obtained by using

the known boundary conditions of the strain distribution to calculate the unknown variables  $A_1, B_1, C_1, A_2, B_2, C_2$  and  $d_1$ . The failure load/width is obtained by using the equations 4.32 and 4.33 to give the stress distribution in the joint, and considering equilibrium of the joint. Details of the analysis are given in Appendix B.

This analysis is the general analysis in which it is assumed that at failure the strain distribution in the joint includes strains from both regions of the shear stress-strain curve. However, as will be shown later, for fusion bonding, it was found unnecessary to consider region 1 of the shear stress-strain curve in the analysis. It was found that for overlap lengths less than those where failure resulted from adherend failure, the failure strain distribution was completely defined by region 2 of the stress-strain curve. It was, therefore, possible to considerably simplify the analysis of the joint.

#### 4.2.2.1 Calculation of Critical Overlap Length

In order to simplify the analysis, it is first necessary to calculate the maximum overlap length for which the strain distribution can be described only by considering region 2 of the shear stress-strain curve. In this analysis, because of the symmetry of the strain distribution, the critical half overlap length ( $c_{cr}$ ) is obtained by considering only half the overlap. The analysis uses equation 4.36

$$\gamma = A_2 \cosh(2\lambda_2 s_2) + B_2 \sinh(2\lambda_2 s_2) + C_2 \quad (4.36)$$

The following boundary conditions are used in the solution,

$$s_2 = 0 \quad , \quad \frac{d\gamma}{ds_2} = 0 \quad (4.38)$$

$$s_2 = 0 \quad , \quad \gamma = \gamma_{1L} \quad (4.39)$$

$$s_2 = c_{cr} \quad , \quad \gamma = \gamma_{2L} \quad (4.40)$$

$$s_2 = c_{cr} \quad , \quad \frac{d\gamma}{ds_2} = \frac{(1 - \nu^2)}{Etn} P \left[ 1 + \frac{3k}{k_b} \left[ 1 + \frac{n}{E} \right] \right] \quad (4.41)$$

$$\frac{P}{2} = \int_{s_2=0}^{s_2=c_{cr}} (G_1 \gamma_{1L} + G_2 (\gamma - \gamma_{1L})) ds_2 \quad (4.42)$$

Equation 4.38 is a statement of symmetry of the stress distribution,  
and, therefore,

$$\gamma = A_2 \cosh(2\lambda_2' s_2) + C_2 \quad (4.43)$$

Equation 4.39 gives

$$C_2 = \gamma_{1L} - A_2 \quad (4.44)$$

and 4.40 with 4.43 and 4.44 yields

$$\gamma_{2L} = A_2 \cosh(2\lambda_2' c_{cr}) + \gamma_{1L} - A_2 \quad (4.45)$$

Equation 4.41 gives

$$2\lambda_2' A_2 \sinh(2\lambda_2' c_{cr}) = \frac{P(1 - \nu^2)}{Et\eta} \left[ 1 + \frac{3k}{k_b} \left[ 1 + \frac{\eta}{E} \right] \right] \quad (4.46)$$

From 4.42, it can be determined that

$$\frac{P}{2} = G_1 \gamma_{1L} c_{cr} + G_2 A_2 \left[ \frac{\sinh(2\lambda_2' c_{cr})}{2\lambda_2'} - c_{cr} \right] \quad (4.47)$$

The equations 4.45, 4.46, 4.47, and 4.2 were solved simultaneously by computer to obtain  $A_2$ ,  $c_{cr}$ ,  $P$  and  $k$ . This, therefore, gave the maximum overlap length  $\ell_{cr} = 2c_{cr}$ , for which the strain distribution in the joint at failure was fully described by region 2 in the shear stress-strain curve.

#### 4.2.2.2 Determination of Failure Load when Strain Distribution is Confined to Region 2 of Shear Stress-Strain Curve

In this analysis the overlap length of the specimen is less than  $\ell_{cr}$ , calculated in the previous section. A similar analysis is performed to that for the calculation of  $c_{cr}$ . The following boundary conditions are used in the calculation of the constants in equation 4.36 and in the determination of  $P$  at failure

$$s_2 = 0, \quad \frac{dy}{ds_2} = 0 \quad (4.48)$$



$$s_2 = c, \quad \gamma = \gamma_{2L} \quad (4.49)$$

$$s_2 = c, \quad \frac{d\gamma}{ds_2} = \frac{P(1 - v^2)}{E t \eta} \left[ 1 + \frac{3k}{k_b} \left( 1 + \frac{\eta}{t} \right) \right] \quad (4.50)$$

$$\frac{P}{Z} = \int_{s_2=0}^{s_2=c} (G_1 \gamma_{1L} + G_2 (\gamma - \gamma_{1L})) ds_2 \quad (4.51)$$

Equation 4.48 is a statement of symmetry and gives

$$\gamma = A_2 \cosh(2\lambda_2' s_2) + C_2 \quad (4.52)$$

Equation 4.49 with 4.52 gives

$$\gamma_{2L} = A_2 \cosh(2\lambda_2' c) + C_2 \quad (4.53)$$

From equation 4.50,

$$2\lambda_2' A_2 \sinh(2\lambda_2' c) = \frac{P(1 - v^2)}{E t \eta} \left[ 1 + \frac{3k}{k_b} \left( 1 + \frac{\eta}{t} \right) \right] \quad (4.54)$$

Using equation 4.51, it can be deduced that

$$\frac{P}{Z} = G_1 \gamma_{1L} c + G_2 \left[ \frac{A_2 \sinh(2\lambda_2' c)}{2\lambda_2'} + C_2 c - \gamma_{1L} c \right] \quad (4.55)$$

Solving simultaneously the equations 4.53 to 4.55 together with equation 4.2 by computer, gives the values for  $A_2, C_2, k$  and the failure load/width,  $P$ , for the particular joint configuration.

#### 4.2.3 Material Properties for Calculations

##### 4.2.3.1 Adhesive Material Properties

In Chapter 3, the adhesive shear properties of PEEK were determined using the Thick Adherend Specimen. In order to use this curve in the shear analysis, the curve had to be approximated by an elastic-plastic and bi-elastic representation. In Table 4.1, the values of the various properties required for the analysis are given, and in Figure 4.1 and Figure 4.3, the PEEK shear stress-strain curve is shown with the two approximations. The curve obtained in Chapter 3 with the failure shear stress of  $66.07 \times 10^6 \text{ N/m}^2$  was used in the calculations, to ensure that a conservative estimate of joint strength was made.

The PEEK shear stress-strain curve was put onto computer by manually taking at least forty points from the curve recorded during testing. The area under the curve was then calculated using the Trapezoidal Rule for integration, and the intersection point of the two lines in the approximations calculated using the equations derived in Appendix B.

There was very little information available on the peel properties of PEEK. ICI have produced data sheets, (Reference 28),

which give information on the bulk properties of PEEK tested in tension. A value of  $E_C = 3.6 \times 10^9 \text{ N/m}^2$  was given for a specimen tested in uniaxial tension. In Reference 29, Loss and Kedward give a formula for correcting  $E_C$  obtained in uniaxial tests, for the case of biaxial stress present at the end of a joint. This is given as

$$E_{C,bi} = \frac{E_C}{(1 - \nu_C^2)} \quad (4.56)$$

where  $\nu_C$  is the Poisson's ratio for the adhesive.

This value for  $E_{C,bi}$  can then be corrected using equation 4.21 given by Hart-Smith to allow for the transverse deformations of the adherends under peel. This gives a value for PEEK of  $E_C' = 1.11 \times 10^9 \text{ N/m}^2$

#### 4.2.3.2 Adherend Properties

Data sheets from ICI, (Reference 30), provided some information on the properties of unidirectional APC-2 material. However, for the properties of laminates containing angled plies, Westland Helicopters analysed the laminates on computer using the program CAMEL 4, (Reference 31), based on the theory presented in the Engineering Sciences Data Unit sheets 75002, (Reference 32). The program calculates the pseudo-homogeneous in-plane and flexural stiffnesses and Poisson's ratio of laminated flat plates.

There was no information available regarding the transverse properties of laminates of APC-2. Therefore, in order to give an approximate value for the transverse modulus of the adherend, the Young's modulus for 90° laminates was used. The value for the transverse strength of APC-2 laminates and PEEK film was not known. After discussing with Westlands the results of some of their preliminary transverse tension tests, a conservative value of  $100.0 \times 10^6 \text{ N/m}^2$  was taken, with a maximum value of  $120.0 \times 10^6 \text{ N/m}^2$ . All material properties used in the calculations are given in Table 4.1.

The general lack of information regarding adherend and PEEK adhesive properties, highlights the need for more research and mechanical testing of the material, in order to expand the data base and enable more accurate modelling of structures utilizing these materials.

#### 4.2.4 Failure Curve Plots

The analyses described in the preceding sections were used to produce plots of the failure load/width against overlap length for various joint parameters. These are shown in the following sections, and used to compare the experimental and theoretical results.

The three curves of peel, adhesive shear and adherend failure were superimposed to clearly show the dominant failure mode for any overlap length. The curve giving the lowest value for the load/width for any given overlap length, determines the type of failure mode for

that overlap length. The peel failure mode curve was produced from the solution of equation 4.24. The conservative value of  $100 \times 10^6 \text{ N/m}^2$  was taken as the transverse strength unless otherwise stated. The adhesive shear failure curve was obtained from the elastic-plastic analysis of Section 4.2.1. Equation 4.18 was used to calculate the critical overlap length, and then equations 4.15 to 4.17 together with 4.2 were solved for overlaps greater than this value. The adherend failure curve was produced from the solution of equation 4.29. Since all the laminates tested had  $0^\circ$  fibres in the outermost ply,  $\epsilon_{x,\max}$  was taken equal to the ultimate tensile strain for a unidirectional laminate. All equations were solved for the case of plane stress.

### 4.3 Results and Discussion

#### 4.3.1 Adherend Failure

In Chapter 2, the influence of adherend type on joint strength was examined. It was found that specimens manufactured from laminates containing angled plies, and an overlap length of only 20mm, failed due to adherend failure. Only unidirectional laminates with this overlap length showed failure in the bondline. This demonstrated the importance of being able to predict adherend failure for fusion joints, since bond strength was sufficient to produce failure in the parent material for relatively small overlap lengths.

Figure 4.4 shows a comparison between the experimental results for adherend failure of several laminates, and the theoretically predicted values. Equation 4.29 was solved by computer for the value of  $P$ , the failure load/width, for the case of plane stress. All of the laminates tested contained  $0^\circ$  fibres in the outermost ply, and it was observed that failure of the adherend was restricted to this outermost ply. Failure of the specimen was, therefore, taken to occur when  $\epsilon_{x,\max}$  equalled the ultimate tensile strain for a unidirectional laminate.

For the  $0^\circ$ , 8 ply laminate, adherend failure was observed to occur for an overlap length of 40mm. However, for laminates containing angled plies, an overlap length of 20mm was sufficient to produce failure in the adherend. From Figure 4.4, it can be seen that equation 4.29 consistently underestimated the failure load/width

for all laminate types, with a maximum error of 15% for laminate  $(0,0,+45,-45)_s$ . The best correlation was achieved with the  $(0,+45,-45,0)_s$  laminate, the lay-up which most closely approximates isotropic material. A degree of error may have been introduced from the calculation of  $E$  and  $E_f$  from the Westlands program, but this could only be checked by comparing the predicted and actual values of these properties for the individual laminates. However, the fact that good correlation was observed when the laminate properties were calculated and not measured must be considered a bonus.

For practical purposes, the agreement between the experimental and theoretical values was very good, with failure being predicted within 10% of the measured value for all but one of the laminates tested.

#### 4.3.2 Influence of Overlap Length on Joint Strength

In Section 4.2, all three types of failure mode were discussed, and the analysis for each presented. It was assumed that each type of failure was independent of the others, and that failure occurred when a critical stress or strain was achieved in the joint or adherend. In reality, it is probable that a combination of stresses will result in failure of the joint, but to date no failure criterion taking into account all the stresses has been demonstrated to be particularly successful. One of the most important joint parameters influencing joint strength is overlap length. Often in a practical design, the adherend thickness and bondline thickness will be determined by other design parameters and processing limitations,

which leaves joint overlap length as the only variable to control joint strength. The influence of overlap length on joint strength, and consequently failure mode, must, therefore, be accurately known.

The analyses of Section 4.2 can be used to look at the likely type of failure mode for any particular joint parameter. Figures 4.5 and 4.6 show the three curves for the three failure modes superimposed for laminate types 1 and 2 respectively, and show the failure load/width  $P$  as a function of overlap length  $l$ . It is obvious that the curve giving the lowest value for  $P$  for any given overlap length, will determine the type of failure mode likely to occur for that particular joint geometry.

From Figure 4.5, it can be seen that for unidirectional material, and for very short overlap lengths, the failure mode is likely to be shear failure of the adhesive. For intermediate overlap lengths, the peel stresses become dominant, giving way to shear failure of the adhesive at slightly higher overlap lengths. The joint strength is ultimately limited by the strength of the adherend material, and this occurs for very long overlap lengths.

It can be seen from Figure 4.5, that as the overlap length increases, the peel stresses are alleviated, giving a potentially higher load/width at failure. The shear failure curve for unidirectional material is found to be a straight line over a wide range of overlap lengths. This is a result of the stress distribution at failure being confined to the plastic region of the elastic-plastic approximation, and all points on this curve have the



same average shear stress at failure. The adherend failure curve shows a levelling of the load/width at failure, and this is reflected in a drop in the average shear stress at failure for all the points on the curve. The correlation between the experimental and theoretical values was within 10% over the range of overlap lengths tested.

Figures 4.6(a) and 4.6(b) show the correlation between the theoretical and experimental values for the laminate  $(0,0,+45,-45)_s$ . In Figure 4.6(a), it can be seen that although the experimental points lie on the adhesive shear failure curve for small overlap lengths, the peel analysis predicts a much lower strength than observed. It is felt that this is a result of not knowing accurately the adhesive peel properties of PEEK. Until these are measured, no comment can be made on the likely accuracy of the peel analysis itself.

Figure 4.6(a) was produced using the conservative figure of  $100.0 \times 10^6 \text{ N/m}^2$  for the ultimate transverse strength of the adherend or PEEK film. Figure 4.6(b), shows the results for the peel stress analysis using a value of  $120.0 \times 10^6 \text{ N/m}^2$  for the transverse strength. A much better correlation between theory and experiment was achieved, since the loads required to induce peel failure had been increased.

The adhesive shear failure curve in Figure 4.6 shows two different parts to the curve. The initial straight line is for joint geometries which are fully plastic at failure, as previously described. In the second part, a curve of reduced slope is seen, and

this is for joint geometries which have a combination of both plastic and elastic adhesive deformation in the joint at failure.

For the  $(0,0,+45,-45)_s$  laminate, the correlation between theory and experiment was excellent for overlap lengths where adhesive shear failure took place. The prediction of adherend failure was within 15% of actual measured value, with the failure load consistently underestimated. The prediction of peel failure was generally inaccurate due to the lack of information regarding peel material properties, although correlation was fair when reasonable values for these material properties were used.

Overall, correlation between theory and experiment was very good and generally within 15% over a range of overlap lengths and for different laminate types. The importance of being able to predict shear failure was shown, since this effectively gives the ultimate average shear stress which can be possibly achieved by the joint. The effect of the other two failure modes, namely peel and adherend failure, is to reduce the achievable joint strength from this potential ultimate shear strength.

#### 4.3.3 Bi-Elastic Analysis

As explained previously, it was of interest to examine the effect of better modelling of the shape of the shear stress-strain curve on the predicted joint strength. Figure 4.7 shows the comparison between the curve for elastic-plastic modelling and bi-elastic modelling, for a range of laminate types. For the bi-elastic

modelling, only the joint overlaps where the stress distribution was confined to region 2 of the shear stress-strain curve were considered. From Section 4.2.2, equations 4.45 to 4.47 together with 4.2, were solved to determine the critical overlap for the bi-elastic model. Equations 4.53 to 4.55 together with 4.2 were then solved to give the value of  $P$  for various values of  $l$  below the critical overlap length. Adherend failure of the laminate removes the necessity to look at overlaps outside this range.

It is immediately obvious that for all the laminate types examined, there is very little difference between the two curves. For example, the worst difference for a 20mm overlap was for the  $(0,0,+45,-45)_s$  laminate, with a difference of only 2.4%. This demonstrates that it is probably not worth the extra computing time necessary to model the joint using a bi-elastic approximation.

Figure 4.8 shows the variation of shear strain and stress over half the overlap length, for a 20mm overlap specimen of the three types of laminate at failure. The strain distribution was plotted by using equation 4.52 with the values of the constants  $A_2$  and  $C_2$  solved for a 20mm overlap specimen at failure. Equation 4.33 was then used to obtain the stress distribution for the bi-elastic model. Although there is a significant variation of shear strain in the joint, this equates to uniform shear stress for the elastic-plastic analysis, and to only a slightly varying shear stress for the bi-elastic analysis.

It is concluded that for this particular adhesive shear stress-strain curve, bi-elastic modelling of the curve is

unnecessary, and that elastic-plastic modelling is quite sufficient.

#### 4.3.4 Peel Stress Distribution

In Chapter 2, examination of the failure surfaces of unidirectional specimens by SEM revealed that at the ends of the joint, the matrix of the adherend was pulled up between the fibres. It was concluded that this was a consequence of high normal stresses in this region of the joint prior to failure. Figure 4.9 shows a plot of the peel stresses present in a 20.3mm overlap unidirectional specimen at failure. This was obtained using equation 4.22. It is significant that there is an extremely sharp rise in peel stresses within the last 1mm of the overlap. This observation supports the conclusions in Chapter 2, and highlights the importance of considering these stresses in the joint, due to their very concentrated nature.

#### 4.3.5 Influence of Bondline Thickness on Joint Strength

In Chapter 2, an investigation was made of the effect of bondline thickness on resulting joint strength. It was found that increasing bondline thickness resulted in an increase in observed joint strength. Figure 4.10 shows the effect of bondline thickness on the predicted joint strength. It can be seen that the effect of increasing the bondline thickness is a reduction of the peel stresses in the joint, thereby reducing the likelihood of this failure mode. The influence of bondline thickness on the peel stresses is quite significant and is a result of the  $(E_c't / E_n)$  parameter in equation

The influence of increasing bondline thickness on the shear adhesive failure is to increase the range of overlap lengths for which failure will occur when the joint is still fully plastic. Increasing bondline thickness, therefore, produces a more uniform strain distribution in the joint.

The effect of bondline thickness on adherend failure is very small. Increasing the bondline thickness, only reduces the failure load/width for adherend failure by a few percent.

These results explain the observations made in Chapter 2. The strength of fusion joints produced without introducing excess PEEK film into the joint were disappointing. From the results discussed above, it can be easily concluded that this was a result of the thin bondline introducing very high peel stresses into the joint at relatively low load levels. The effect of increasing the bondline thickness, by introducing a PEEK film into the joint, was to reduce these peel stresses, resulting in a much higher load/width at failure. Increasing bondline thickness increases the likelihood of failure due to shear failure of the PEEK film.

These results may also explain an observation made by the engineers at Westland Helicopters, that for fusion joints produced with 90° fibres in the outermost ply, a stronger joint was obtained, as compared to those with 0° fibres in the outermost ply. Although similar tests were not conducted in this research work, the

observations made on the influence of bondline thickness on the peel stresses present in a joint, may explain this result. 90° fibres in the outermost ply of any adherend would have the effect of increasing the thickness of the bondline, although there would be an effective change in the properties of the bondline within this ply. This would have had the effect of reducing the peel stresses present in the joint, thereby increasing the observed joint strength if failure had been a result of peel failure. It must be emphasised, however, that the joints tested by Westlands were produced by a practical process, which produced a joint strength significantly less than that observed in Chapter 2. The practical process would have introduced a degree of inefficiency into the joint, as more fully discussed in Chapter 5. However, the explanation given above would still explain the results from the testing program, if peel had been the dominant mode of failure.

#### 4.3.6 Influence of Adherend Thickness on Joint Strength

Figure 4.11 demonstrates the effect of adherend thickness on joint strength. It is immediately obvious that the mode of failure most influenced by changing the adherend thickness, and, therefore, of most concern, is peel failure. Increasing the adherend thickness results in an increase in the peeling stresses in the joint.

The effect of an increase in adherend thickness on shear failure of the adhesive, is to extend the range of overlap lengths for which the joint is fully plastic at failure. The effect on adherend failure, is, as would be expected, to increase the load carrying

potential of the adherend. Undoubtedly, for thick adherends, the most dominant failure mode will be peel failure over a wide range of overlap lengths.

#### 4.4 Conclusions

The following conclusions were drawn from the work:

- (1) Good correlation between theory and experiment was observed, with the difference usually within 15%.
- (2) Good correlation was achieved for shear failure of the adhesive, with observed joint strengths approaching the ultimate shear strength of the adhesive, ( $66.07 \times 10^6 \text{N/m}^2$ ), within the appropriate overlap length ranges.
- (3) The adherend failure analysis developed, predicted the failure loads of laminates containing unidirectional fibres in the outermost ply within 15%, (on average 10%), of observed strength.
- (4) There was not a great deal of confidence expressed in the accuracy of the prediction of peel failure. This was considered mainly due to the lack of information regarding the peel and transverse properties of PEEK and APC-2 material.
- (5) The very small difference found between the prediction of shear failure using an elastic-plastic approximation and bi-elastic approximation of the shear stress-strain curve, did not merit the additional computation necessary in the solution of the mathematically more complex bi-elastic



analysis.

(6) It was shown that the peel stresses were very concentrated at the ends of the joint overlap. This was found to be in agreement with the conclusions of chapter 2, where it was felt that the presence of high normal stresses in the bondline, were responsible for the observed failure surface.

(7) An increased bondline thickness was found to alleviate the peel stresses within the joint.

(8) Increasing the adherend thickness was found to significantly aggravate the peel stresses in the bondline, giving an associated reduction in the predicted joint strength.

## CHAPTER 5

### SPOT WELDING OF APC-2

#### 5.1 Introduction

Although the feasibility of fusion bonding was proved in Chapter 2, the development of practical techniques is required before the joint can be successfully and economically incorporated into a design. Much undocumented work is being carried out into the development of such techniques, since the commercial rewards of a developed and successful technique would be quite considerable. Among the techniques being looked at are induction welding, ultrasonic welding and resistance welding.

Stein, et al., (References 33-35), published work describing the development of an induction welding technique. A toroid induction heater was used to heat a perforated metallic foil susceptor in the bondline. This enabled heating to be focussed in the bondline. The shear strengths obtained for this technique were given as  $48\text{N/mm}^2$  for an overlap length of 25.4mm using quasi-isotropic APC-2 adherends. From the results shown in Figure 4.4, it can be seen that for this laminate lay-up and overlap length, failure would almost certainly be due to adherend failure in the outermost plies unless very thick adherends were used. It is difficult to assess the efficiency of this technique by comparison with the joint strengths obtained in Chapter 2 without all the information regarding the specimen geometry

used.

During the development of ultrasonic and resistance welding, the control of temperature has been found to be the most important processing parameter. This is in agreement with the observations of Chapter 2, where joint strength was found to be very dependent on processing temperature. In ultrasonic welding, the adherends are vibrated together in order to produce heat in the bondline, and it can be appreciated that controlling the bondline temperature would be extremely difficult. With resistance welding, metal wire is placed in the bondline, and heating is achieved by passing an electric current through the wires. However, again control of bondline temperature is found to be extremely difficult. Although there is no published work regarding the strengths of joints obtained with ultrasonic or resistance welding, it is thought that strengths do not exceed  $40\text{N/mm}^2$ .

Another concern with many of the above techniques, is the presence of metal wires and steel foils in the joint after welding has taken place. There is concern over the danger of metal corrosion degrading the joint, and of the possibility of lightning strike on an aircraft resulting in unacceptably high currents passing through the metal inserts. Although it has been tried to use the carbon fibres of the adherends to replace the metal inserts, difficulty in maintaining laminate quality has been experienced.

It was felt that it may be possible to overcome some of the problems discussed above, by the development of a direct heating

technique for producing "spot welds" in APC-2. The techniques described above have been developed in an attempt to concentrate heating in the bondline. This would have the advantage of restricting the melting of the adherends to only the first few layers of the adherend. However, as has been shown, there are significant problems in controlling the bonding temperature. A direct heating technique would consist of heating the bondline through the thickness of the composite using an easily controlled temperature source. This report describes the development of such a technique, and compares the joint strength obtained with the results of Chapter 2. The effect of bonded area shape on joint strength is also examined, by using the experimental technique of Chapter 2 to produce round welds in APC-2 specimens.

## 5.2 Experiment

Two types of specimen were manufactured and tested in the following work. In Sections 5.2.1 to 5.2.3, the work described is concerned with the specimens produced by spot welding. In Section 5.2.4, the work is concerned with specimens produced by using the experimental arrangement described in Chapter 2.

### 5.2.1 Spot Welding Equipment

In order to provide through-the-thickness heating of the composite, a heated copper pad was used. This was incorporated into a hot tool mounted on a rotatable frame. Also mounted on this frame was an unheated copper tool, which provided fast cooling of the welded area after bonding. This rotatable frame allowed either tool to be brought quickly and accurately into position. The whole assembly was mounted on a commercially available drill stand, which provided vertical movement of the welding tools.

Figure 5.1 shows the general arrangement of the equipment. The consolidation pressure was obtained through weights applied to the handle of the drill stand. The specimen to be bonded was placed in a metal picture frame mounted on an insulating block. Careful control of the hot tool temperature was obtained through a digital temperature controller, and the power output was controlled through a "burst fire" power controller.

Two hot tools, or spot welders, were developed. The first was

developed round a 100 Watt soldering iron heating element, and consisted of a copper core with a welding head 15mm square (SW1). For reasons discussed later, however, this was replaced with a second spot welder with a 200 Watt heating element and an 11mm diameter welding head (SW2). The details of this spot welder are shown in Figure 5.2. Figure 5.3(a) shows a photograph of the experimental arrangement, and Figure 5.3(b) a photograph of SW2 heating a specimen.

#### 5.2.2 Specimen Preparation for Spot Welding

The specimens were produced from pre-fabricated unidirectional 8 ply laminates of APC-2. Vacuum bag consolidated laminates were preferred because of their superior fibre orientation. Strips of composite were cut from the parent laminate and then reduced in width so that a good fit between composite and picture frame was achieved. The only surface preparation made prior to bonding was degreasing with acetone.

In all specimens a piece of 0.1mm thick Stabar film was included in the bondline. A piece of 0.1mm thick stainless steel was used between the upper surface of the top adherend and the copper tool, in order to give a good surface finish. Figure 5.4 shows the specimen lay-up.

Tests were conducted in order to obtain the temperature distribution and temperature-time curves of the specimens during processing. Thermocouples were, therefore, imbedded in the composite surface. Channels were prepared in the composite using a small power

tool, and the thermocouples bonded into place.

### 5.2.3 Spot Welding Heating Cycle

Two types of heating cycle were examined for spot welding.

#### 5.2.3.1 Single Weld

In this process, the tool is preheated to a desired temperature and then brought down on the specimen. Heating of the specimen then takes place under consolidation pressure. After heating for a given time, the hot tool is removed and the cold tool brought into place. Cooling of the specimen takes place under the same consolidation pressure. It is essential that a quick change is made between hot and cold tool (normally less than ten seconds).

#### 5.2.3.2 Array Weld

This type of weld is made by making a series of small single welds in succession. The hot tool is applied for a short time at several points on the overlap before cooling takes place with the cold tool. Again consolidation pressure is applied during the cycle, and time between each change is kept to a minimum.

The particular array chosen for this work was a series of five spot welds as shown in Figure 5.5. The 200 Watt spot welder was used in this type of weld. Initially a spot weld was made at position 1 for two minutes, and then moved to position 2 for two minutes. This

continued until all five areas had been heated for two minutes. Finally position 1 was heated for a further two minutes. This was felt necessary since the adherends tended to spring apart as the welder was moved from position 1 to position 2, and it also ensured that the area was heated to the required bonding temperature. Cooling finally took place with the cold tool for two minutes. The total processing time was 15 minutes with the tool preheated to 550°C and the consolidation pressure between 0.28 and 0.34MPa (40 to 50psi). The power output from the tool was set at 200 Watts, which enabled the tool to be kept between 545 and 550°C during the process.

#### 5.2.4 Round Welds

It was recognised that spot welding would produce bonds in the composite which were not rectangular in shape, and concern was expressed as to the influence of welded area shape on the joint strength. In order to obtain information regarding this, a technique was developed to manufacture round welds in APC-2 using the experimental arrangement described in Chapter 2.

8 ply unidirectional APC-2 laminates were used as the adherends, and the surface was prepared by degreasing with acetone. 0.1mm thick 450 Grade film was used to form a 15mm diameter round weld between two adherends, with a specimen overlap length of 20mm. This film type was used in preference to Stabar film because of its higher viscosity and, therefore, less tendency to run during processing. The round piece of PEEK was tacked into place with a soldering iron, and then two layers of Kapton film were introduced around the PEEK



film to ensure bonding of the two adherends only at the round weld. Although the layers of Kapton stuck to the adherends, no transfer of load could take place between the two layers, thus ensuring load was only carried by the round weld.

#### 5.2.5 Specimen Testing

All the specimens were tested in tension on a 250kN Instron tensile testing machine. A plot of load against deformation for one of the spot welded specimens is shown in Figure 5.6. This was obtained by placing a displacement transducer across the joint.

Microscopic examination of the spot welded specimen failure surface and cross-section was undertaken, and the results are discussed later.

### 5.3 Results and Discussion

In the following work, all of the discussion is concerned with specimens produced by spot welding except for Section 5.3.2.3, where the specimens were produced using the experimental arrangement described in Chapter 2.

#### 5.3.1 Specimen Temperatures During Spot Welding

The following discussion is based on work conducted using thermocouples imbedded in the surface of the composite. The temperatures quoted are representative of the majority of the specimens tested. Occasionally, however, it was found that the temperatures measured were slightly different from those given below. The difference was generally less than 7% and was probably due to the difficulty in ensuring that the thermocouples were buried to the same depth in each specimen.

##### 5.3.1.1 Single Weld

Tests were undertaken to obtain the temperature distribution and temperature-time curves for the specimens during welding. In Chapter 2 it was found that joint strength was very sensitive to processing temperature. Heating a joint to 340°C produced little or no bonding. At 360°C some bonding did take place, but the results were very scattered. By increasing the processing temperature to 380°C, however, consistently strong joints were obtained. It was felt, therefore, that if temperatures between 370 and 380°C could be

achieved in this process, strong reliable joints would be produced. In Reference 35, Stein, et al., also found that it was only possible to bond APC-2 with PEEK when processing temperatures were above 371°C.

It was found that tool preheat temperature and power output were the most important parameters for achieving the required temperatures. Figure 5.7 shows the temperature-time curve for a specimen heated with the 100 Watt square pad welder (SW1). The tool was preheated to 550°C before being applied to the specimen. It can be seen that the top temperature did not rise above 430°C, and that the temperature at the bondline reached 367°C within ten minutes. It was also observed that the hot tool never managed to recover the set temperature of 550°C during processing. Thermocouples placed at 5mm each side of the centre thermocouple also showed that there was a non-uniform temperature distribution over this area.

In view of these results it was decided that an improved tool design would be to increase the tool power output and reduce the area of the heated pad. It was hoped that this would allow the tool to achieve the set temperature throughout the process, and also enable a more uniform temperature distribution to be achieved in the bondline. The reduced pad area would also allow the tool to be moved to form an array weld within the 20x16mm overlap area of the standard specimen.

Figure 5.8 shows the temperature-time curve for a specimen heated with the 200 Watt 11mm diameter spot welder. Again it can be seen that the maximum temperature on the top surface is 432°C. Here,

however, this is held throughout the process; unlike in Figure 5.7, where the temperature on the top adherend drops from an initial value of around 430°C, down to 416°C. In Figure 5.8 it can also be seen that the temperature in the bondline rises to 373°C after ten minutes, which is approaching the optimum temperature of 380°C. The temperature distribution for this tool was not significantly better than for the SWI welder, with a 20°C to 30°C drop in temperature being observed in the bondline 5mm from the centre of the overlap.

#### 5.3.1.2 Array Weld

Joint strength not only depends on reaching the required bonding temperature, but also depends on the area of the bond which achieves this bonding temperature. Although the above results show that the bonding temperature was achieved in the bondline at the centre of the overlap, the strength of specimens produced using this "single weld" approach were disappointing. This was a consequence of the non-uniform temperature distribution in the specimen.

Since heating of the composite in the surrounding area takes place during processing, it was felt that it may be possible to increase the area bonded by moving the weld head to various positions on the overlap. It was found that the preheating of an area prior to the application of the hot tool resulted in the bonding temperature being reached very quickly. In a short time, therefore, several areas of the overlap could be heated, resulting in a larger bonded area and a stronger joint as compared to a joint produced from a single weld processed for the same time.

Figure 5.9 demonstrates this result. Area 2 is heated to 320°C while the heating of area 1 takes place. When the tool is moved to position 2, a temperature of 387°C is reached within one minute, with a final temperature of 390°C being reached at the end of the two minute period.

A similar result is obtained for the heating of the centre position of the array. Although during the first weld the central area reached a temperature of only 362°C, on reapplication of the hot tool for the final weld of the array, a temperature of between 370 and 380°C was achieved.

#### 5.3.1.3 Adherend Temperature

With this type of welding technique it is necessary to heat the top adherend to a higher temperature than the required temperature at the bondline. It was generally found that the top temperature had to be about 60°C above the required temperature of the bondline. The maximum temperature recorded for the adherend during processing was a value of 458°C. This was obtained during reapplication of the hot tool to the central area during the array weld. It may be possible to reduce this by a suitable change in the order of heating or by a reduction of tool temperature.

For the moment very little information is available regarding the effect on APC of temperatures above the normal processing level. Tests at ICI have been conducted on APC held at a temperature of

420°C for two hours. Some degradation of the matrix took place, but this was reduced considerably when the time of heating was reduced to one hour. Since the average maximum temperature experienced by the composite in this process is around 430°C, and the fact that it is experienced for only a few minutes at most, it is unlikely that much damage, if any, takes place in the composite. However, this would certainly be an area for further work.

#### 5.3.1.4 Specimen Cooling

In order to achieve optimum crystallinity in PEEK and APC, it is essential that the cooling rate is between 10°C/min and 700°C/min. The introduction of the cold copper tool facilitated rapid cooling. During the process this was applied for 2 minutes. However after only one minute, the temperature in both the bondline and the top adherend was below 100°C. This gives an average cooling rate over this period of between 270°C/min and 360°C/min.

#### 5.3.2 Strength Tests

##### 5.3.2.1 Specimens Produced Using SWI

From Chapter 2 it was noted that joints processed at 360°C produced random joint strengths, and this is reflected in the results obtained using SWI. Three specimens were produced under the same conditions (8 minutes heating, 34psi consolidation pressure). The strengths of these joints were measured at 0.9, 2.0 and 5.6kN. As can be seen, a very random strength was obtained. Although bonding

temperatures may have been achieved at the centre of the weld, lower temperatures away from the centre would produce this result.

#### 5.3.2.2 Specimens Produced Using SW2

Figure 5.10 shows the failure loads for joints produced using SW2. The very large improvement in strength achieved by using the spot welder to produce an array weld over that for a single weld processed for the same time is immediately obvious. The average value for the array weld in Figure 5.10 is 10.9kN compared to 1.9kN for a single weld heated for the same time (twelve minutes). This represents a five fold improvement. Figure 5.10 also shows that the average failure load for a two minute weld is 0.98kN. Therefore, a joint produced using 5 single welds could be expected to carry 4.9kN. The array weld with 5 welded areas, however, produced a joint strength at least twice as great. It is also seen that specimens heated for 12 minutes did not produce strengths very much stronger than those heated for only two minutes. These observations suggest that there is probably not only an optimum heating time for each weld in an array, but also an optimum spacing of these welds.

The importance of weld spacing is demonstrated in Figure 5.10 and Table 5.1. Although Figure 5.10 shows that there is considerable scatter in the failure loads of the array welds, Table 5.1 shows that this corresponds to a large variation in the bonded areas of these specimens. This was a result of the weld head being positioned by hand during processing. Each specimen, therefore, was not produced with the same weld spacing, which in turn influenced the area bonded.

Perhaps the most important observation which can be made from these results, concerns the average shear stress at failure. In Chapter 2 it was found that the shear stress at failure for specimens bonded with 0.1mm thick Stabar film was  $64.5\text{N/mm}^2$ . From Table 5.1 it can be seen that the average shear stress at failure for the array welds was  $60\text{N/mm}^2$ , which is very close to the standard set in Chapter 2. It is important to note that this value is independent of bonded area, which again agrees with the results in Chapter 2. This suggests that with the correct weld spacing, this process would be capable of producing large bonded areas with high average shear stresses at failure. This would be reflected in a very high failure load.

#### 5.3.2.3 Round Welds

The specimens produced using the experimental arrangement described in Chapter 2, with a 15mm diameter round weld in an overlap of 20mm, produced an average joint strength of  $59\text{N/mm}^2$ . In Chapter 2, the specimens produced with a square weld of  $15\text{mm} \times 15\text{mm}$ , produced an average shear strength of  $61\text{N/mm}^2$ . It is, therefore, possible that a round weld will show a slight reduction in strength, but this reduction is extremely small and could probably be explained by taking account of experimental error. The influence of weld area shape on joint strength, therefore, appears very small.



### 5.3.3 Consolidation Pressure During Spot Welding

The consolidation pressure is important in determining not only the joint strength, but also the surface finish of the top adherend. A sufficient pressure must be used in order to overcome any curvature of the laminate and ensure good contact between components. However, too high a pressure must be avoided since this causes excessive fibre movement to take place. In this work a pressure was applied which provided a compromise.

Unfortunately, the rig developed did not allow very accurate measurement of the consolidation pressure to be made. Therefore, the effect of consolidation pressure on joint strength could not be accurately measured. The experience of the operator when preparing this work, however, suggests that the higher the consolidation pressure the stronger the joint.

### 5.3.4 Surface Finish of Spot Welded Specimens

Generally the surface finish on the top adherend was not too bad. The single weld specimens showed a very good surface finish with very little fibre movement. Since the whole of the top adherend did not melt in this process, a good deal of support was provided to the fibres in the melt region from the unheated areas.

In the case of the array weld, the majority of the top surface melted, with an associated increase in fibre movement. This was still not excessive, however, with the picture frame simulating the

support which would be provided when welding in a wide laminate.

The PEEK on the top adherend did not show any significant degradation after processing. However, future work could look at this in more detail, since a visual examination only gives an indication of the condition of the PEEK after processing.

During the array welding, the PEEK tended to flow from the area of the weld. This left the laminate surface with a matt finish compared to the glossy finish of the parent laminate. This may, however, be prevented by introducing a clamping frame to contain the PEEK within the welded area during processing. Figure 5.11 shows a photograph of the surface of the top adherend of a specimen after array welding.

#### 5.3.5 Failure Surface Examination

Figure 5.12 shows photographs of the failure surface of an array welded specimen. The diagram in this figure highlights the three areas which were distinguished on all specimens.

Figure 5.12(a) shows the failure surface of the top adherend. The central area, (Area 1 in Figure 5.12(c)), was very black in appearance, and this was the area used in the calculation of the average shear stress. This area corresponds to a matt black area on the bottom adherend, (see Figure 5.12(b)), and was considered as the main bonded area.

Bordering this area was a piece of PEEK film which had not fully melted, (Area 2 in Figure 5.12(c)), and had only bonded to the top adherend. There was no corresponding area observed on the bottom adherend, and this region was regarded as contributing little strength to the joint. During initial loading of the specimen, creaking of the joint was heard, and it was believed that this was the breaking of any weak bonding which had taken place in Area 2.

Area 3 in Figure 5.12(c) was the area of the film which had only softened during processing. No bonding took place in this region. Before processing, the Stabar film was transparent. After processing, however, the film in this region changed to a light brown colour and was opaque. This is believed to be due to the cooling rate of the film. During manufacture of the Stabar film, very fast cooling is achieved, and this produces the transparent appearance. However, under the slower cooling rate of the welding process, this transforms into an opaque appearance.

#### 5.3.6 Microscopic examination

An array weld was sectioned through the centre of the overlap and at 3mm from the end of the top adherend, in order to examine the quality of the bondline achieved.

In Chapter 2, where vacuum consolidation was used, excellent uniformity of bondline combined with good wetting of the fibres was achieved. Figure 5.13(a) shows the cross-section through the middle of the array weld. It is seen here that the bondline varied in

thickness. Measurement of the bondline thickness showed that it varied between 0.13mm and 0.05mm over the specimen width. However, the use of a higher viscosity film would have probably enabled better control of the bondline to be achieved. Overall there was good wetting of the fibres, with very few voids present in the bondline.

In Figure 5.13(b) the cross-section of the joint 3mm from the end of the top adherend is shown. In the bondline it is immediately obvious that random bonding has been achieved, with large voids present. This represents the limit of the bonded area. Most significant from this section of the joint, however, is the high void content of the upper adherend. This must have been a result of the plies separating while molten. This would happen when the hot tool was moved to another position within the array. Again the introduction of a clamping frame would help to prevent this occurring, by supplying a consolidation pressure around the boundary of the weld.

#### 5.3.7 Processing Time

There is no doubt that the weakness of this spot welding technique in comparison to other fusion bonding techniques being developed, is the length of time taken to process a joint. However, it has been shown in this work that by using the hot tool to form an array weld instead of a single weld, the efficiency of the technique can be increased many times. There is no reason to doubt, therefore, that with refinement, this technique will be able to produce efficient high strength joints in shorter cycling times than quoted

here.

The length of processing time, however, may restrict this technique to use on an automatic rig. Here, several hot tools could be used simultaneously to produce panels bonded by several array welds. These array welds could overlap to produce a continuous weld. The relative cheapness of the tool and ease of control and operation, would be an advantage if used in this manner. Large panels could, therefore, be bonded in one quick and simple operation.

#### 5.3.8 Future Developments

The work presented here only demonstrates the feasibility of using a direct heating method to produce fusion bonds. Considerable development and refinement is required before the process could be accepted as an alternative means of producing reliable bonds in APC-2.

Future work should include:

- the development of larger and more efficient heated tools to produce larger bonded areas in shorter times.
- the development of a clamping frame to reduce both fibre and PEEK movement and prevent ply separation during processing.
- the optimization of weld spacing and heating time for array welds.

-the extension of the technique to bonding of large structures.

#### 5.4 Conclusions

The use of direct heating to produce fusion bonds in APC-2 has been demonstrated. A welding technique has been developed which produces strong joints which compare very closely with those produced in Chapter 2. The following conclusions were drawn from the investigation:

(1) Tool preheat temperature and power output were important parameters in achieving the required bonding temperatures.

A 200 Watt copper tool, preheated to 550°C, was found to achieve these temperatures in a reasonable time.

(2) Single weld processing resulted in bonding temperatures being achieved after ten minutes. Array welding, however, reduced this time to two minutes per weld, and produced much larger bonded areas than those for single welds.

(3) Top adherend temperatures were around 430°C during processing, and this was considered acceptable.

(4) Array welding produced a five fold improvement in joint strength over single welding for the same time. The results suggested that there is probably not only an optimum heating time for each spot weld in an array, but also an optimum spacing of these welds.

(5) The average shear stress at failure for the array welds

was  $60\text{N/mm}^2$ . This compares very closely with the value of  $64.5\text{N/mm}^2$  measured in Chapter 2.

(6) Using the high temperature oven and vacuum bag technique of Chapter 2, it was shown that weld shape has very little influence on average shear stress at failure.

(7) The surface finish of the top adherend was better than anticipated. It was felt that the introduction of a clamping frame surrounding the weld site would help to reduce both fibre and PEEK movement during processing.

(8) Failure surface examination of the specimens revealed three distinct areas. These included an area where full bonding was achieved, where partial bonding was achieved and a region where no bonding of the film took place.

(9) Microscopic examination of the joint cross-section at the middle of the joint revealed excellent wetting of the fibres with few voids present. At the ends of the overlap, however, an increase in the void content of the upper adherend was discovered. It was concluded that this was due to ply separation as the hot tool was moved during the process. The introduction of a clamping frame would probably help to alleviate this problem.



## CHAPTER 6

### CONCLUSIONS

A high temperature oven in combination with a vacuum bag was used to prove the feasibility of fusion bonding. This produced a high standard of joint strength, and provided specimens for the investigation and identification of the important parameters influencing joint strength.

It was shown that joint strength was very sensitive to processing temperature. Processing at 380°C was found to give the strongest joints with very little scatter of results. Simple degreasing of the surfaces with acetone was found to be a satisfactory method of surface preparation prior to bonding. The use of trichloroethane for surface degreasing is not recommended, since the tendency for PEEK to absorb chlorinated solvents produced joints with a great deal of voids and with associated reduced strengths.

The measured shear stress-strain curve for PEEK was very non-linear, with a shear stress at failure of between 66 and 72N/mm<sup>2</sup>, and an ultimate shear strain of 1.9 to 2.1. In the development of the shear specimen, the properties of the PEEK film used in the bondline was found to be important in the control of bondline thickness. The higher viscosity PEEK film, 450 Grade, produced a void free and more uniform bondline compared to Stabar film. However, Stabar film demonstrated better adhesion to the aluminium

adherends of the thick adherend specimen.

The theoretical work of Hart-Smith was used to compare experimental and theoretical results. Good correlation was observed, and all results were predicted within 15%.

Hart-Smith's model for adherend failure was modified to consider the strain distribution in the adherends rather than the stress distribution. The correlation between the measured and predicted results was within 15%, (on average 10%), for laminates containing 0° fibres in the outermost ply. It was found that fusion bonding produced such strong joints that laminates containing angled plies failed from adherend failure with only a 20mm overlap length.

The measured shear stress-strain curve for PEEK was used to compare Hart-Smith's elastic-plastic analysis with a bi-elastic analysis developed for single-lap joints. This provided the opportunity of investigating the effect of more accurate modelling of the shape of the shear stress-strain curve. It was shown that the very small difference between the two results did not merit the additional computation required for the solution of the mathematically more complex bi-elastic analysis. It was shown that the measured joint strengths approached the ultimate shear strength of the PEEK within the appropriate overlap length ranges where adhesive shear failure dominated.

There was not a great deal of confidence expressed in the accuracy of the prediction of peel failure. This was considered

mainly due to the lack of information regarding the peel and transverse properties of PEEK and APC-2 material. Future work should include measurement of these properties to enable modelling of these stresses, since they play such an important role in single-lap joint behaviour.

Using the adherend, shear (elastic-plastic) and peel failure analyses, plots were produced of the failure load/width versus overlap length for various joint parameters. This provided an opportunity to investigate the influence of these parameters on the likely failure mode for various overlap lengths. Correlation between predicted and observed failure was good, with shear or peel failure dominant for small overlap lengths, and adherend failure limiting the joint strength for long overlaps.

It was shown that increasing bondline thickness alleviates the peel stresses in a joint, and this agreed with the experimental observation that a thicker bondline produced a stronger joint. This result suggests that all joints should be produced with a film of PEEK introduced into the bondline. Joints produced utilizing the surface layer of PEEK in the adherend for the bondline, will fail at reduced loads due to the presence of high peel stresses. It was similarly shown from the theoretical analysis, that increasing adherend thickness aggravates the peel stresses in the bondline, giving an associated reduction in the predicted joint strength.

It was demonstrated that a practical technique employing direct heating of the bondline through the thickness of the composite, was

capable of producing accurate control of processing temperature and a joint strength approaching the shear strength of PEEK. It was found that tool preheat temperature and power output were important parameters in achieving the required bonding temperature.

It was found more efficient to use the spot welding technique to produce several welds, to form an array of welds, rather than single welds. The effect of weld shape was also investigated, and it was concluded that this had very little influence on joint strength.

In view of the influence of bondline thickness on joint strength, practical techniques may benefit from the use of higher viscosity PEEK films, since this will enable easier control of bondline thickness to be achieved.

## REFERENCES

- (1) Hart-Smith, L.J., "Mechanically Fastened Joints for Advanced Composites - Phenomenological Considerations and Simple Analysis," *Fibrous Composites in Structural Design*, Plenum Press, New York, 1980, pp. 543-574.
- (2) Oplinger, D.W., "On the Structural Behaviour of Mechanically Fastened Joints in Composite Structures," *Fibrous Composites in Structural Design*, Plenum Press, New York, 1980, pp. 575-602.
- (3) Collings, T.A., "The Strength of Bolted Joints in Multi-Directional CFRP Laminates," *Composites*, Jan. 1977, pp. 43-56.
- (4) Vinson, J.R., Sierakowski, R.L., "Joining of Composite Material Structures," *The Behaviour of Structures Composed of Composite Materials*, Martinus Nijhoff Publishers, 1986, Chapter 8.
- (5) Hillier, W.D., "Fibre Reinforced Thermoplastic Fabrication Technology for Helicopter Primary Structure," Paper presented at RAeS Composite Workshop, Yeovil, May 1987.
- (6) Duthie, A.C., "Fibre Reinforced Thermoplastics in Helicopter Primary Structure," Paper presented at RAeS Composite Workshop, Yeovil, May 1987.

- (7) Kutscha, D., "Mechanics of Adhesive Bonded Lap-Type Joints: Survey and Review," Forest Products Laboratory, AFML-TDR-64-298, Dec. 1964.
- (8) Hart-Smith, L.J., "Adhesive-Bonded Single-Lap Joints," NASA CR 112236, Jan. 1973.
- (9) Private Communication, ICI Chemicals and Polymers Group, Wilton, Middlesbrough, Feb. 1987.
- (10) Renton, W.J., "Structural Properties and Adhesives, Vols. 1 and 2," AFML-TR-78-127, Sep. 1978.
- (11) Althof, W., Klinger, G., "Environmental Effects on the Elastic-Plastic Properties of Adhesives in Bonded Metal Joints," Royal Aircraft Establishment Library Translation 1999, Jan. 1979.
- (12) Krieger, R.B., "Stiffness Characteristics of Structural Adhesives for Stress Analysis in Hostile Environment," American Cyanamid Company, Oct. 1975.
- (13) "Araldite Bonding, Surface Preparation and Pretreatments," Ciba-Giegy, Instruction Manual A.15k, Nov. 1980.
- (14) Ojalvo, I.U., Eidinoff, H.L., "Bond Thickness Effects Upon Stresses in Single-Lap Adhesive Joints," *AIAA Journal*, Vol. 16, March 1978.

(15) Private Communication, ICI Chemicals and Polymers Group, Wilton, Middlesbrough, Aug. 1987.

(16) Sinclair, J.H., Chamis, C.C., NASA Technical Paper 1081, National Aeronautics and Space Administration, Washington DC, Dec. 1977.

(17) Johannesson, T., Sjoblom, P., Sleden, R., "The Detailed Structure of Delamination Fracture Surfaces in Graphite/Epoxy Laminates," *Journal of Materials Science*, 19, 1984, pp. 1171-1177.

(18) Volkersen, O., "Die Niet Kraft vertelung in Zug bean Spruchten Neit verb bind ungen mit Konstanten Lasch enguerschnitten," *Luftfahrt forschungen*, 15, 1938, pp. 41-47.

(19) Goland, M., Buffalo, N.Y., Reissner, E., "The Stresses in Cemented Joints," *Journal of Applied Mechanics*, March 1944, pp. A-17-A-27.

(20) Dickson, J.N., Hsu, T.M., McKinney, J.M., "Development of an Understanding of the Fatigue Phenomena of Bonded and Bolted Joints in Advanced Filamentary Composite Materials, Vol. 1, Analysis Methods," AFFDL-TR-72-64, June 1972.

(21) Grimes, G.C., Greimann, L.F., Wah, T., "The Development of Nonlinear Analysis Methods for Bonded Joints in Advanced Filamentary Composite Structures," Technical Report AFFDL-TR-72-97, Sept. 1972.

- (22) Renton, W.J., Vinson, J.R., " The Analysis and Design of Composite Material Bonded Joints Under Static and Fatigue Loadings," AFOSR-TR-73-1627, Aug. 1973.
- (23) Renton, W.J., Vinson, J.R., "The Analysis and Design of Anisotropic Bonded Joints, Report No. 2," AFOSR-TR-75-0125, Aug. 1974.
- (24) Renton, W.J., Vinson, J.R., "The Efficient Design of Adhesive Bonded Joints," *Journal of Adhesion*, Vol. 7, 1975, pp. 175-193.
- (25) Sharpe, W.N., Muha, T.J., "Comparison of Theoretical and Experimental Shear Stress in the Adhesive Layer of a Lap Joint Model," *Proceedings of the Army Symposium of Solid Mechanics*, AMMRC-74-9, 1974, pp. 23-41.
- (26) Oplinger, D.W., "Stress Analysis of Composite Joints," *Proceedings of the Fourth Army Materials Technology Conference - Advances in Joining Technology*, Sept. 1975, pp. 405-452.
- (27) Hart-Smith, L.J., "Adhesive-Bonded Double-Lap Joints," NASA-CR-112235, Jan. 1973.
- (28) "Vitrex PEEK, A Guide to Grades for Injection Moulding," Imperial Chemical Industries PLC, Lit. Ref. VK2/0785, 1985.
- (29) Loss, K.R., Kedward, K.T., "Modelling and Analysis of Peel and Shear Sresses in Adhesively Bonded Joints," *Proceedings of the AIAA/ASME/ASCE/AHS 25th Structures, Structural Dynamics and Materials*



(30) "Property Data of Aromatic Polymer Composite, APC-2/Hercules Magnamite AS4 Carbon Fibre," Imperial Chemical Industries PLC, Fiberite Data Sheet 3a, 1986.

(31) C.A.M.E.L. 4, "The Stiffness, Stress and Thermal Analysis of Flat Laminated Orthotropic Plates," SDS/S153A, Version B, Westland Helicopters Ltd, June 1984.

(32) "Stiffnesses of Laminated Flat Plates," Engineering Sciences Data Unit, Item No. 75002, Jan. 1975.

(33) Stein, B.A., Tyeryar, J.R., Hodges, W.T., "Rapid Adhesive Bonding Concepts," NASA TM-86256, June 1984.

(34) Stein, B.A., Hodges, W.T., Tyeryar, J.R., "Rapid Adhesive Bonding of Advanced Composites and Titanium," *Proceedings of the AIAA/ASME/ASCE/AHS 26th Structures, Structural Dynamics and Materials Conference*, AIAA Paper No. 85-0750-CP, April 1985.

(35) Stein, B.A., Hodges, W.T., Tyeryar, J.R., "Rapid Adhesive Bonding of Thermoplastic Composites and Titanium with Thermoplastic Adhesives," *Journal of Aircraft*, Vol. 23, No. 7, July 1986, pp. 545-546.

## APPENDIX A

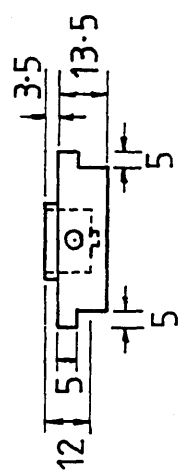
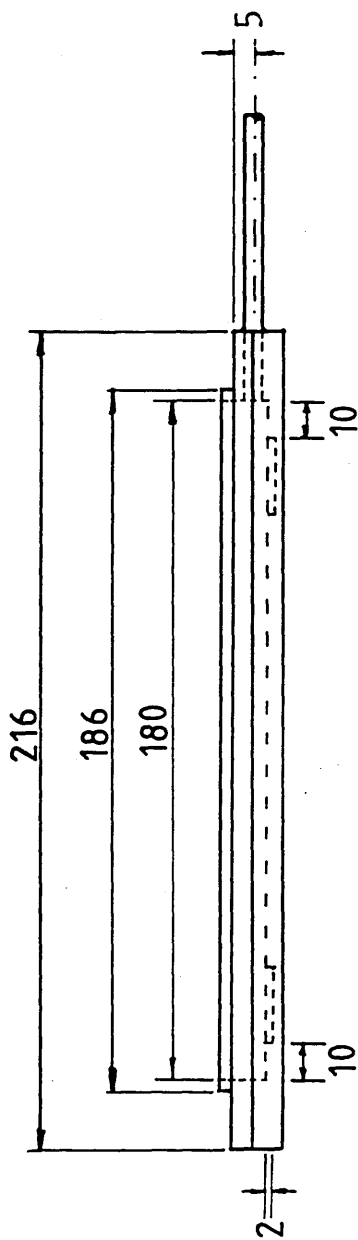
FIGURE A.1: Vacuum Plate for Thick Adherend Specimen

FIGURE A.2: Inner Loading Block

FIGURE A.3: Outer Loading Block

FIGURE A.4: Extensometer Pick-up Attachment

FIGURE A.5: Extensometer Support



NOTES

MATERIAL: MILD STEEL  
COPPER PIPE SILVER SOLDERD  
TO PLATE

DIMENSIONS IN mm

IJM 3/10/86

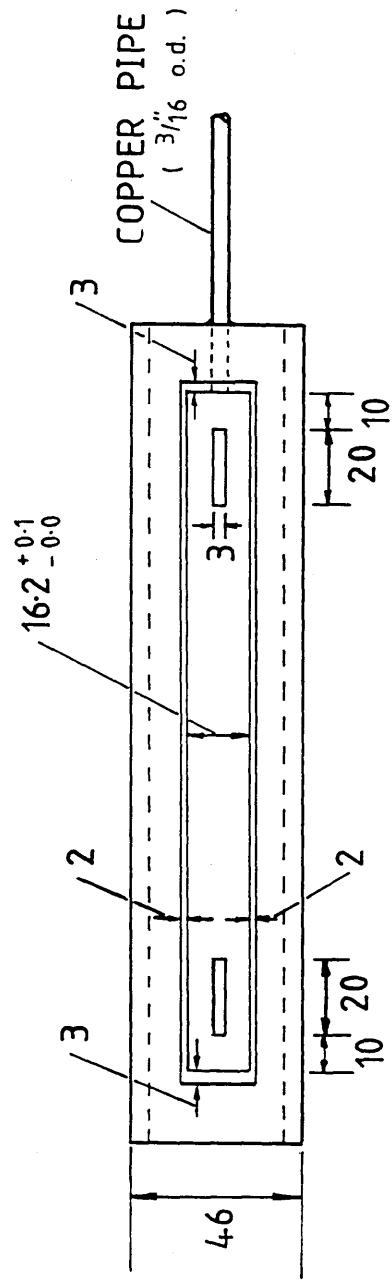


FIGURE A.1: VACUUM PLATE FOR THICK ADHEREND SPECIMEN

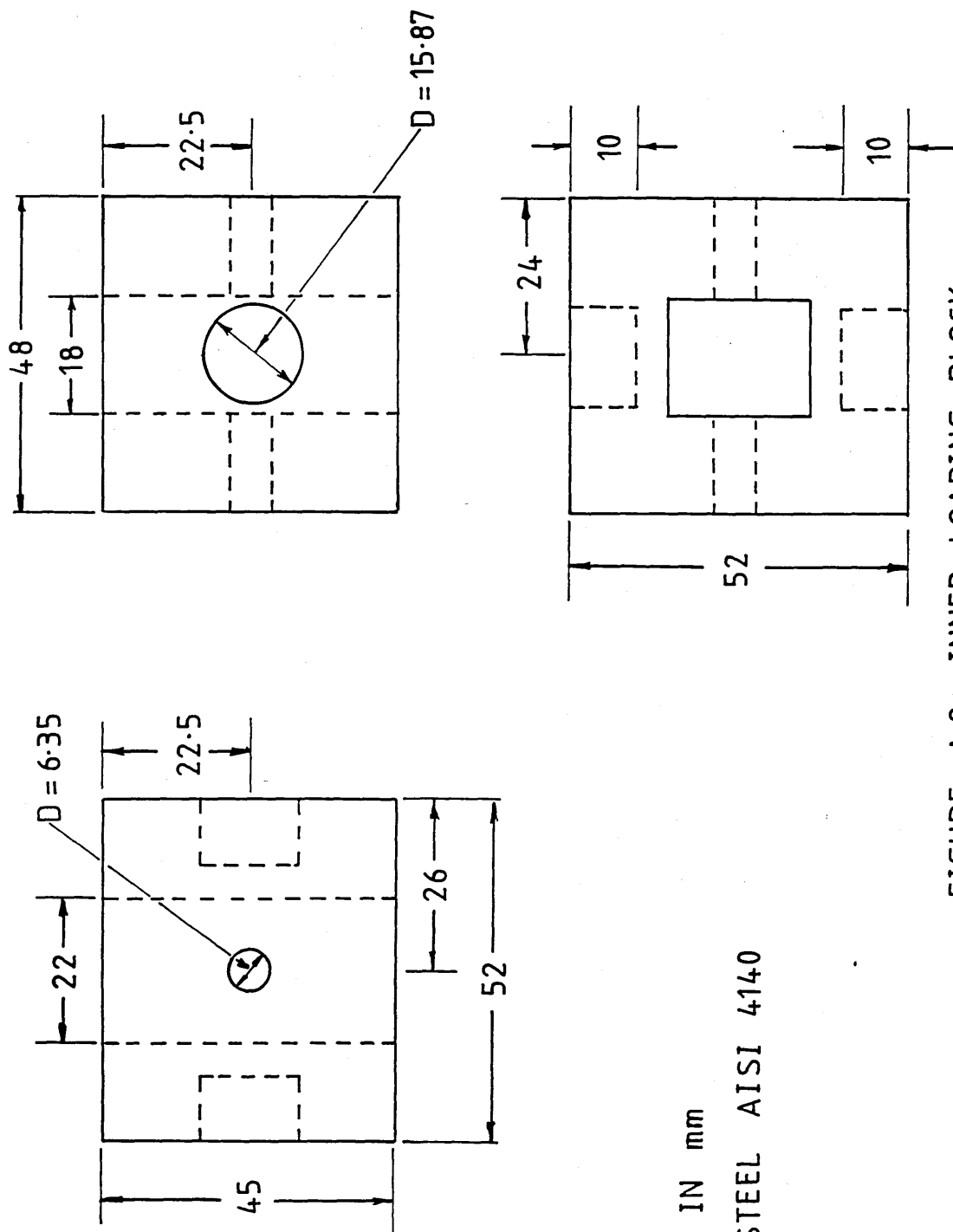
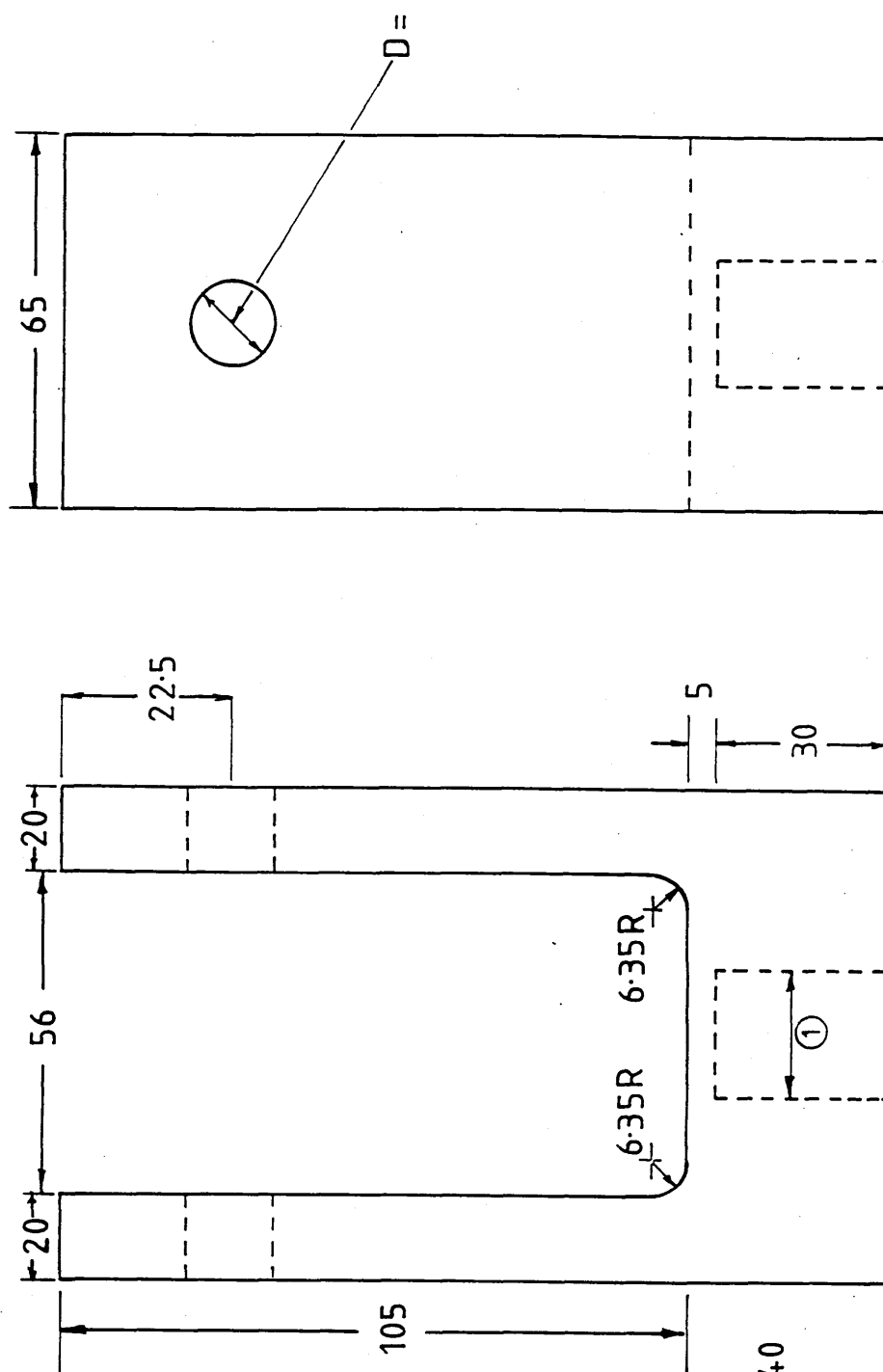


FIGURE A.2: INNER LOADING BLOCK

DIMENSIONS IN mm  
MATERIAL: STEEL AISI 4140

LJM 16/12/86



NOTE

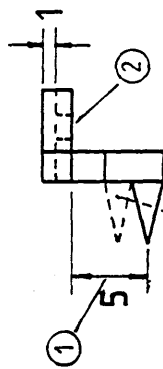
① HOLE TAPPED FOR  
7/8 UNC

DIMENSIONS IN mm

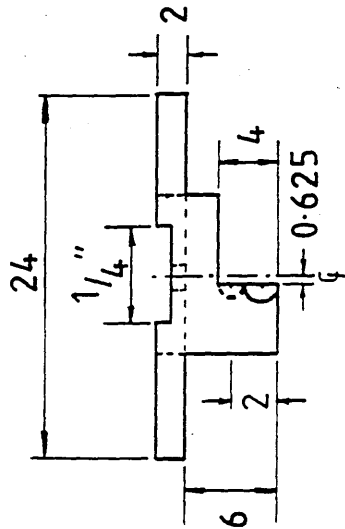
MATERIAL: STEEL AISI 4140

IJM 16/12/86

FIGURE A.3: OUTER LOADING BLOCK



ONLY ON BOTTOM  
ATTACHMENT



#### NOTES

- ① POSITION OF POINT CRITICAL.
- ② HOLE TAPPED FOR EXTENSOMETER SCREW.

MATERIAL: STEEL

DIMENSIONS IN mm  
(unless otherwise stated)

IJM 5/8/86

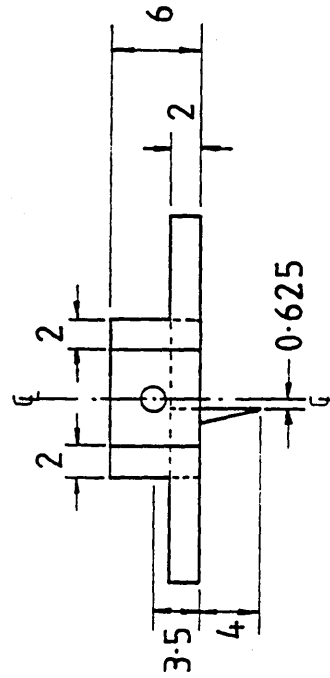
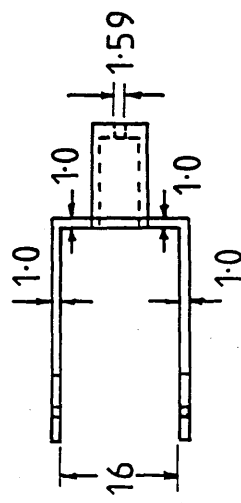
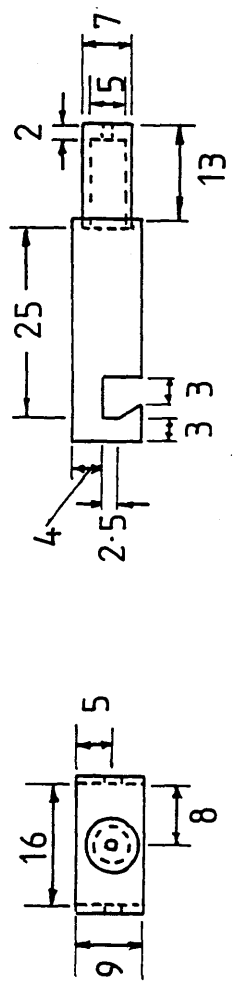


FIGURE A.4: EXTENSOMETER PICK-UP ATTACHMENT



MATERIAL: MILD STEEL

ALL DIMENSIONS IN mm

IJM 6/1/87

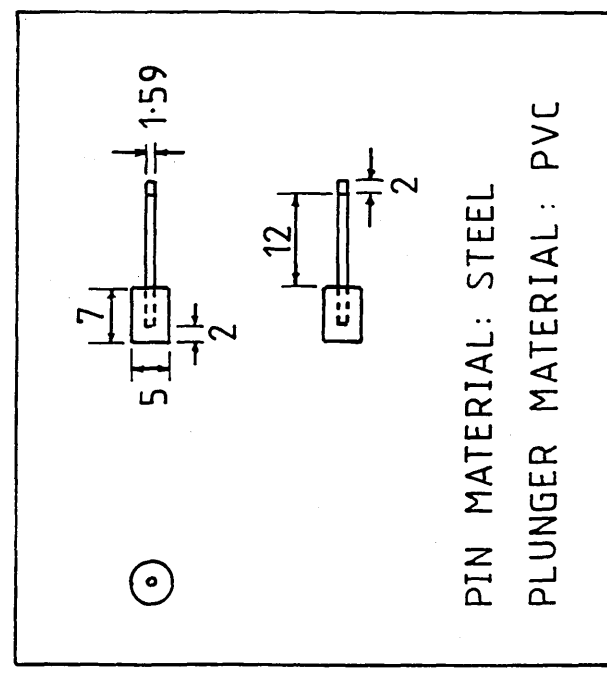


FIGURE A.5: EXTENSOMETER SUPPORT

## APPENDIX B

### MATHEMATICAL DERIVATIONS

#### B.1 Correction for Metal Deformation in Thick Adherend Specimen

From experimental measurement of the dummy specimen, the metal deformation was measured as

$$u_d = 3.0 \times 10^{-9} F \quad 0 \leq F \leq 6000N \quad (B.1)$$

In the actual specimen there is a bondline, and, therefore,  $u_d$  has to be corrected for the smaller amount of metal present. Taking the distance between the extensometer measurement points across the bondline as  $a$ , and the bondline thickness as  $n$ , the actual metal deformation is given by

$$u_m = u_d \left[ \frac{a - n}{a} \right] \quad (B.2)$$

Hence if  $u_s$  is the measured displacement of the bonded specimen during test, the adhesive deformation,  $u_c$ , is given by

$$u_c = u_s - u_m \quad (B.3)$$



## B.2 Bi-Elastic Modelling for Shear Failure

In the bi-elastic analysis, the shear stress-strain curve is considered in two regions as shown in Figure 4.3. Taking  $u_2$  and  $u_3$  as the longitudinal displacements of the adherends immediately adjacent to the adhesive in regions 2 and 3 of the joint, (Refer to Figure 4.2), and considering the stress-strain relations for the adherends in plane strain

$$\left. \begin{aligned} \frac{du_2}{ds} &= \frac{(1 - \nu^2)}{Et} \left[ T_2 + \frac{6M_2}{k_b t} \right] \\ \frac{du_3}{ds} &= \frac{(1 - \nu^2)}{Et} \left[ T_3 - \frac{6M_3}{k_b t} \right] \end{aligned} \right\} \quad (B.4)$$

Now considering equilibrium of the elements in Figure 4.2, moment equilibrium gives

$$\left. \begin{aligned} \frac{dM_2}{ds} - V_2 + \tau \left[ \frac{t + n}{2} \right] &= 0 \\ \frac{dM_3}{ds} - V_3 + \tau \left[ \frac{t + n}{2} \right] &= 0 \end{aligned} \right\} \quad (B.5)$$

while longitudinal force equilibrium gives

$$\left. \begin{aligned} \frac{dT_2}{ds} + \tau &= 0 \\ \frac{dT_3}{ds} - \tau &= 0 \end{aligned} \right\} \quad (B.6)$$

and transverse force equilibrium gives

$$\left. \begin{aligned} \frac{dV_2}{ds} + \sigma_c &= 0 \\ \frac{dV_3}{ds} - \sigma_c &= 0 \end{aligned} \right\} \quad (B.7)$$

The shear strain is taken as

$$\gamma = \frac{u_3 - u_2}{n} \quad (B.8)$$

Differentiation of B.8 and substitution of equations B.4 to B.7 gives

$$\frac{d\gamma}{ds} = \frac{1}{n} \left[ \frac{du_3}{ds} - \frac{du_2}{ds} \right] = \frac{(1 - \nu^2)}{nEt} \left[ T_3 - T_2 - \frac{6}{k_b t} (M_3 + M_2) \right] \quad (B.9)$$

$$\frac{d^2\gamma}{ds^2} = \frac{(1 - \nu^2)}{nEt} \left[ 2\tau - \frac{6}{k_b t} (V_3 + V_2 - \tau(t + n)) \right] \quad (B.10)$$

$$\frac{d^3\gamma}{ds^3} = \frac{(1 - \nu^2)}{nEt} \left[ 2 + \frac{6}{k_b} \right] \frac{d\tau}{ds} \quad (B.11)$$

assuming that  $(1 + n/t) \approx 1$ .

The problem is formulated by considering the shear stress-strain curve in two regions, as shown in Figure 4.3. The stress-strain relation for each region is given by

$$\tau = G_1 \gamma \quad \text{where } 0 \leq \gamma \leq \gamma_{1L} \quad (B.12)$$

$$\tau = G_1 \gamma_{1L} + G_2 (\gamma - \gamma_{1L}) \quad \text{where } \gamma_{1L} \leq \gamma \leq \gamma_{2L} \quad (B.13)$$

The co-ordinates for describing the strain distribution in the joint for  $\gamma$  in equations B.12 and B.13, are  $s_1$  and  $s_2$  respectively. The origin of  $s_2$  is taken at  $s_1 = d_1$ , where  $d_1$  is an unknown term.

Considering equation B.11 for  $0 \leq \gamma \leq \gamma_{1L}$  and substituting  $\tau = G_1 \gamma$

$$\frac{d^3\gamma}{ds_1^3} = (1 - \nu^2) \left[ 1 + \frac{3}{k_b} \right] \frac{2G_1}{Et n} \frac{d\gamma}{ds_1} \quad (B.14)$$

Using the notation

$$\lambda_1^2 = \frac{2G_1}{Etn} \quad \text{and} \quad (\lambda_1')^2 = \frac{(1 - v^2)}{4} \left[ 1 + \frac{3}{k_b} \right] \lambda_1^2$$

The solution of B.14 is

$$\gamma = A_1 \cosh(2\lambda_1' s_1) + B_1 \sinh(2\lambda_1' s_1) + C_1 \quad (\text{B.15})$$

Similarly for  $\gamma_{1L} \leq \gamma \leq \gamma_{2L}$

$$\gamma = A_2 \cosh(2\lambda_2' s_2) + B_2 \sinh(2\lambda_2' s_2) + C_2 \quad (\text{B.16})$$

with  $\lambda_2^2 = \frac{2G_2}{Etn}$  and  $(\lambda_2')^2 = \frac{(1 - v^2)}{4} \left[ 1 + \frac{3}{k_b} \right] \lambda_2^2$

The solution of the problem is obtained by solving for the unknown variables  $A_1, B_1, C_1, A_2, B_2, C_2$  and  $d_1$ . These are obtained from the following boundary conditions

$$s_1 = 0, \quad \frac{d\gamma}{ds_1} = 0 \quad (\text{B.17})$$

$$s_1 = d_1, \quad s_2 = 0 \quad \gamma = \gamma_{1L} \quad (\text{Two equations}) \quad (\text{B.18})$$

$$s_1 = d_1, \quad s_2 = 0 \quad \frac{dy}{ds_1} = \frac{dy}{ds_2} \quad (\text{B.19})$$

$$s_1 = d_1, \quad s_2 = 0 \quad \frac{d^2\gamma}{ds_1^2} = \frac{d^2\gamma}{ds_2^2} \quad (\text{B.20})$$

$$s_2 = c - d_1, \quad \gamma = \gamma_{2L} \quad (\text{B.21})$$

$$s_2 = c - d_1, \quad \frac{dy}{ds_2} = \frac{P(1 - \nu^2)}{nEt} \left[ 1 + \frac{3k}{k_b} \left[ 1 + \frac{n}{t} \right] \right] \quad (\text{B.22})$$

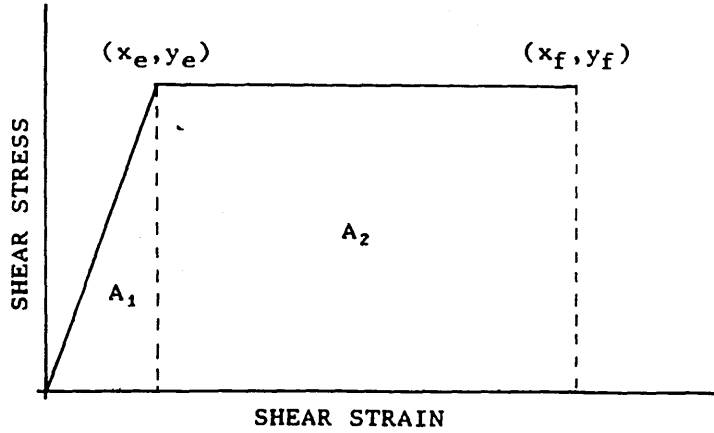
Failure is assumed when  $\gamma = \gamma_{2L}$  at the end of the overlap. The load/width at failure,  $P$ , is obtained from

$$\frac{P}{2} = \int_{s_1=0}^{s_1=d_1} G_1 \gamma ds_1 + \int_{s_2=0}^{s_2=(c-d_1)} (G_1 \gamma_{1L} + G_2 (\gamma - \gamma_{1L})) ds_2 \quad (\text{B.23})$$

B.3 Calculation of Intersection Points for Elastic-Plastic and  
Bi-Elastic Shear Stress-Strain Curve Representations

B.3(a) Elastic-Plastic Representation

The approximation to the actual shear stress-strain curve is made as shown below, with  $(x_e, y_e)$  the co-ordinates of the intersection point



The area under the approximate curve,  $A_c$ , is given by

$$A_c = A_1 + A_2 \quad (B.24)$$

where

$$A_1 = \frac{1}{2} x_e y_e = \frac{1}{2} x_e y_f \quad (B.25)$$

$$A_2 = y_f (x_f - x_e) \quad (B.26)$$

It is required to obtain the value of  $x_e$ , the x co-ordinate of the intersection point. Therefore, from equation B.24

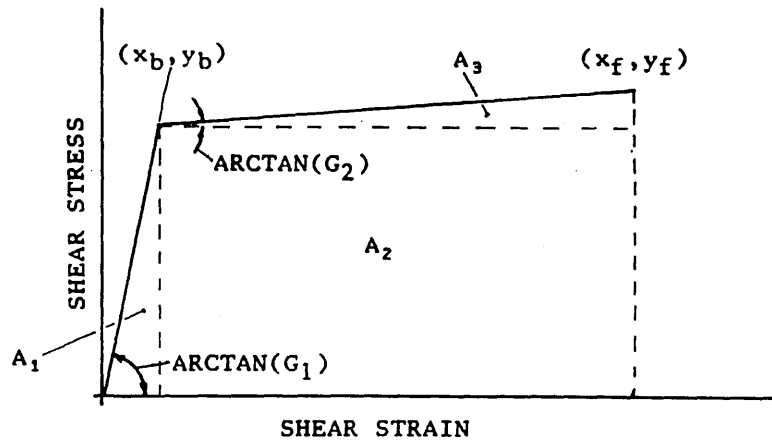
$$A_c = \frac{1}{2} x_e y_f + y_f (x_f - x_e) \quad (B.27)$$

and re-arranging for  $x_e$  gives

$$x_e = 2 \left[ x_f - \frac{A_c}{y_f} \right] \quad (B.28)$$

### B.3(b) Bi-Elastic Representation

For the bi-elastic representation of the shear stress-strain curve, the approximation is made as shown below, with  $(x_b, y_b)$  the co-ordinates of the intersection point



The two lines have a slope of  $G_1$  and  $G_2$  as shown. The line with the slope  $G_2$  was fitted to the actual shear curve in such a manner as to approximate the shape of the shear curve as best as possible. The problem then reduces to the solution of  $(x_b, y_b)$ .

The area under the curve,  $A_c$ , is given by

$$A_c = A_1 + A_2 + A_3 \quad (\text{B.29})$$

where

$$A_1 = \frac{1}{2} x_b y_b \quad A_2 = y_b (x_f - x_b) \quad A_3 = \frac{1}{2} (x_f - x_b) (y_f - y_b) \quad (\text{B.30})$$

Therefore, from equation B.29

$$A_c = \frac{1}{2} x_f y_b + \frac{1}{2} x_f y_f - \frac{1}{2} x_b y_f \quad (\text{B.31})$$

From the equation of a line

$$y_f = G_2 x_f + C \quad (\text{B.32})$$

where  $C$  is the constant of the line given by

$$C = y_f - G_2 x_f \quad (\text{B.33})$$

Since the point  $(x_b, y_b)$  lies on the same line as  $(x_f, y_f)$

$$y_b = G_2 x_b + (y_f - G_2 x_f) \quad (\text{B.34})$$



Therefore, substituting for  $y_b$  into equation B.31 and re-arranging for  $x_b$  gives

$$x_b = \frac{2A_c - x_f(2y_f - G_2x_f)}{(x_fG_2 - y_f)} \quad (B.35)$$

## EXPERIMENTAL ARRANGEMENT

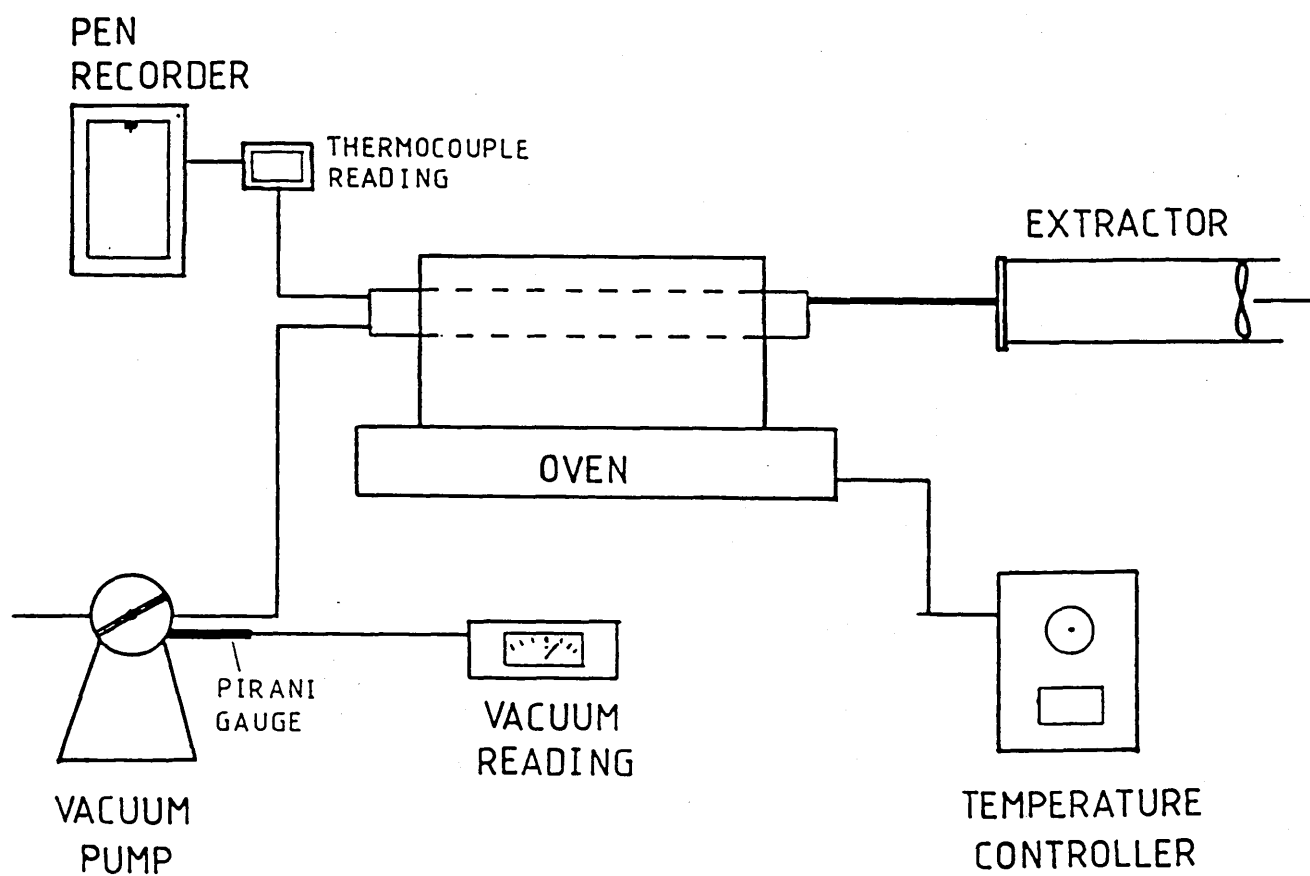
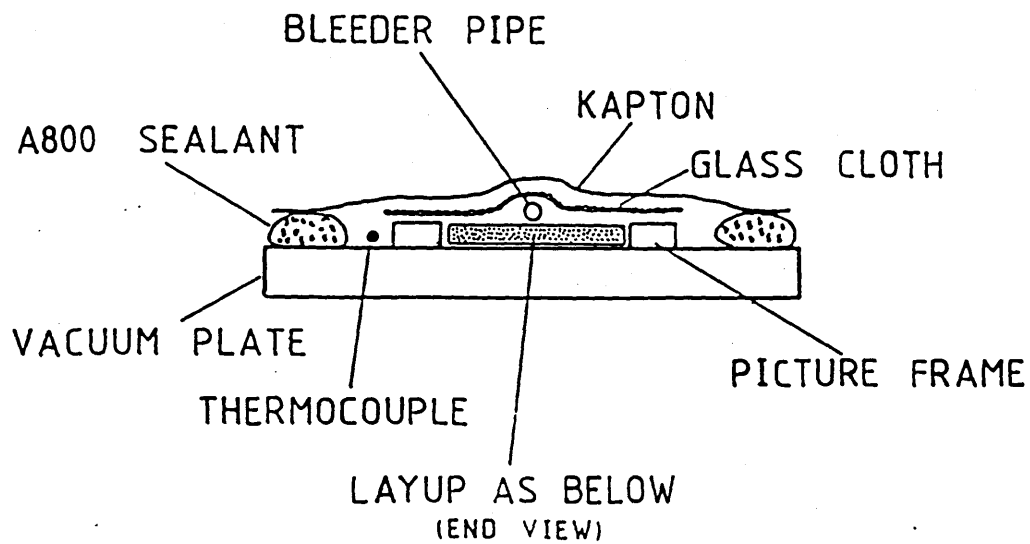






FIGURE 2.1



### VACUUM BAG

#### KEY

-  COMPOSITE
-  PEEK FILM
-  PACKING PIECE
-  STAINLESS STEEL

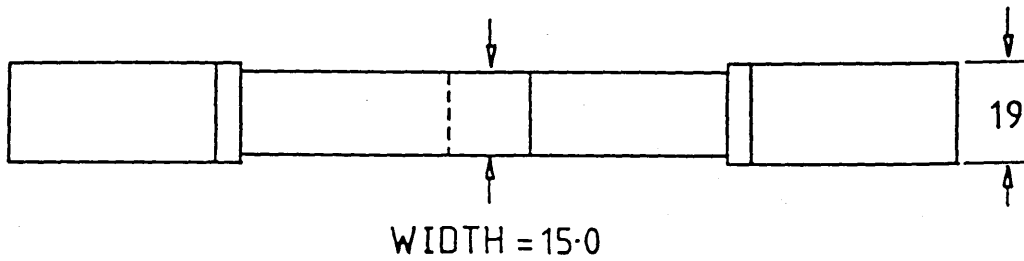
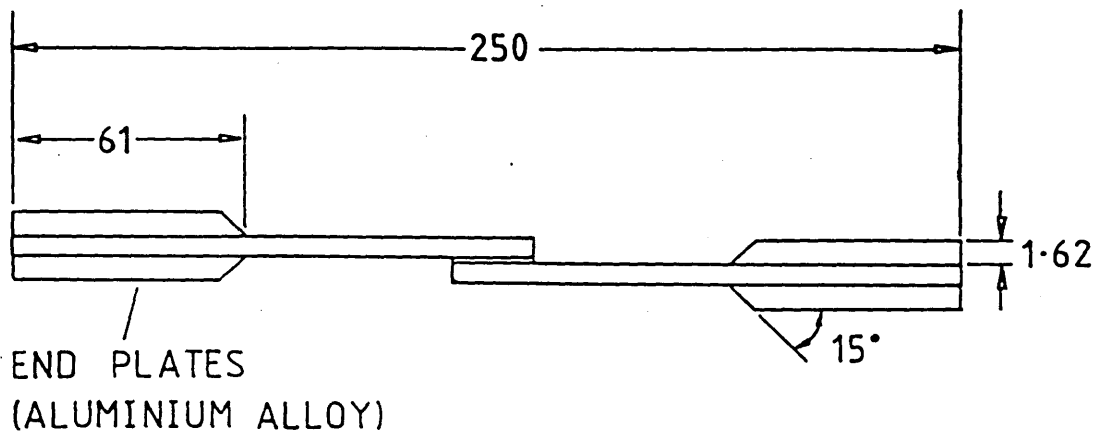


### LAYUP INSIDE PICTURE FRAME

(SIDE VIEW)

FIGURE 2.2

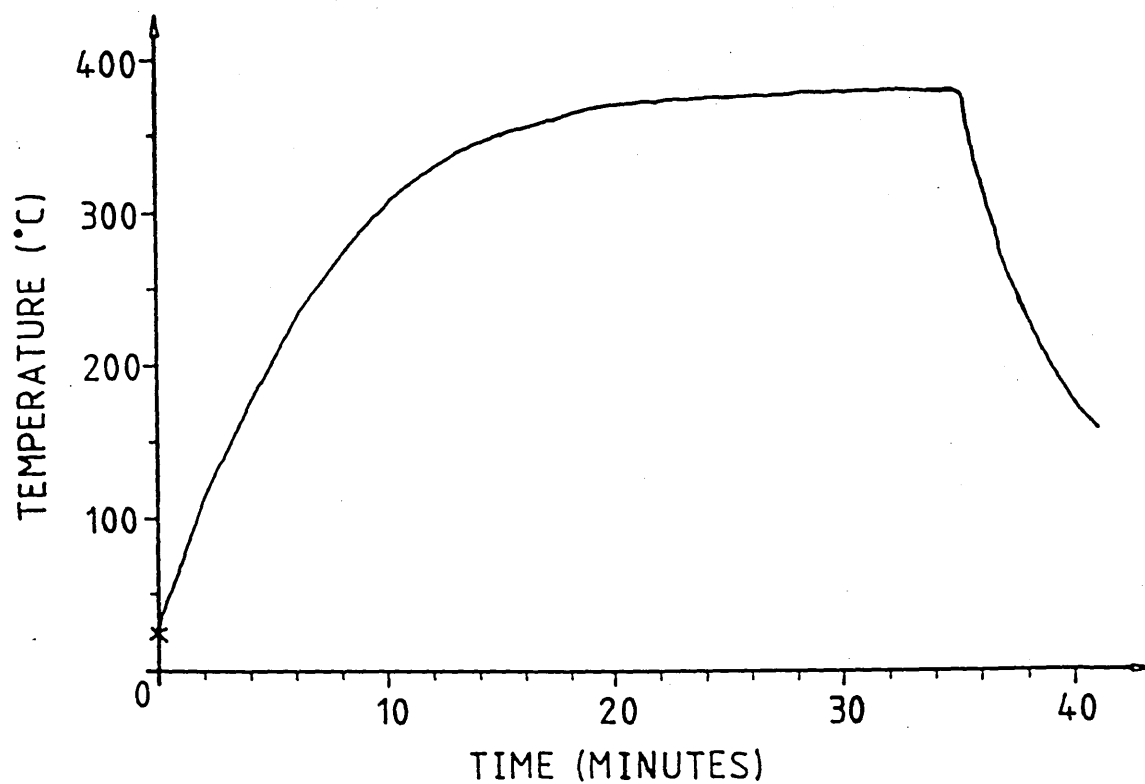
## TEST SPECIMEN



ALL DIMENSIONS IN MM  
NOT TO SCALE

FIGURE 2.3

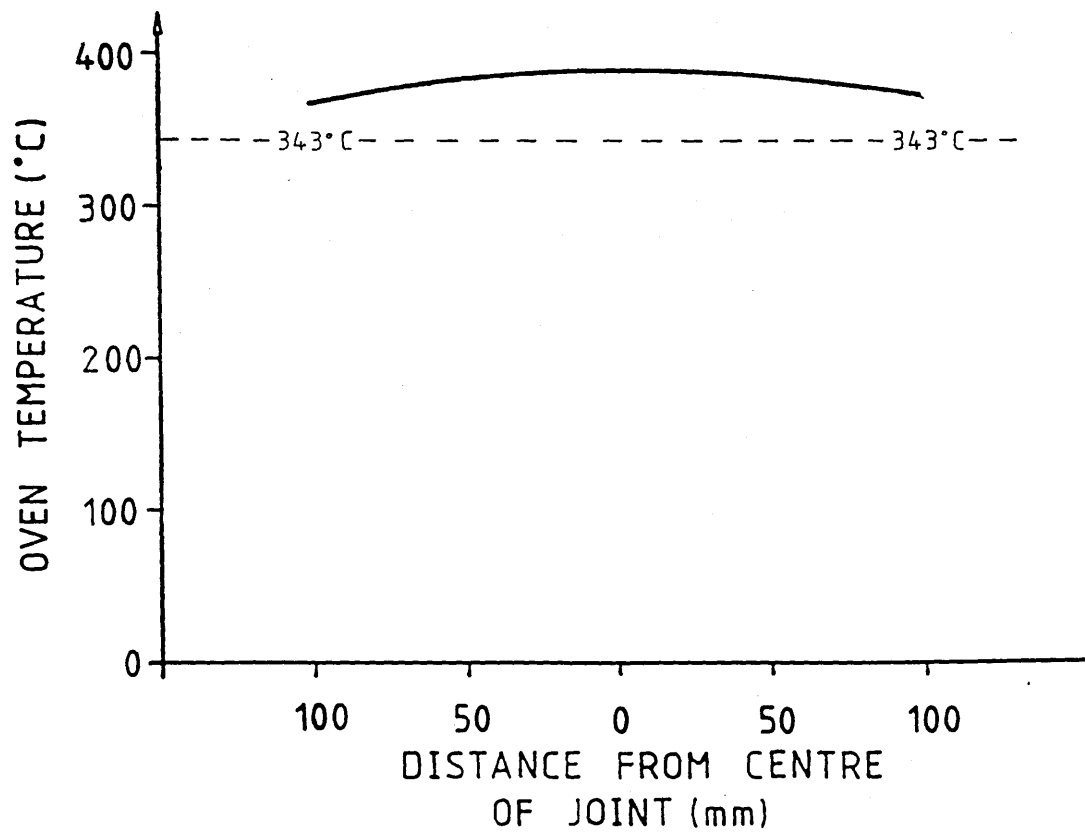
## HEATING CYCLE



Average cooling rate =  $45^{\circ}\text{C}/\text{min}$   
( $380^{\circ}\text{C}$  to  $200^{\circ}\text{C}$ )

FIGURE 2.4

## OVEN TEMPERATURE DISTRIBUTION



PEEK melting point = 343 °C

FIGURE 2.5

## SPECIMEN TESTING

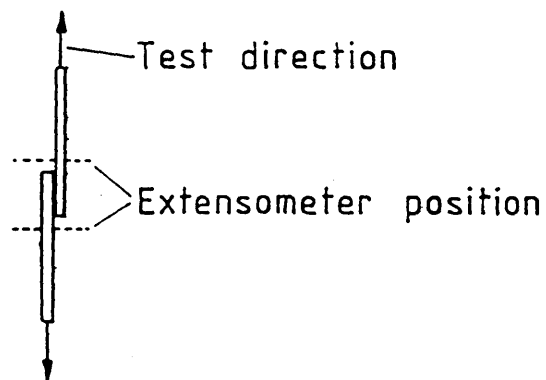
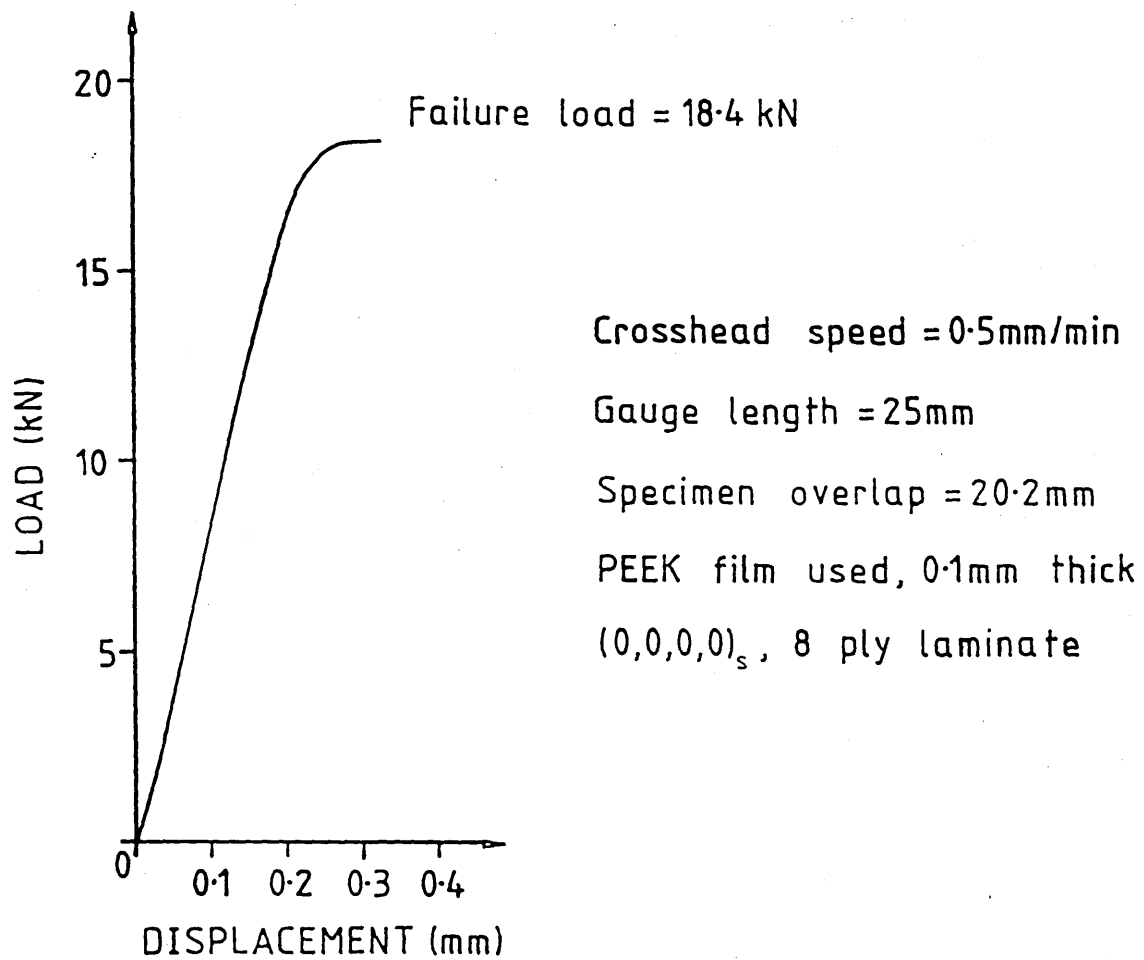
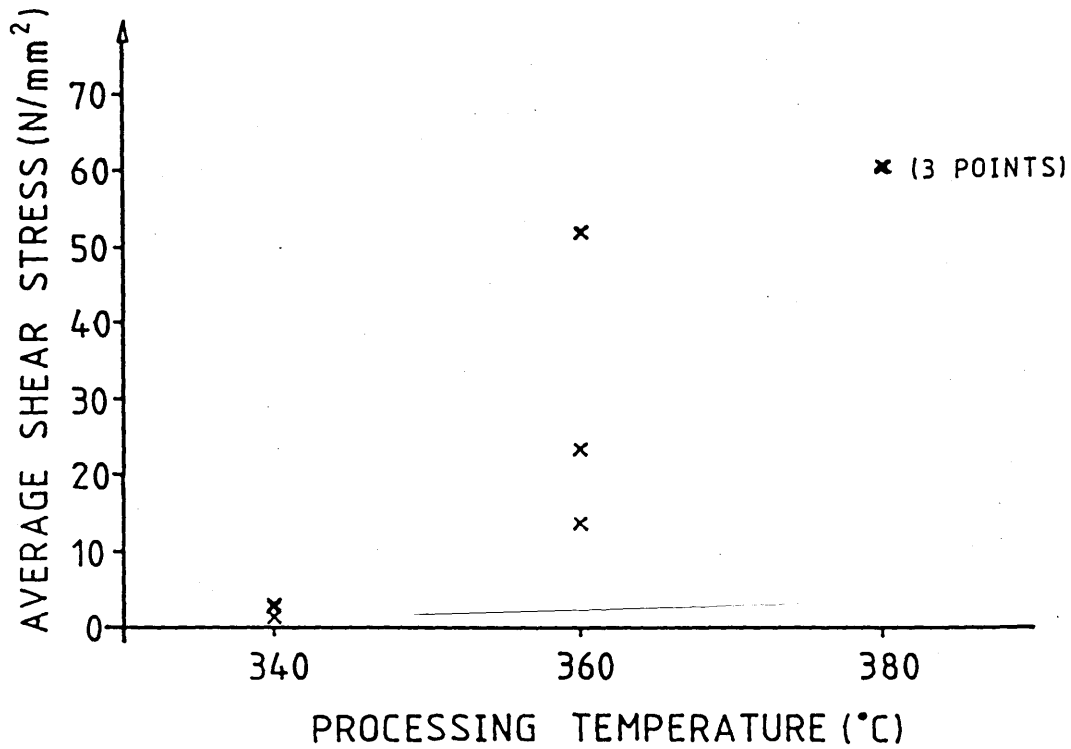


FIGURE 2.6

# INFLUENCE OF PROCESSING TEMPERATURE ON JOINT STRENGTH



Specimen Width(mm)	Specimen Overlap(mm)	Processing Temperature(°C)	Failure Load(kN)	Average Shear Stress(N/mm <sup>2</sup> )
15.0	20.0	340	0.80	2.67
15.0	20.0	340	0.55	1.83
15.0	20.0	340	1.00	3.33
15.0	20.5	360	16.1	52.3
15.0	20.2	360	7.20	23.8
15.0	20.1	360	4.20	13.9
15.0	20.5	380	18.8	61.1
15.0	20.5	380	18.7	60.8
15.0	20.2	380	18.4	60.7

NOTE: 0.1mm thick, 450 Grade PEEK film used in joint.  
Surface cleaning with Acetone.  
Crosshead speed during testing, 0.5mm/min.  
Adherends from 8 ply, unidirectional laminate.

FIGURE 2.7



INFLUENCE OF SURFACE CLEANING  
ON JOINT STRENGTH

Specimen Width(mm)	Specimen Overlap(mm)	Surface Cleaning	Failure Load(kN)	Average Shear Stress(N/mm <sup>2</sup> )
14.96	19.8	TCE	12.3	41.5
14.95	20.0	TCE	12.3	41.1
14.94	20.3	TCE	11.5	37.9
15.00	20.3	Acetone	18.9	62.1
15.00	20.2	Acetone	18.4	60.7
15.00	20.3	Acetone	18.3	60.1

NOTE: TCE = Trichloroethane  
0.1mm thick, 450 Grade PEEK film used in joint.  
Processing Temperature, 380°C.  
Crosshead speed during testing, 0.5mm/min.  
Adherends from 8 ply, unidirectional laminate.

TABLE 2.1

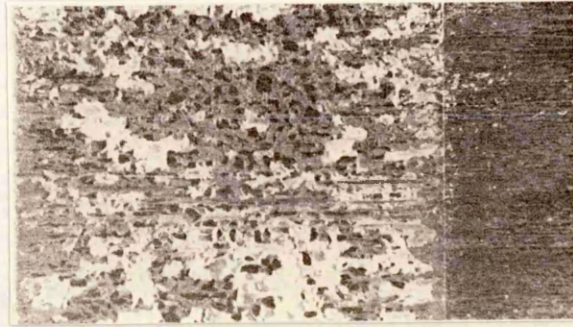


**FIGURE 2.8(a)** Failure surface of specimen  
cleaned with Trichloroethane

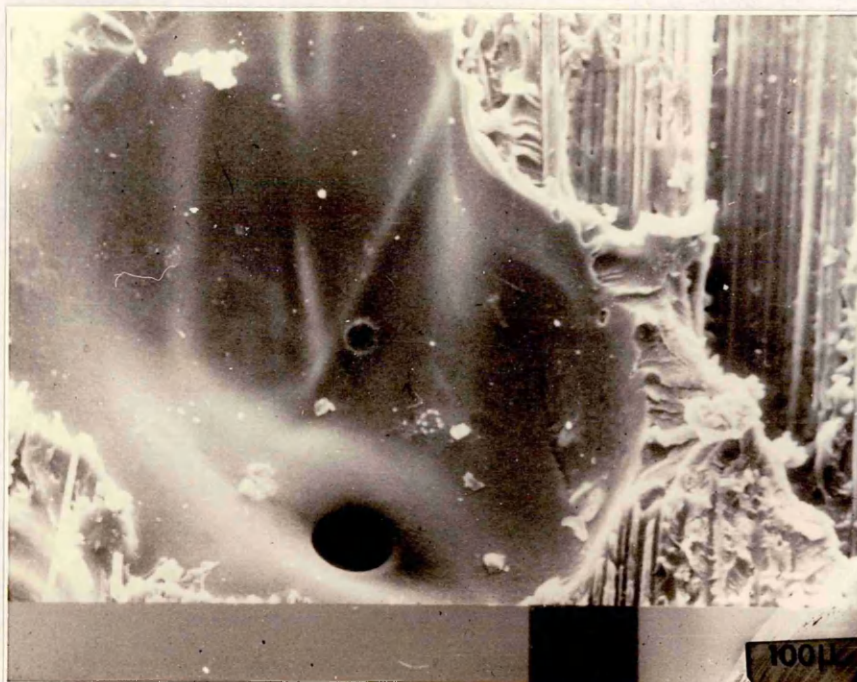
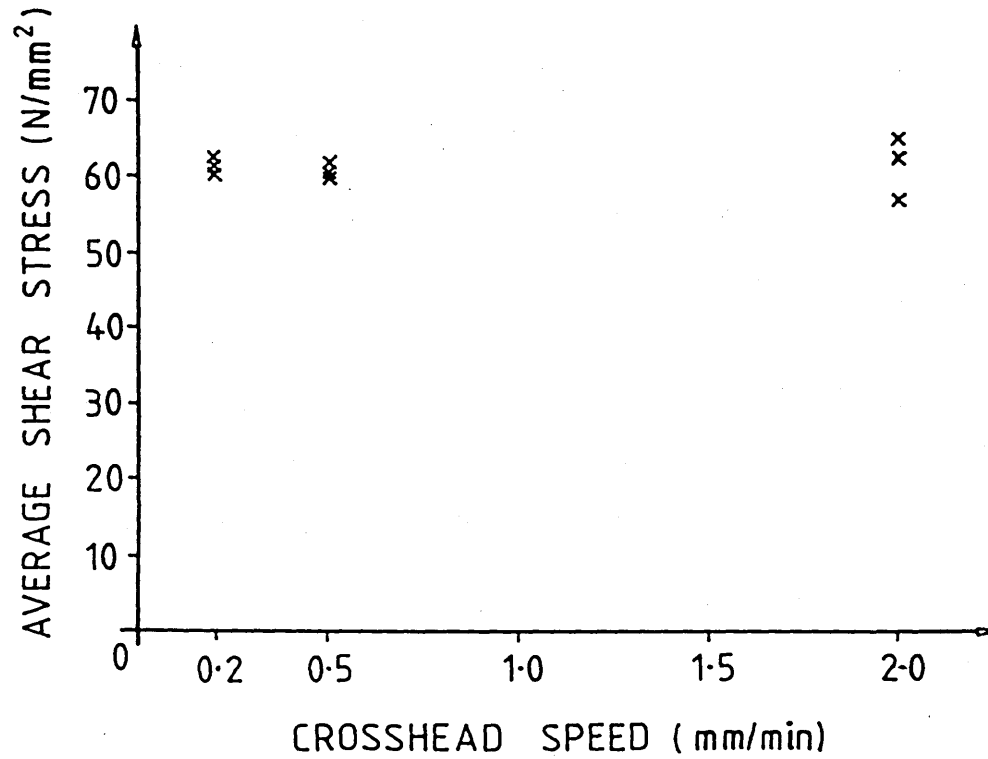


**FIGURE 2.8(b)** SEM micrograph of specimen  
cleaned with Trichloroethane

INFLUENCE OF CROSSHEAD SPEED  
ON JOINT STRENGTH



Specimen Width(mm)	Specimen Overlap(mm)	Crosshead Speed(mm/min)	Failure Load(kN)	Average Shear Stress(N/mm <sup>2</sup> )
15.0	20.2	0.2	19.00	62.7
15.0	20.2	0.2	18.65	61.6
15.0	20.4	0.2	18.55	60.6
15.0	20.3	0.5	18.90	62.1
15.0	20.2	0.5	18.40	60.7
15.0	20.3	0.5	18.30	60.1
15.0	20.2	2.0	19.80	65.3
15.0	20.3	2.0	19.10	62.7
15.1	20.3	2.0	17.50	57.1

NOTE: 0.1mm thick, 450 Grade PEEK film used in joint.  
Surface cleaning with Acetone.  
Processing temperature, 380°C.  
Adherends from 8 ply, unidirectional laminate.

FIGURE 2.9

INFLUENCE OF EXCESS PEEK  
ON JOINT STRENGTH

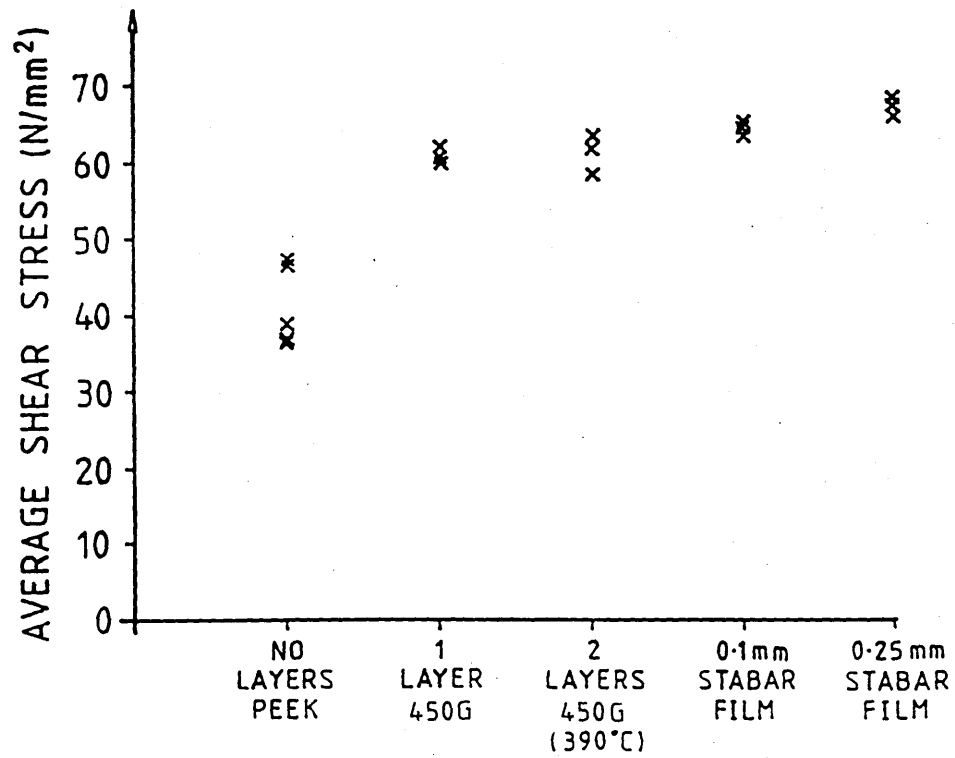


FIGURE 2.10

INFLUENCE OF EXCESS PEEK  
ON JOINT STRENGTH

Specimen Width(mm)	Specimen Overlap(mm)	Film Type	Number of Layers	Average Shear Stress(N/mm <sup>2</sup> )
15.00	20.2	-	0	47.5
15.00	20.3	-	0	46.6
15.00	20.7	-	0	39.0
15.00	20.7	-	0	37.0
14.95	20.4	-	0	36.7
15.00	20.3	A	1	62.1
15.00	20.2	A	1	60.7
15.00	20.3	A	1	60.1
15.00	20.1	A	2	63.8
14.95	20.0	A	2	61.9
14.95	20.0	A	2	58.5
15.10	20.0	B	1	65.4
14.96	20.3	B	1	64.5
14.96	20.2	B	1	63.7
14.94	20.0	C	1	68.6
14.90	20.2	C	1	67.3
14.96	20.2	C	1	66.0

NOTE: Film type A: 430 Grade, 0.1mm thick.  
Film type B: Stabar film, 0.1mm thick.  
Film type C: Stabar film, 0.25mm thick.

Surface cleaning with Acetone.  
Processing temperature, 380°C.  
Crosshead speed during testing, 0.5mm/min.  
Adherends from 8 ply, unidirectional laminate.

TABLE 2.2





FIGURE 2.11(a) Cross-section of joint produced with 0.1mm thick 450 Grade film, (Mag. 50x)

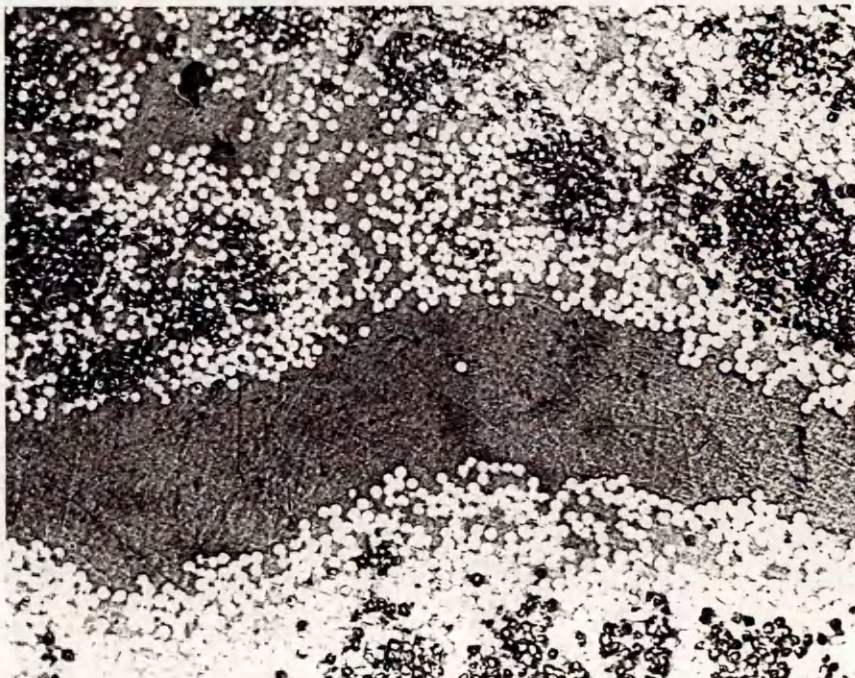


FIGURE 2.11(b) Cross-section of joint produced with 0.1mm thick 450 Grade film, (Mag. 110x)

FIGURE 2.11





FIGURE 2.12(a) Cross-section of joint produced without PEEK film, (Mag. 50x)

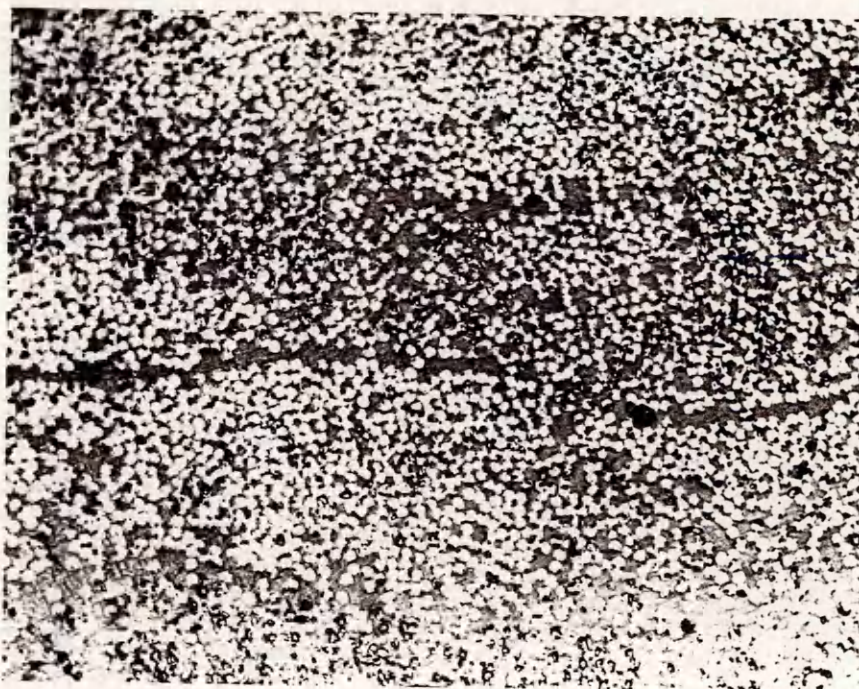
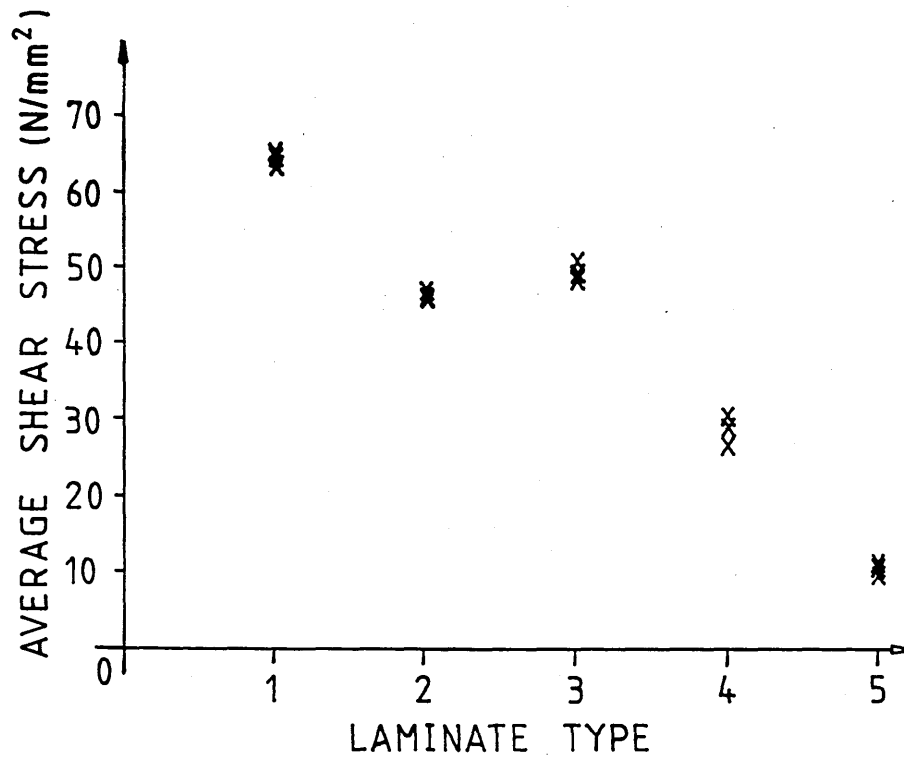


FIGURE 2.12(b) Cross-section of joint produced without PEEK film, (Mag. 110x)

FIGURE 2.12

# INFLUENCE OF LAMINATE LAY-UP ON JOINT STRENGTH



Laminate Type	Laminate Lay-up (8 plies)	Average Shear Stress(N/mm <sup>2</sup> )	Failure Mode
1	(0,0,0,0) <sub>s</sub>	64.5	bondline
2	(0,0,+45,-45) <sub>s</sub>	46.7	adherend
3	(0,+45,-45,0) <sub>s</sub>	49.7	adherend
4	(0,+45,-45,90) <sub>s</sub>	28.8	adherend
5	(+45,-45,+45,-45) <sub>s</sub>	10.9	adherend

NOTE: 0.1mm thick Stabar film used in joint.  
Specimen dimensions: Width=15mm, Overlap=20mm.

FIGURE 2.13



VARIATION OF JOINT STRENGTH  
WITH OVERLAP LENGTH

$(0,0,0,0)_S$ , 8 ply.

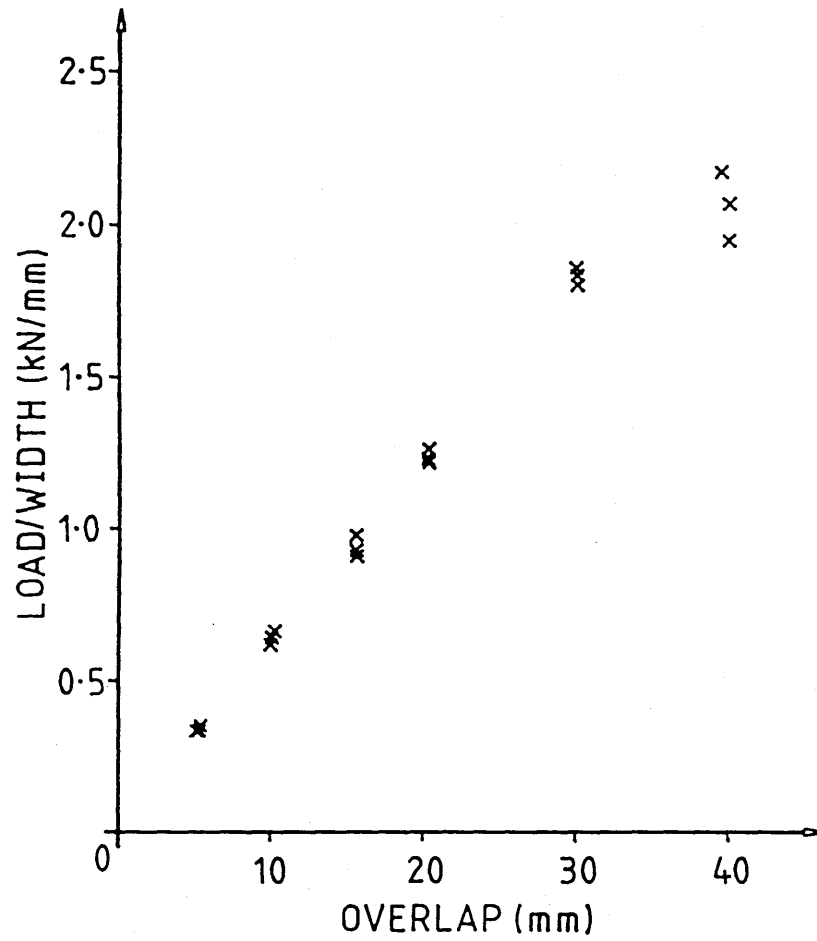


FIGURE 2.14

VARIATION OF JOINT STRENGTH  
WITH OVERLAP LENGTH

(0,0,0,0)<sub>s</sub>, 8 ply.

Specimen Width(mm)	Specimen Overlap(mm)	Failure Load(kN)	Load/Width at Failure(kN/mm)	Average Shear Stress(N/mm <sup>2</sup> )
15.10	5.3	5.5	0.36	68.7
15.00	5.0	5.1	0.34	68.0
15.00	5.3	5.1	0.34	64.2
15.00	10.2	10.0	0.66	65.4
15.00	10.0	9.6	0.64	64.0
15.00	10.0	9.3	0.62	62.0
15.00	15.4	14.7	0.98	63.6
15.00	15.5	14.0	0.93	60.2
15.00	15.5	13.9	0.92	59.8
15.00	20.3	18.9	1.26	62.1
15.00	20.2	18.4	1.23	60.7
15.00	20.3	18.3	1.22	60.1
15.00	30.0	27.9	1.86	62.0
15.00	30.0	27.5	1.83	61.1
15.00	30.0	27.0	1.80	60.0
14.96	39.5	32.5	2.17	55.0
15.00	40.0	31.0	2.06	51.7
15.00	40.0	29.25	1.95	48.8

NOTE: 0.1mm thick, 450 Grade PEEK film used in joint.  
Surface cleaning with Acetone.  
Processing temperature, 380°C.  
Crosshead speed during testing, 0.5mm/min.

TABLE 2.3

VARIATION OF JOINT STRENGTH  
WITH OVERLAP LENGTH

(0,0,+45,-45) , 8 ply.

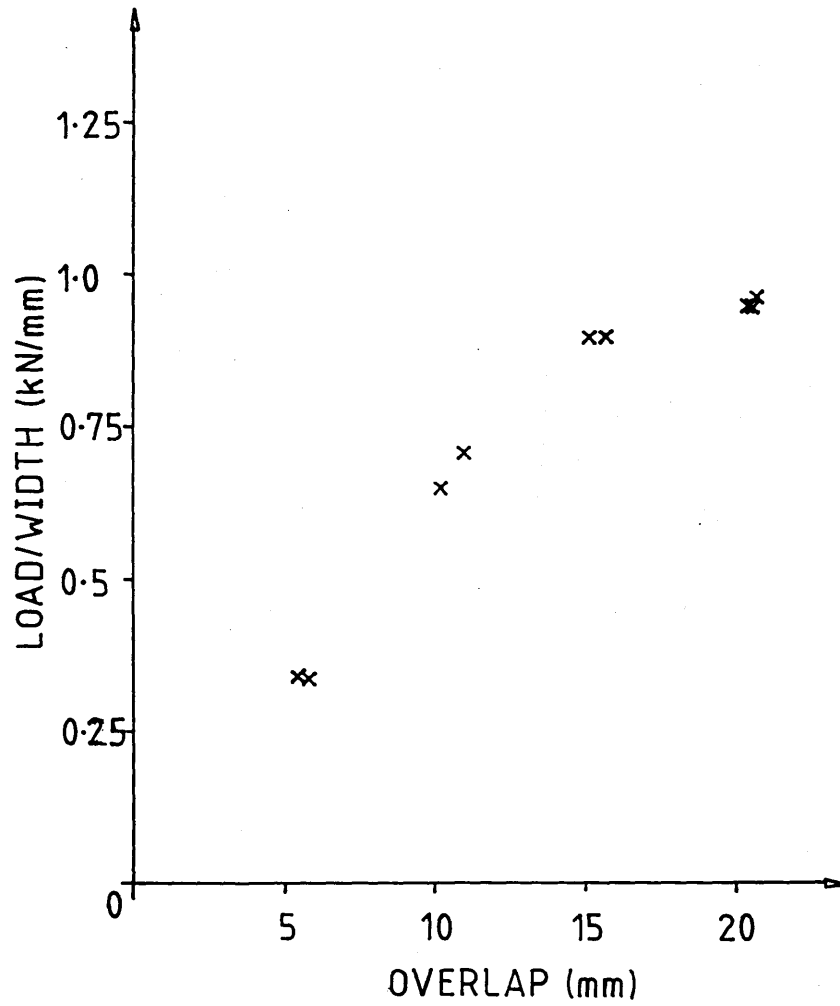


FIGURE 2.15

VARIATION OF JOINT STRENGTH  
WITH OVERLAP LENGTH

(0,0,+45,-45) , 8 ply.

Specimen Width(mm)	Specimen Overlap(mm)	Failure Load(kN)	Load/Width at failure(kN/mm)	Average Shear Stress(N/mm <sup>2</sup> )
15.00	5.44	5.08	0.34	62.2
15.00	5.56	5.08	0.34	60.9
15.00	10.9	10.7	0.71	65.4
14.94	10.1	9.80	0.66	64.9
14.96	15.2	13.5	0.90	59.4
14.96	15.6	13.4	0.90	57.4
14.98	20.6	14.6	0.97	47.3
15.00	20.5	14.3	0.95	46.5
15.00	20.4	14.2	0.95	46.4

NOTE: 0.1mm thick Stabar film used in joint.  
Surface cleaning with Acetone.  
Processing temperature, 380°C.  
Crosshead speed during testing, 2mm/min.

TABLE 2.4



FIGURE 2.16(a) 20mm overlap, 0.1mm thick 450 Grade film



FIGURE 2.16(b) 40mm overlap, 0.1mm thick 450 Grade film



FIGURE 2.16(c) 20mm overlap, no PEEK film in joint



FIGURE 2.16(d) 20mm overlap, 2 layers 0.1 mm thick  
450 grade film

FIGURE 2.16



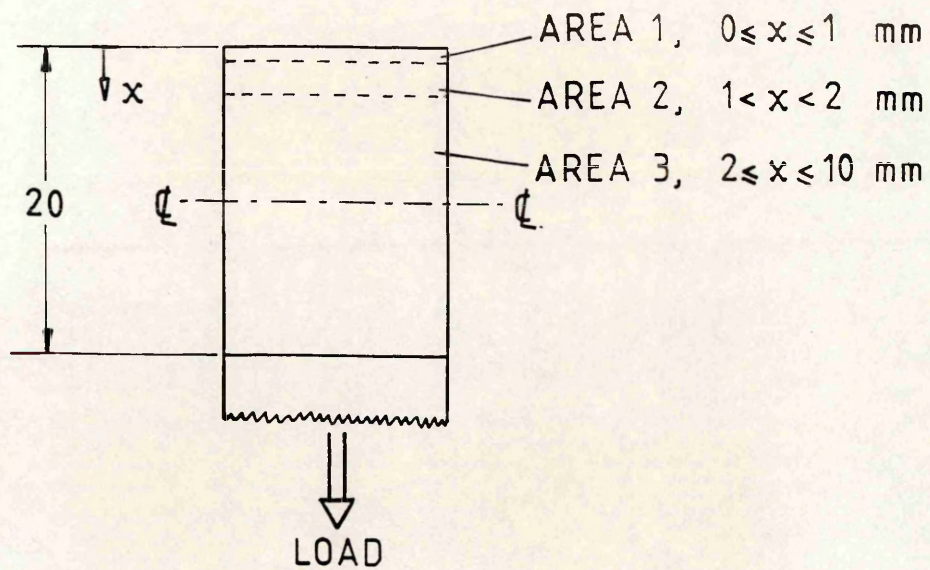


FIGURE 2.17(a) SEM examination Areas

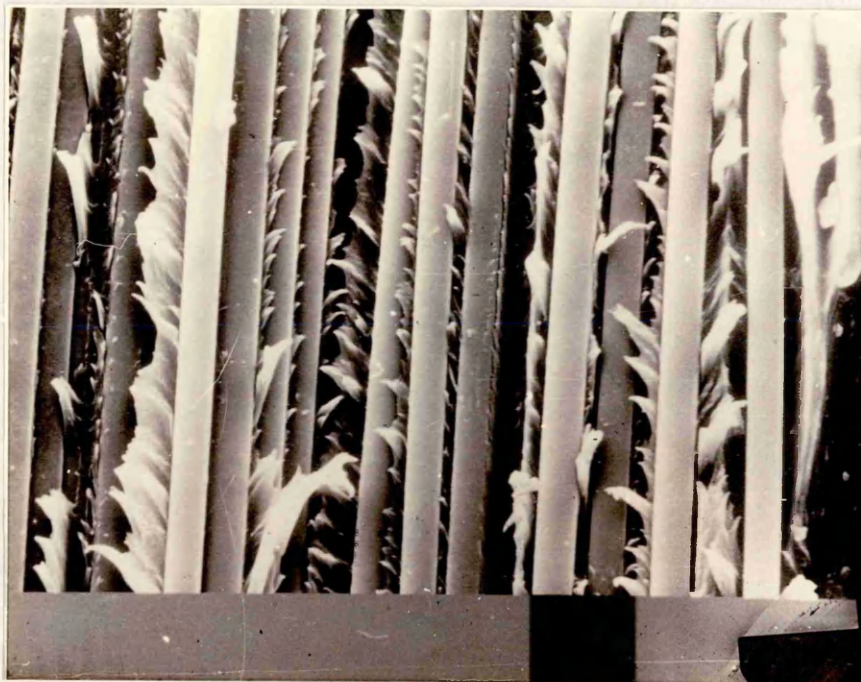


FIGURE 2.17(b) SEM micrograph of joint failure surface in Area 1 of Fig. 2.17(a)

FIGURE 2.17



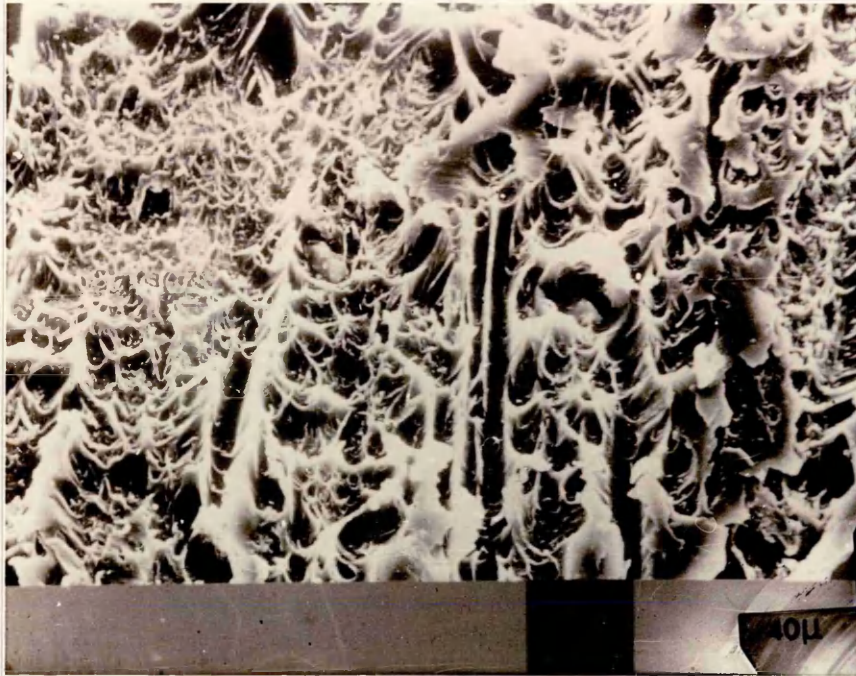


FIGURE 2.18(a) SEM micrograph of joint failure surface in Area 2 of Fig. 2.17(a)

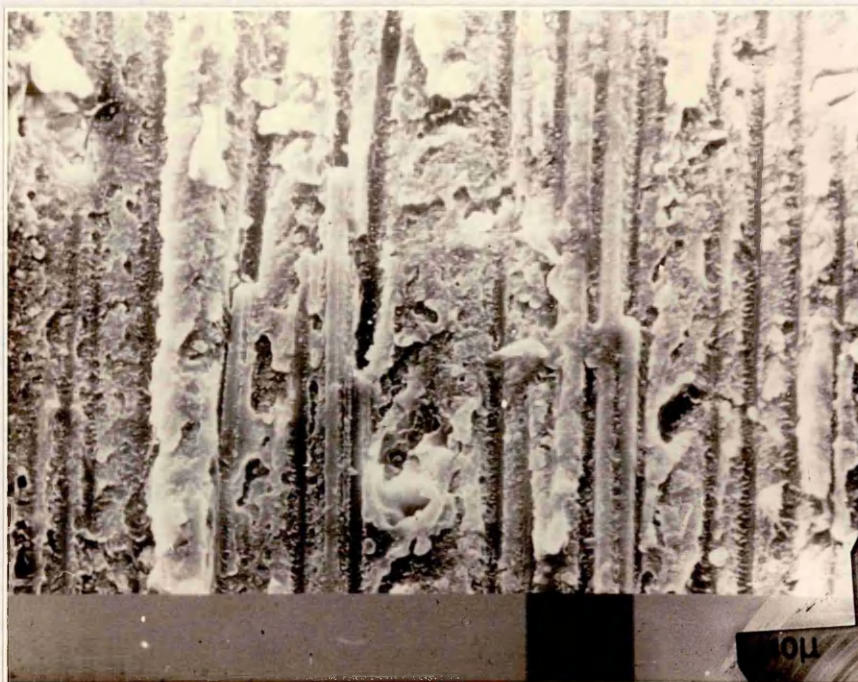
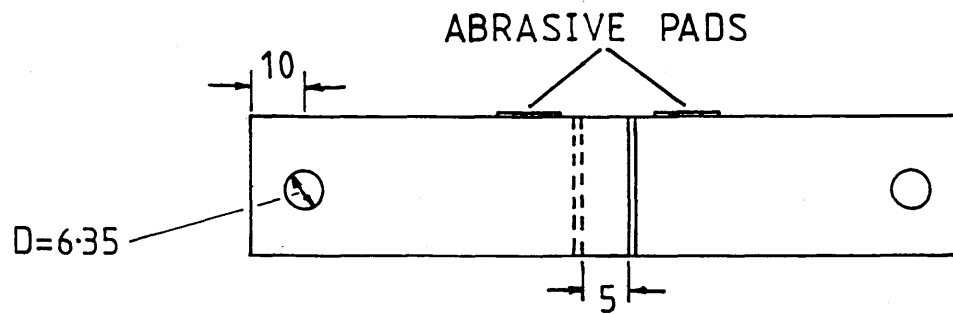
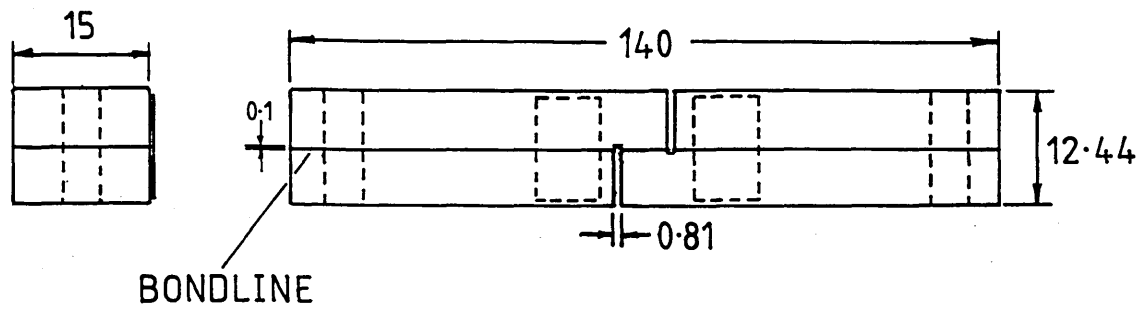


FIGURE 2.18(b) SEM micrograph of joint failure surface in Area 3 of Fig. 2.17(a)

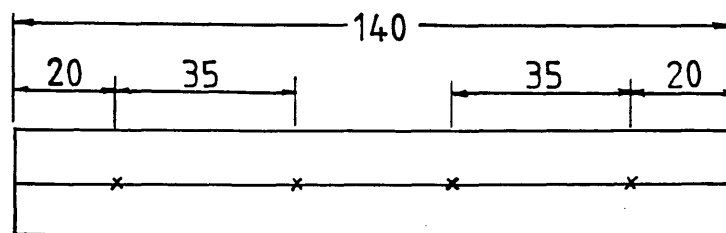
FIGURE 2.18

# DIMENSIONS OF THICK ADHEREND SPECIMEN

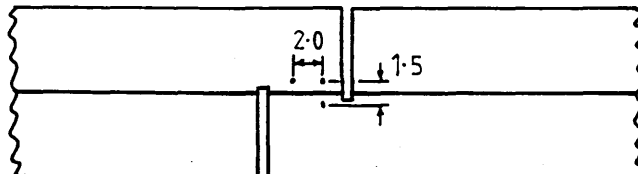


DIMENSIONS IN mm

ALUMINIUM ALLOY L93



POSITION OF BONDLINE  
CONTROL WIRES



POSITION OF EXTENSOMETER  
PICK-UP POINTS

FIGURE 3.1



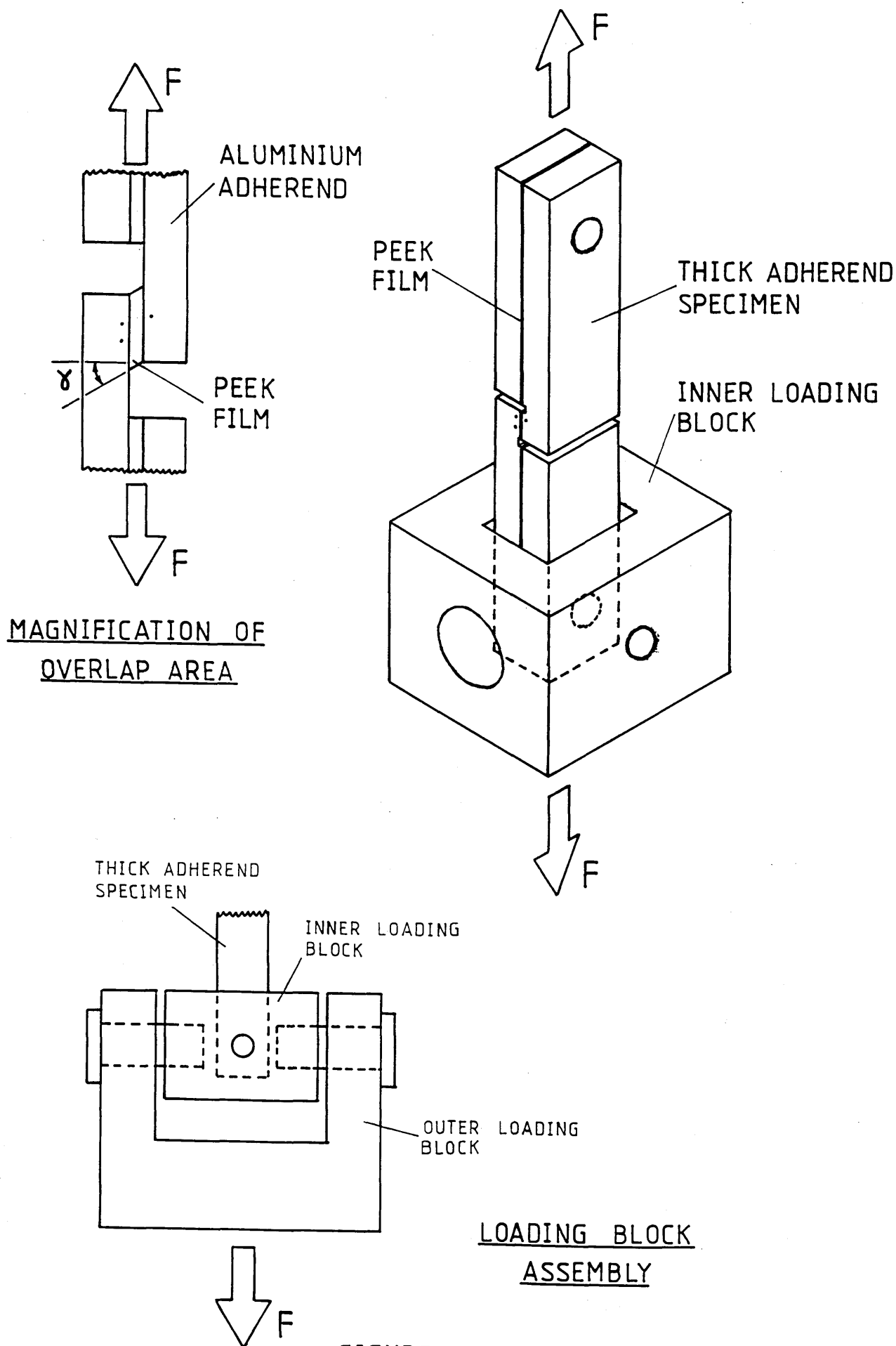


FIGURE 3.2

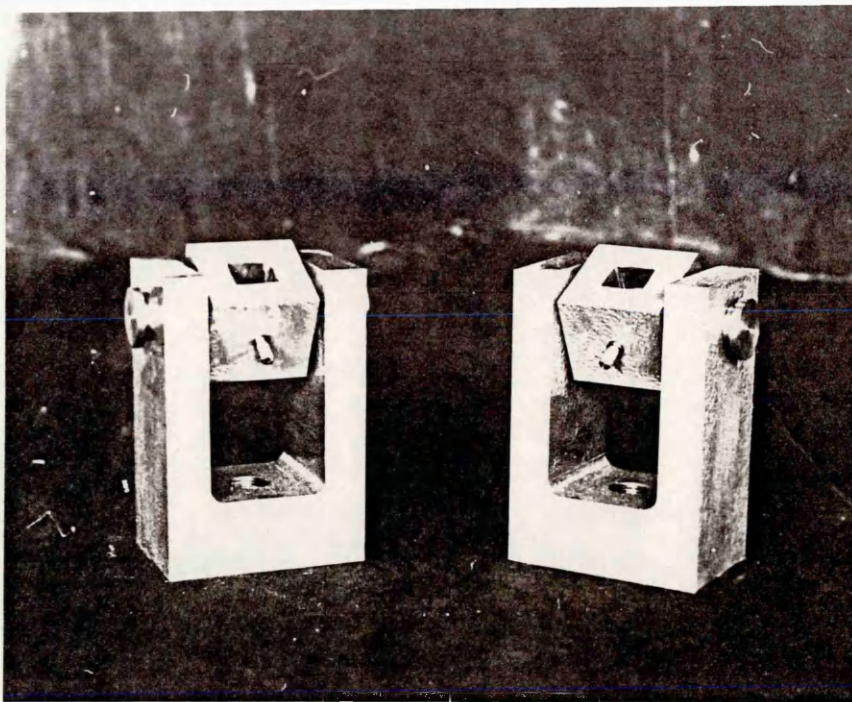


FIGURE 3.3(a) Photograph of thick adherend specimen loading blocks

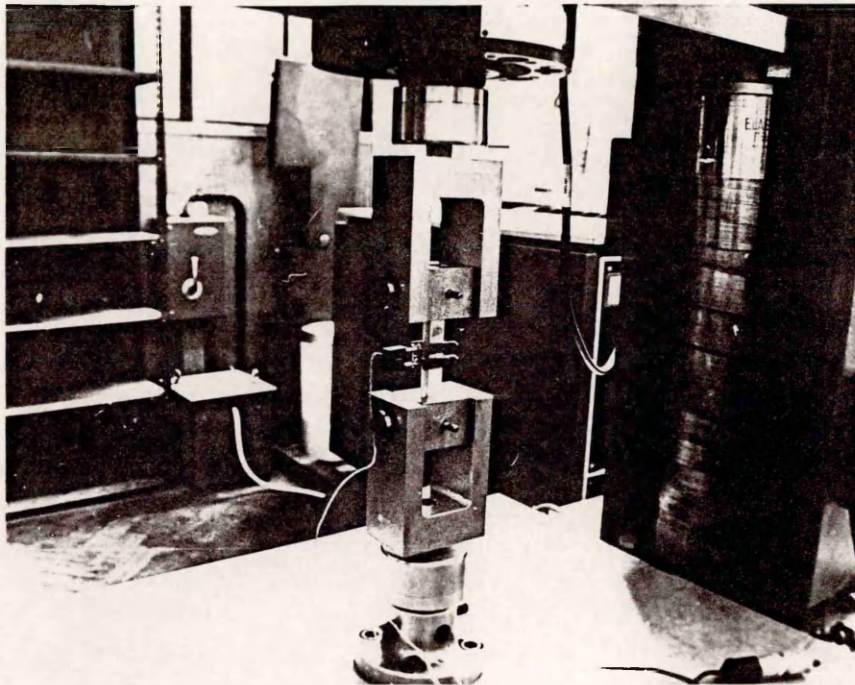
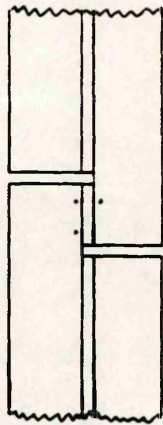


FIGURE 3.3(b) Photograph of loading blocks during testing of specimen

FIGURE 3.3



CORRECT



WRONG

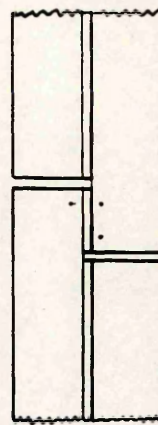


FIGURE 3.4(a) Arrangement of Extensometer  
Pick-Up Points (Ref. 12)

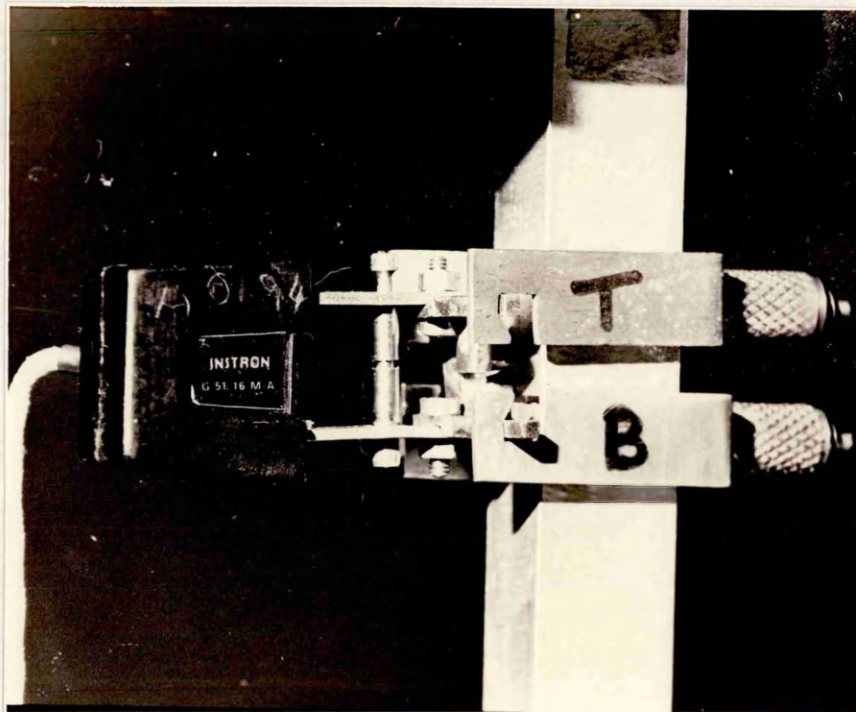


FIGURE 3.4(b) Photograph of extensometer on  
thick adherend specimen

FIGURE 3.4



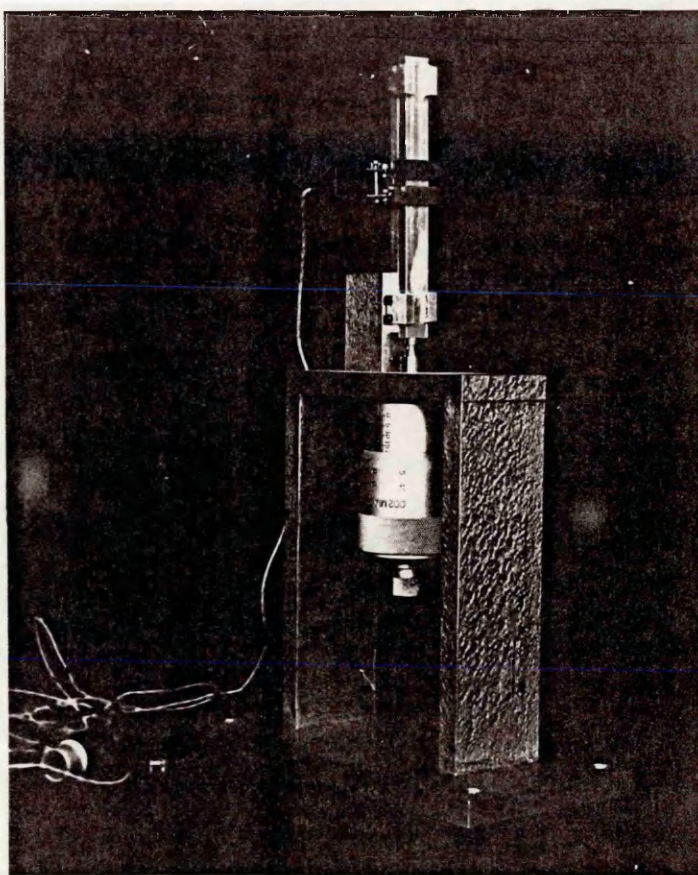


FIGURE 3.5 Photograph of extensometer mounted on calibration frame

	Actual Micrometer Displacements(mm)				
	0.01	0.05	0.10	0.15	0.20
Error at Calibration	+20%	+6%	+2%	0%	-1%
Error after Repositioning	-10%	-12%	-3%	+1%	-0.25%

$$\text{Error} = \frac{\text{measured displacement} - \text{micrometer displacement}}{\text{micrometer displacement}}$$

TABLE 3.1 Errors Recorded on Calibration Frame

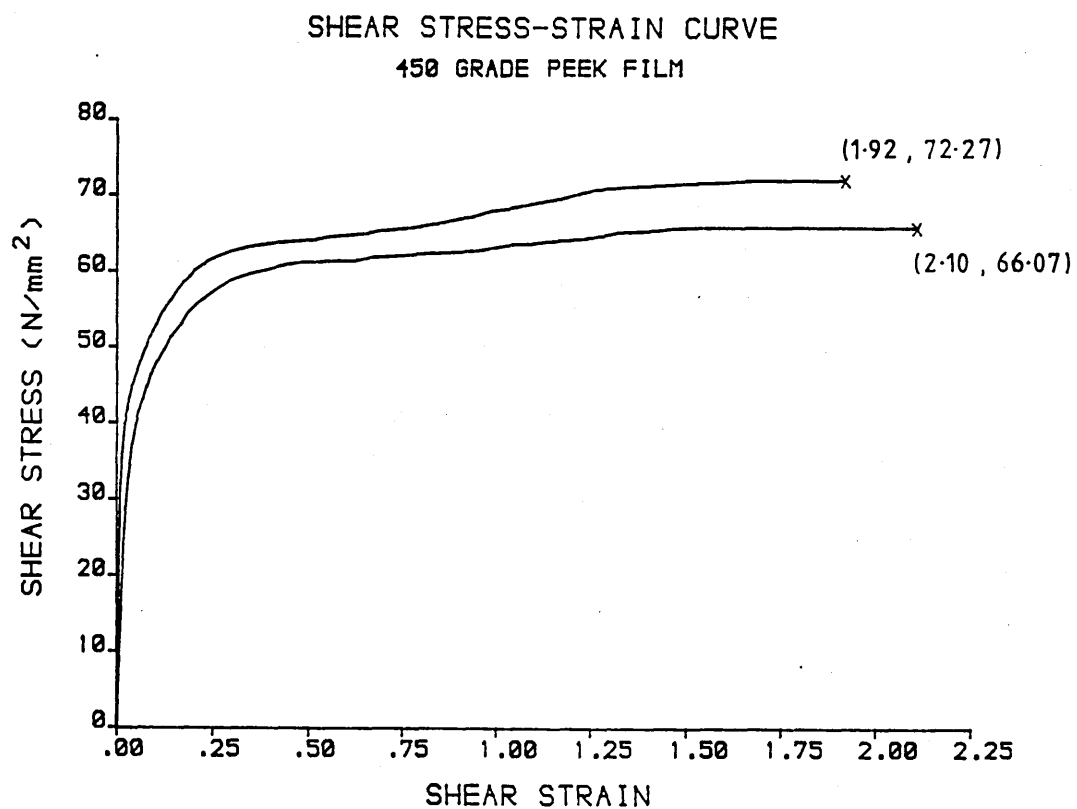
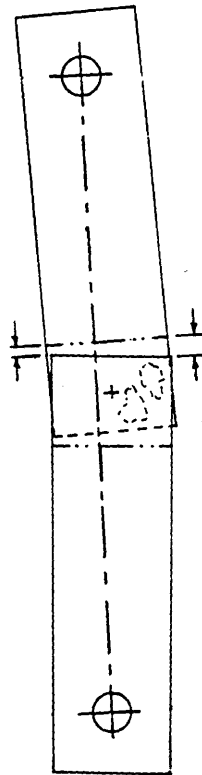
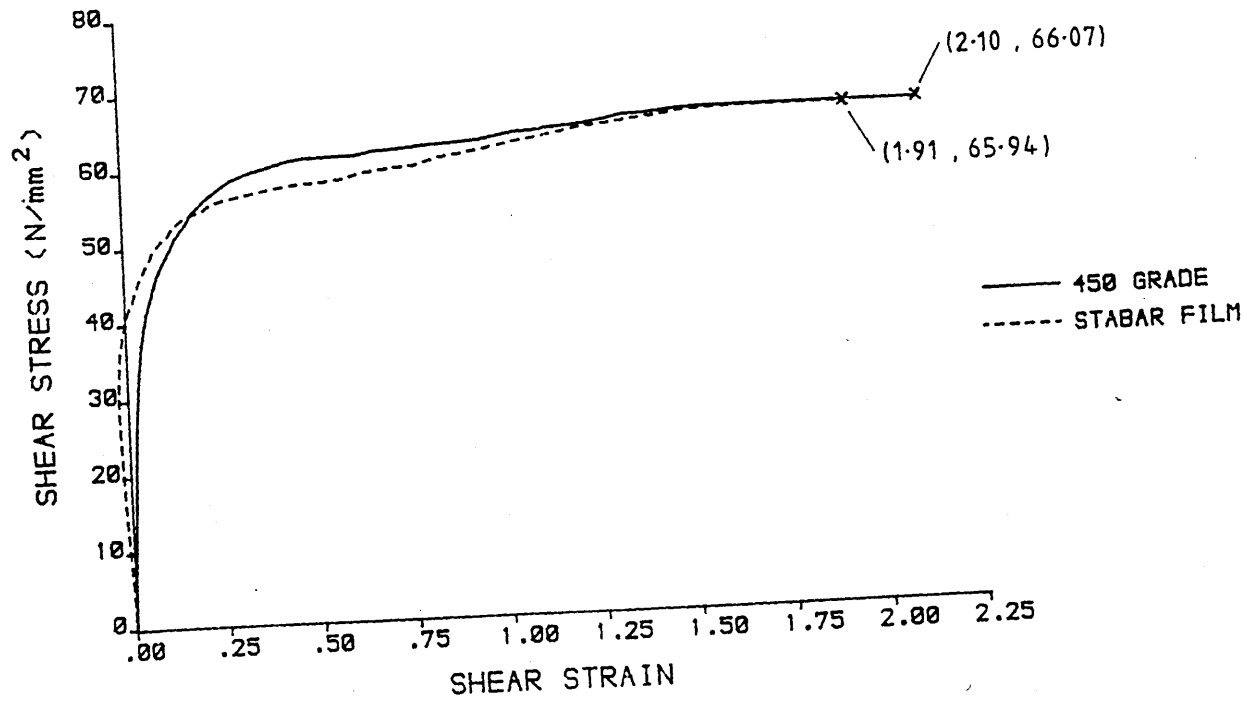


FIGURE 3.6



INFLUENCE OF VOIDS ON  
DISPLACEMENT MEASUREMENT  
(Ref. 12)

FIGURE 3.7



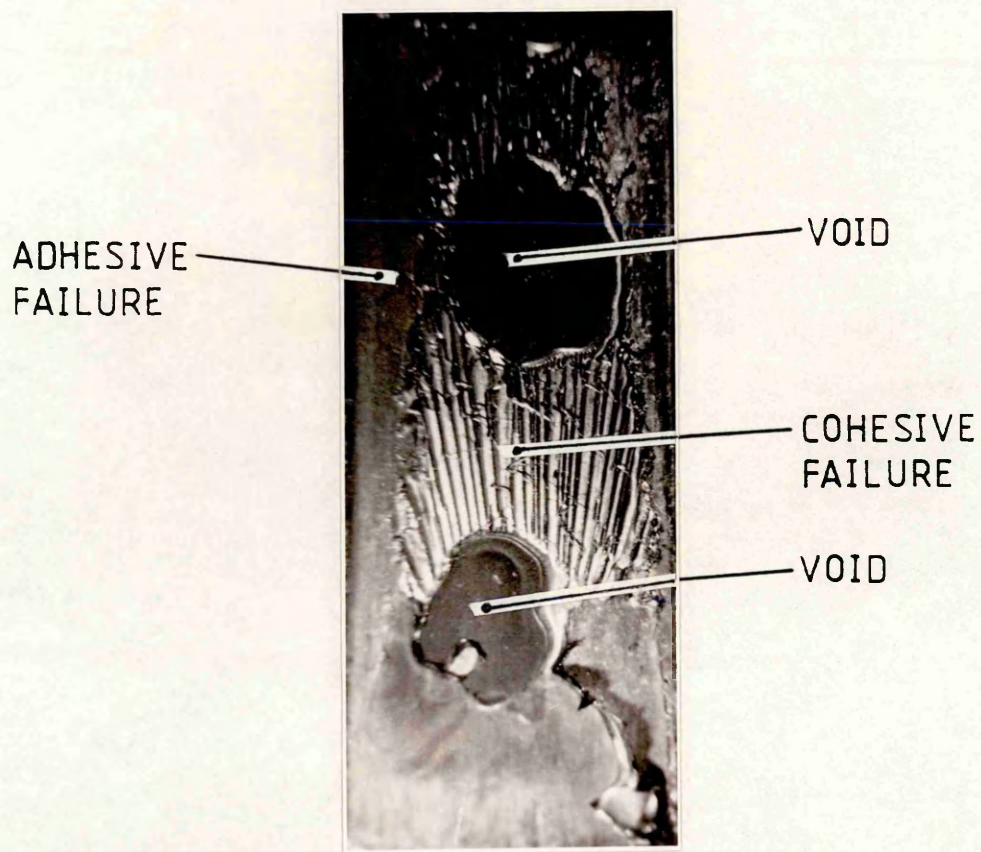


FIGURE 3.8(a) Failure surface of thick adherend specimen, 0.1mm thick Stabar film

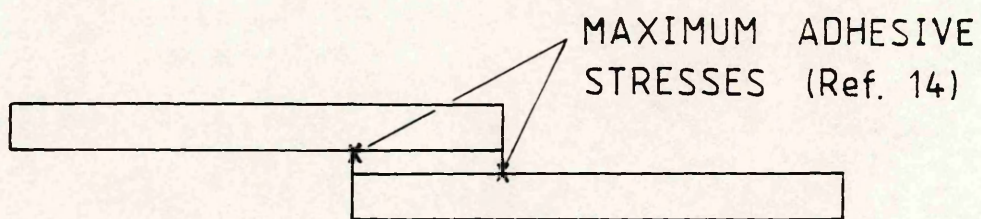


FIGURE 3.8(b)

FIGURE 3.8

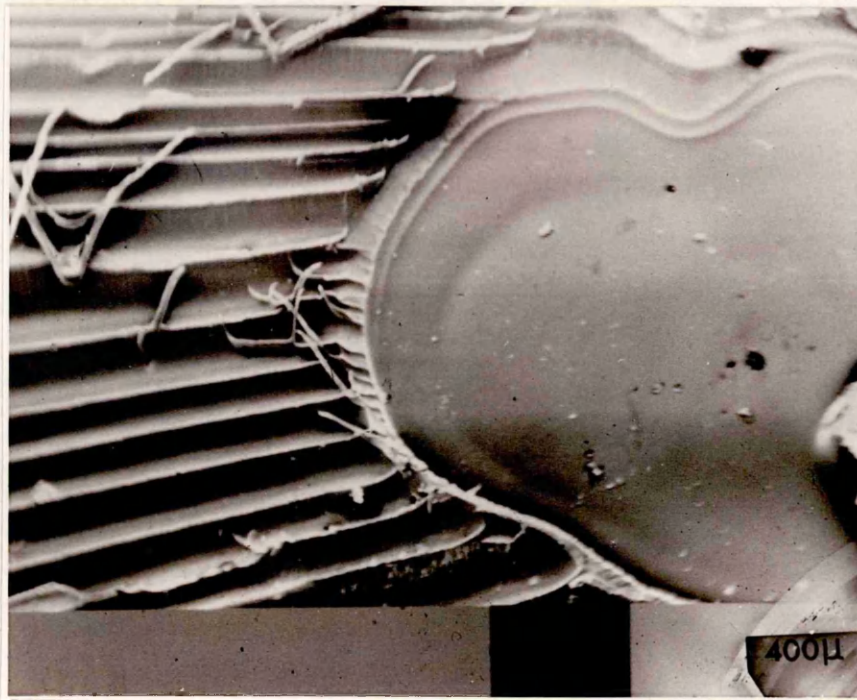


FIGURE 3.9(a) SEM micrograph of failure surface of thick adherend specimen

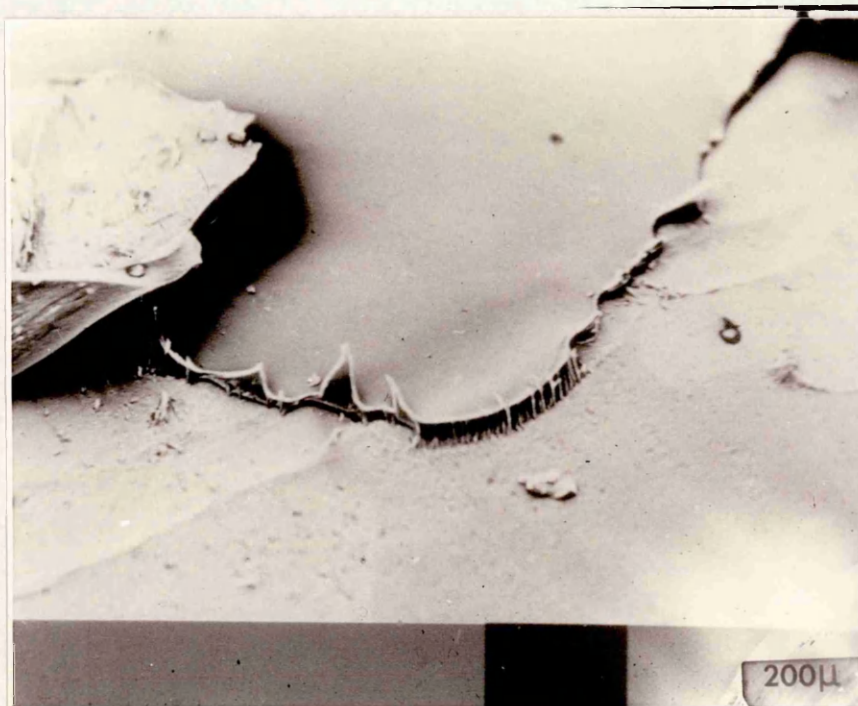


FIGURE 3.9(b) SEM micrograph showing void thickness in bondline of thick adherend specimen

FIGURE 3.9



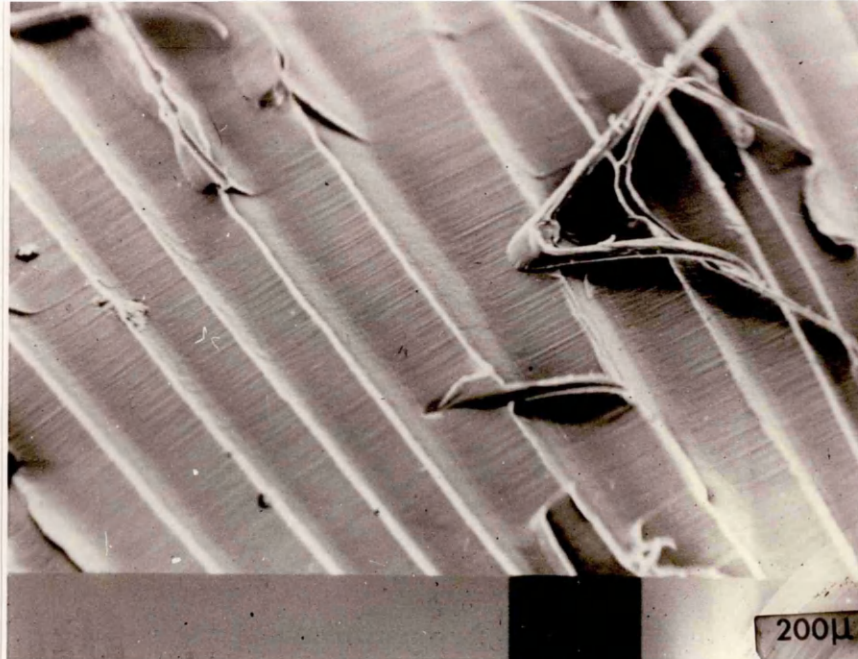


FIGURE 3.10(a) SEM micrograph of cohesive failure in thick adherend specimen

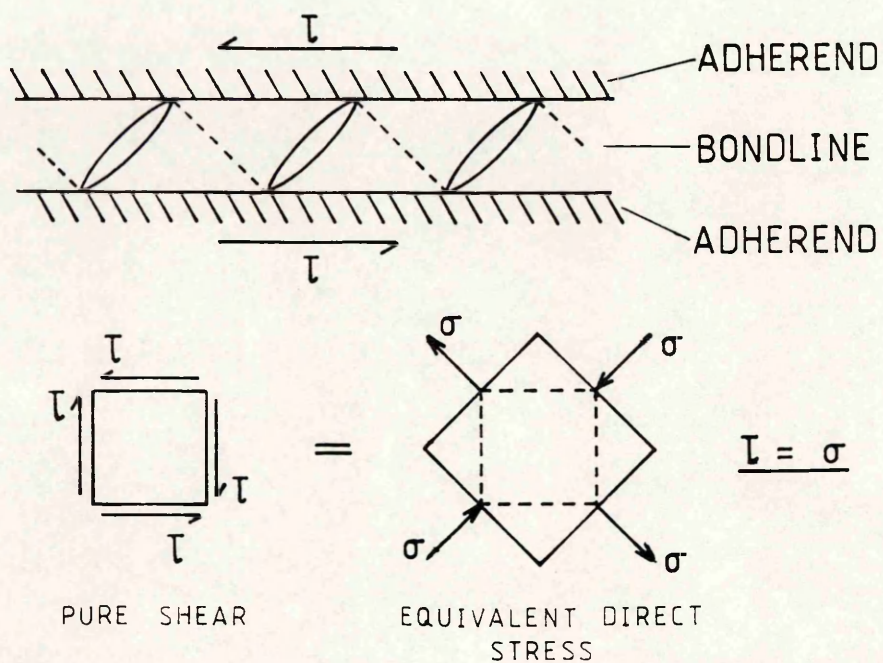
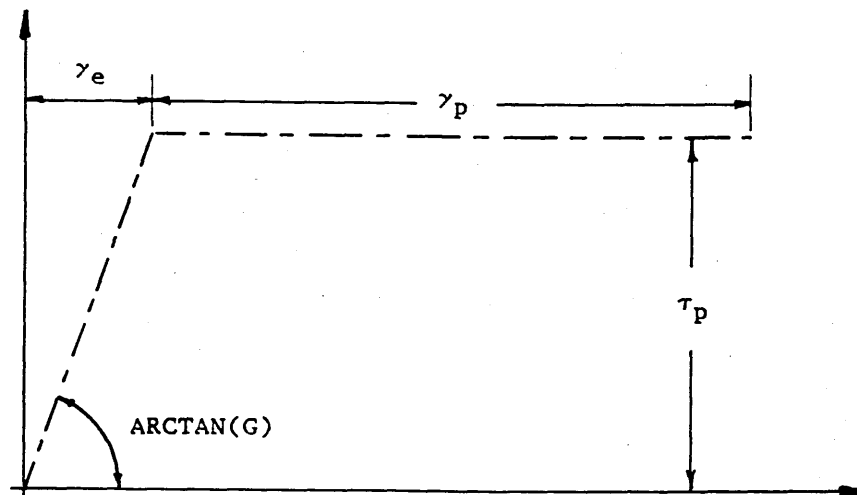


FIGURE 3.10(b) Possible Formation of Cohesive Failure Surface

FIGURE 3.10

# ELASTIC - PLASTIC REPRESENTATION



SHEAR STRESS-STRAIN CURVE  
450 GRADE PEEK FILM

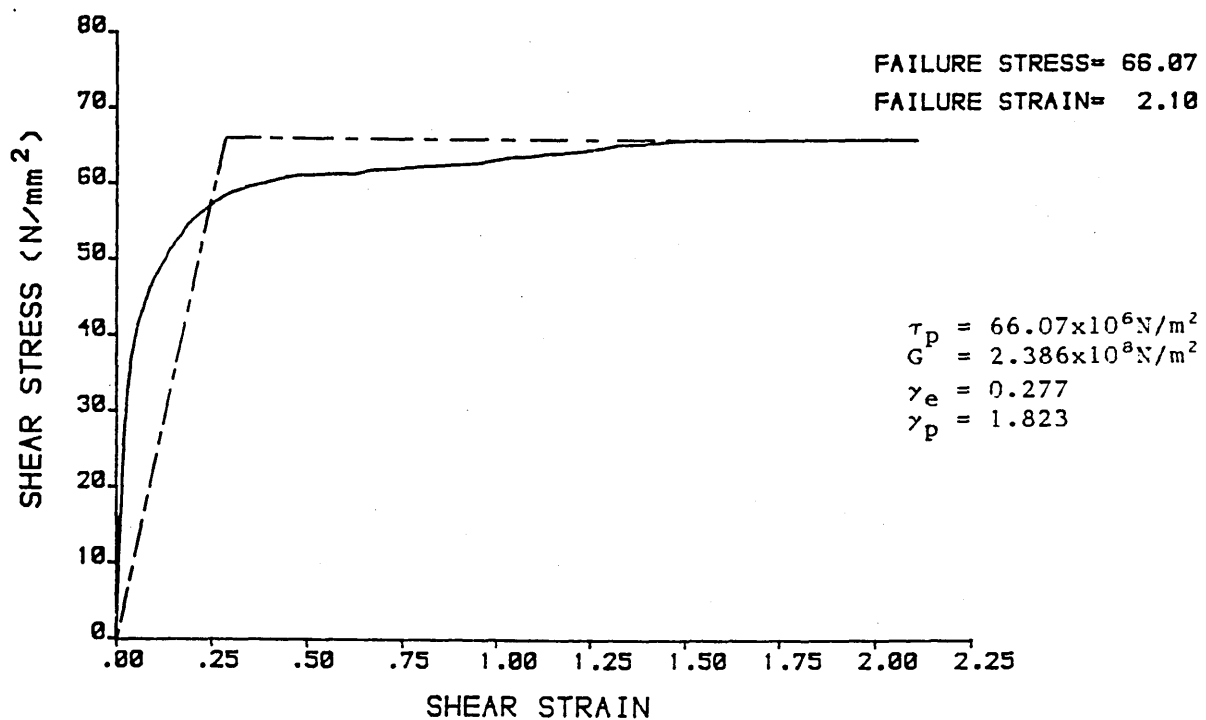
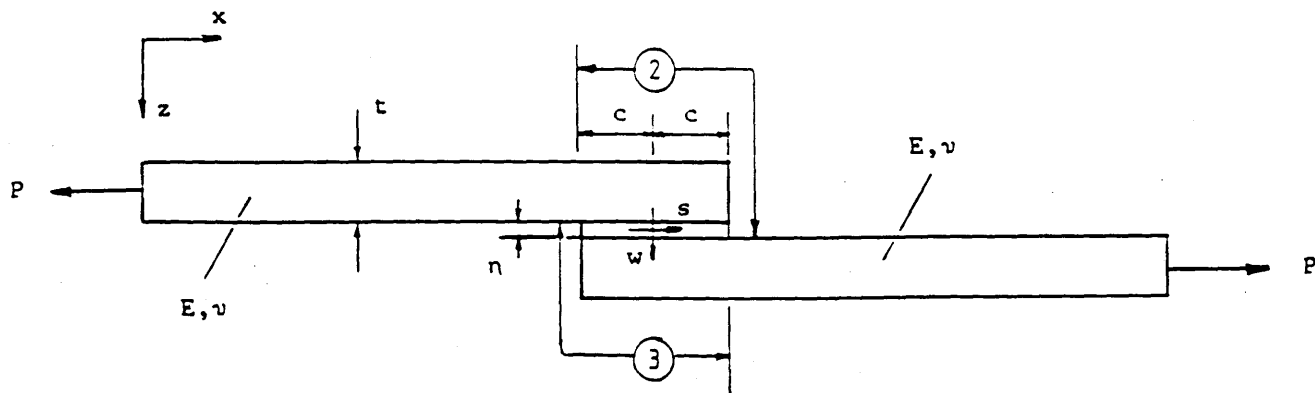
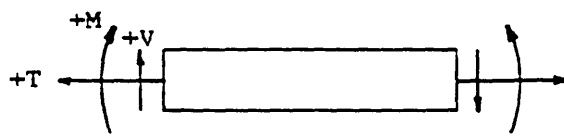


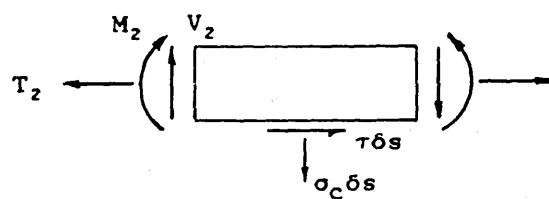
FIGURE 4.1



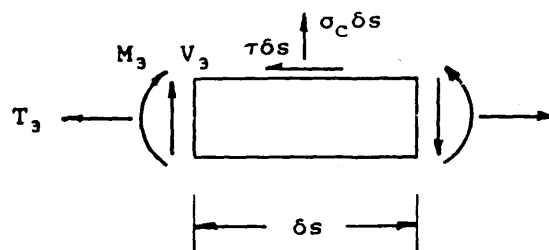
CO-ORDINATE SYSTEM AND NOMENCLATURE  
FOR SINGLE-LAP JOINT



SIGN CONVENTION



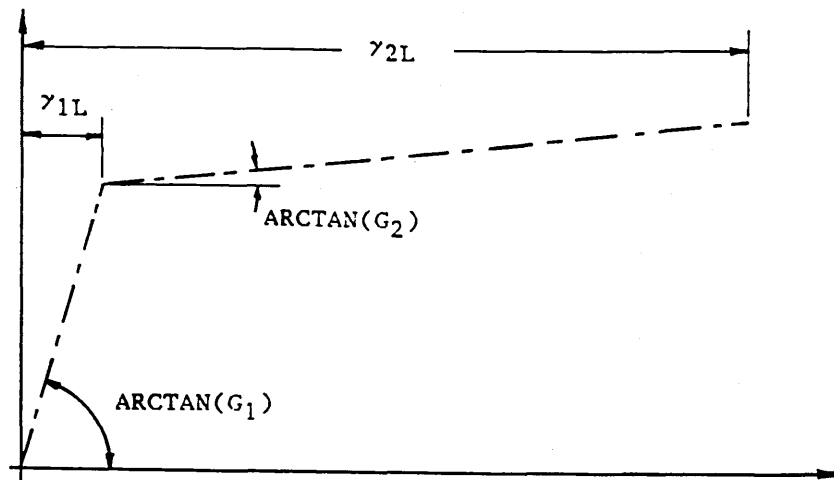
LOADS ON ELEMENT  
OF REGION 2



LOADS ON ELEMENT  
OF REGION 3

FIGURE 4.2

## BI - ELASTIC REPRESENTATION



### SHEAR STRESS-STRAIN CURVE 450 GRADE PEEK FILM

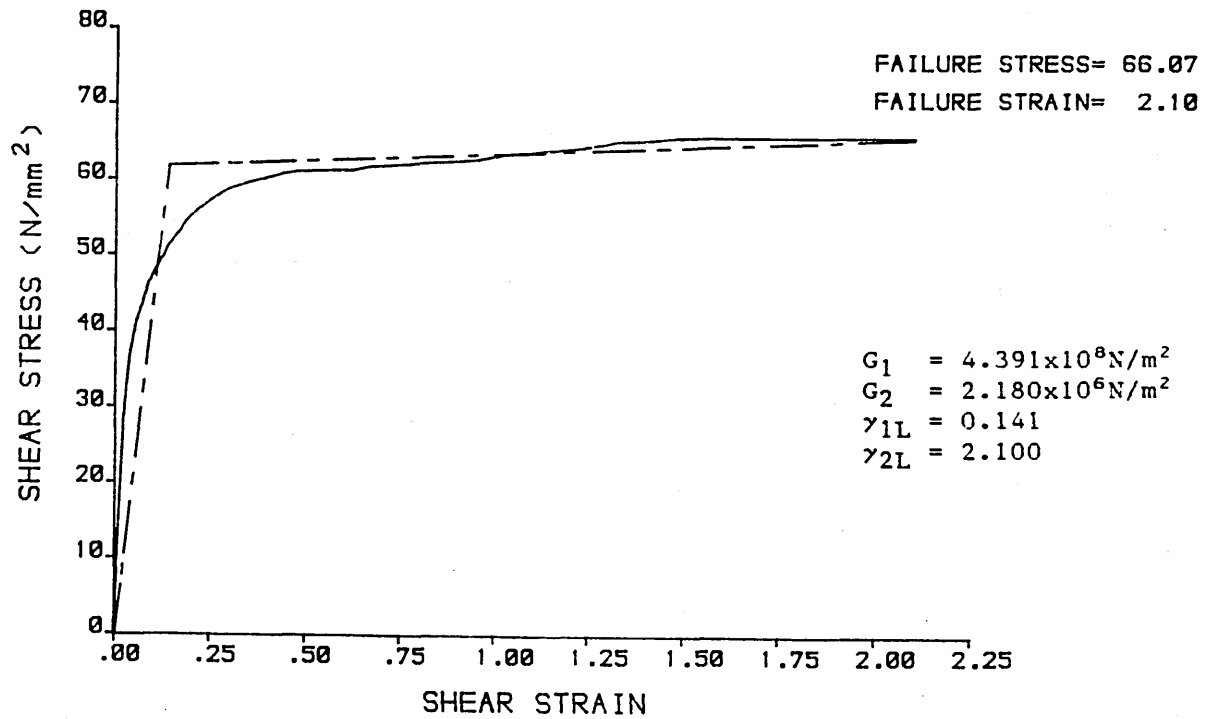


FIGURE 4.3

## ADHESIVE MATERIAL PROPERTIES

### Shear

$$\tau_{ult} = 66.07 \times 10^6 \text{ N/m}^2$$

$$\gamma_{ult} = 2.10$$

Refer to Figures 4.1 and 4.3 for elastic-plastic and bi-elastic approximations to stress-strain curve.

### Peel

$$E_c = 3.6 \times 10^9 \text{ N/m}^2$$

$$E_{c,bi} = 4.37 \times 10^9 \text{ N/m}^2 \quad (\text{Eqn. 4.56})$$

$$E_c = 1.11 \times 10^9 \text{ N/m}^2 \quad (\text{Eqn. 4.21})$$

$$\nu_c = 0.42$$

## ADHEREND MATERIAL PROPERTIES

1)  $(0,0,0,0)_s$ , 8 ply.

$$E = 134 \times 10^9 \text{ N/m}^2$$

$$E_f = 121 \times 10^9 \text{ N/m}^2$$

$$\nu = 0.29$$

$$\sigma_{x,max} = 2130 \times 10^6 \text{ N/m}^2$$

$$\epsilon_{x,max} = 0.0159$$

$$t = 0.0011 \text{ m}$$

2)\*  $(0,0,+45,-45)_s$ , 8 ply.

$$E = 73.3 \times 10^9 \text{ N/m}^2$$

$$E_f = 115 \times 10^9 \text{ N/m}^2$$

$$\nu = 0.681$$

$$t = 0.00103 \text{ m}$$

3)\*  $(0,+45,-45,0)_s$ , 8 ply.

$$E = 73.3 \times 10^9 \text{ N/m}^2$$

$$E_f = 83.5 \times 10^9 \text{ N/m}^2$$

$$\nu = 0.681$$

$$t = 0.0011 \text{ m}$$

4)\*  $(0,+45,-45,90)_s$ , 8 ply

$$E = 48.9 \times 10^9 \text{ N/m}^2$$

$$E_f = 82.3 \times 10^9 \text{ N/m}^2$$

$$\nu = 0.293$$

$$t = 0.001 \text{ m}$$

5)\*  $(+45,-45,+45,-45)_s$ , 8 ply.

$$E = 17.4 \times 10^9 \text{ N/m}^2$$

$$E_f = 17.1 \times 10^9 \text{ N/m}^2$$

$$\nu = 0.749$$

$$t = 0.00107 \text{ m}$$

## Transverse Properties (All Laminates)

$$E_n = 8.9 \times 10^9 \text{ N/m}^2$$

$$\sigma_{n,max} = 100 \times 10^6 \text{ N/m}^2 \quad (\text{conservative value})$$

$$120 \times 10^6 \text{ N/m}^2 \quad (\text{maximum value})$$

\*  $E, E_f$  and  $\nu$  for this laminate calculated using Westland Helicopter's program CAMEL 4, (Ref. 31)

TABLE 4.1

COMPARISON BETWEEN EXPERIMENT AND THEORY  
FOR ADHEREND FAILURE

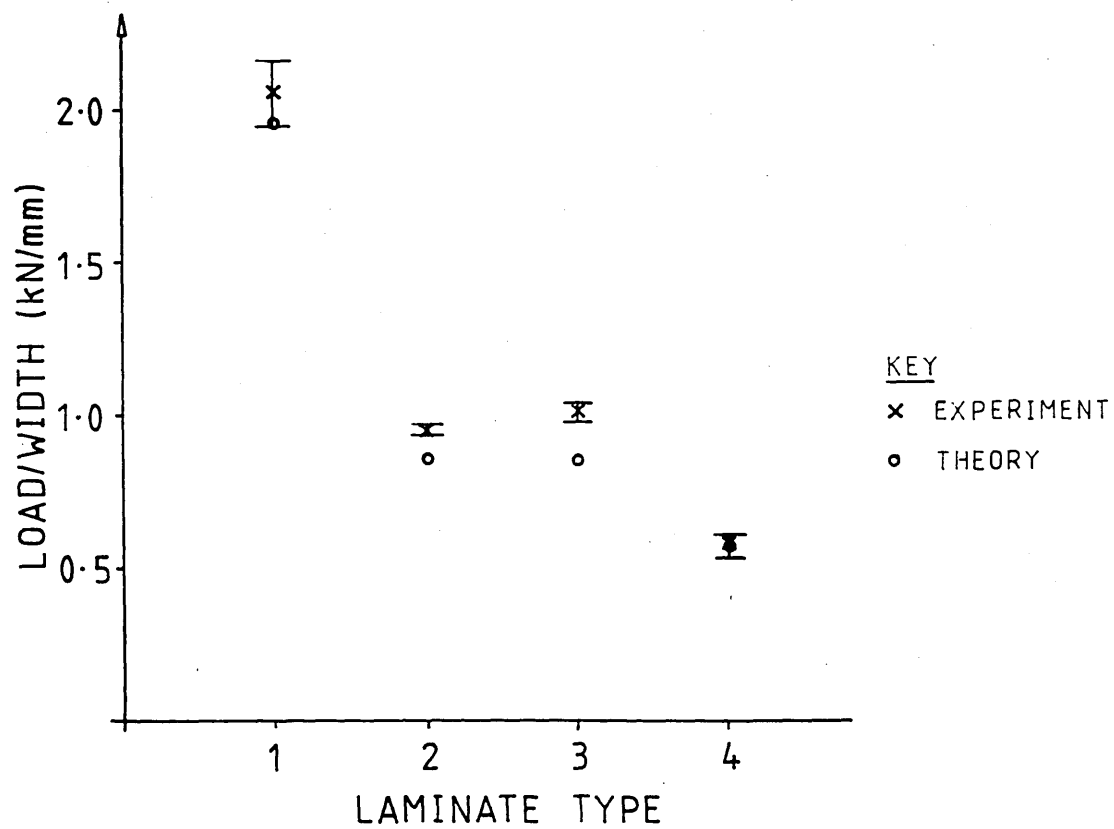


FIGURE 4.4

# INFLUENCE OF OVERLAP LENGTH ON JOINT STRENGTH

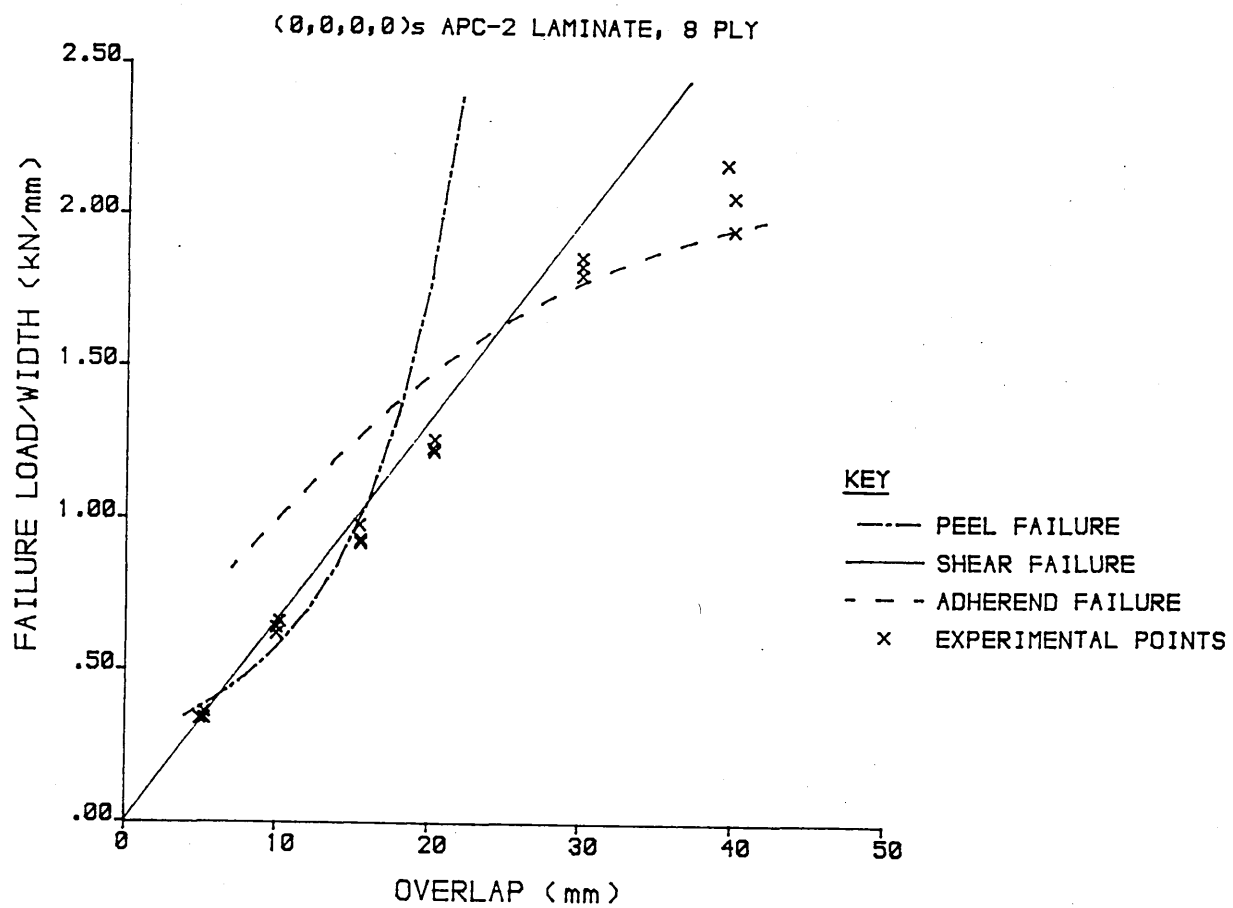


FIGURE 4.5

# INFLUENCE OF OVERLAP LENGTH ON JOINT STRENGTH

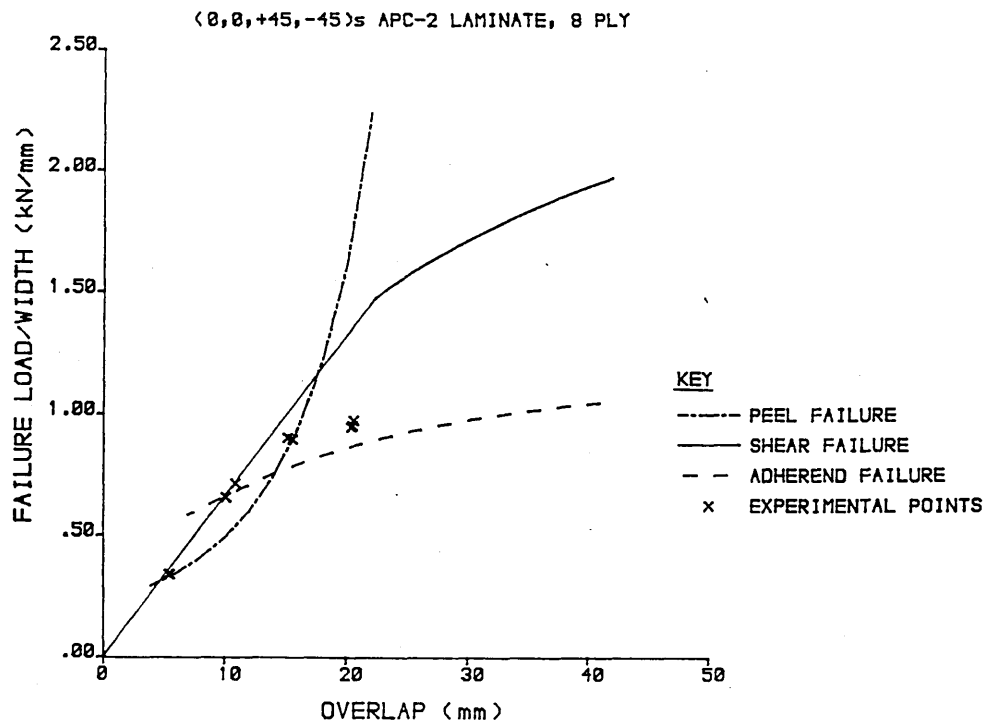


FIGURE 4.6(a) Peel failure curve plotted with  $\sigma_{n,max} = 100 \times 10^6 \text{ N/m}^2$

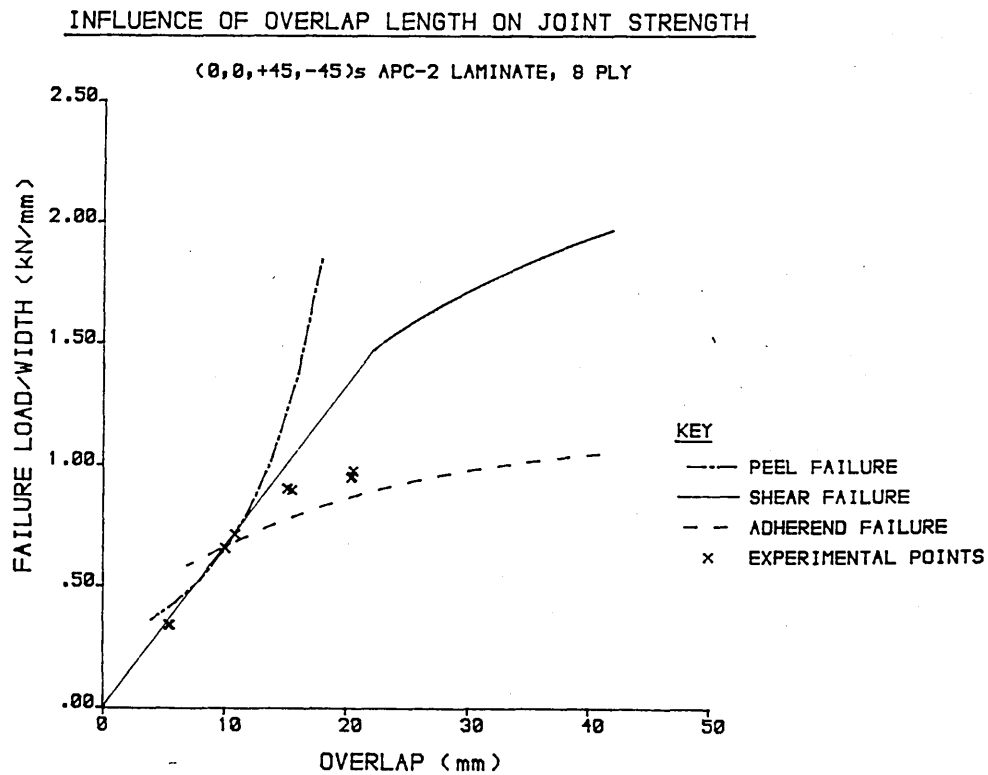
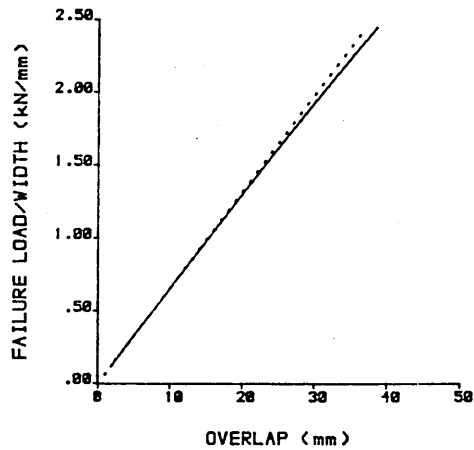


FIGURE 4.6(b) Peel failure curve plotted with  $\sigma_{n,max} = 120 \times 10^6 \text{ N/m}^2$

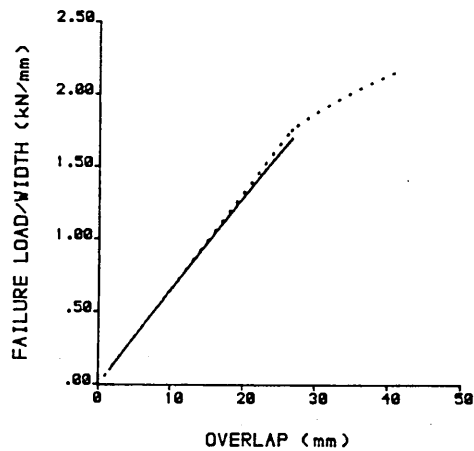


# BI-ELASTIC MODELLING FOR SHEAR FAILURE

$[0,0,0,0]_s$  APC-2 LAMINATE, 8 PLY



$[0,0,+45,-45]_s$  APC-2 LAMINATE, 8 PLY



KEY

----- ELASTIC-PLASTIC  
—— BI-ELASTIC

$[0,+45,-45,0]_s$  APC-2 LAMINATE, 8 PLY

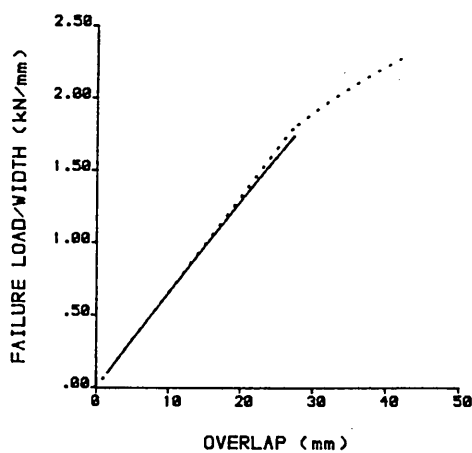
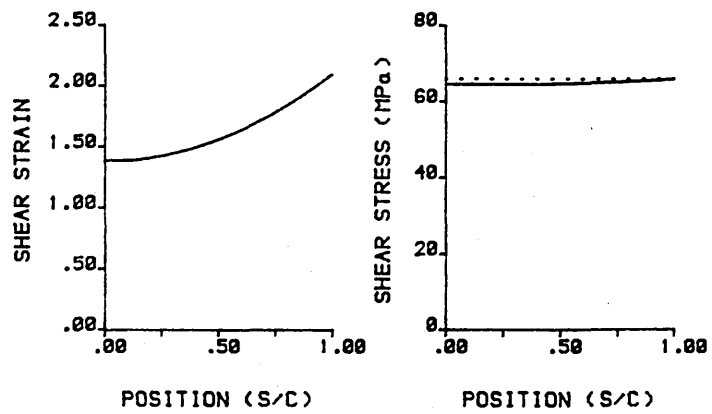
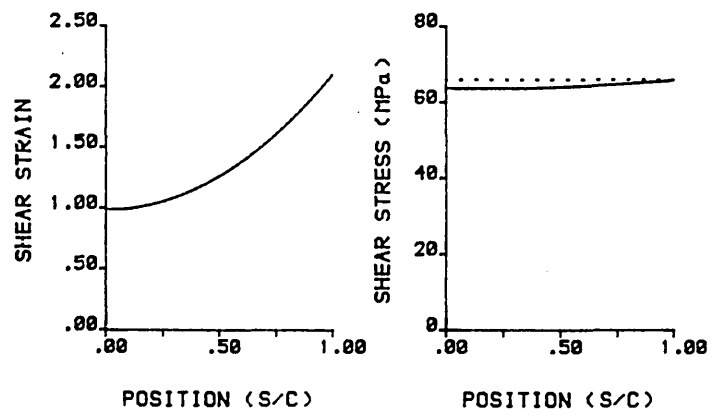


FIGURE 4.7

(0,0,0,0)s APC-2 LAMINATE, 8 PLY



(0,0,+45,-45)s APC-2 LAMINATE, 8 PLY



KEY

..... ELASTIC-PLASTIC  
 — BI-ELASTIC

(0,+45,-45,0)s APC-2 LAMINATE, 8 PLY

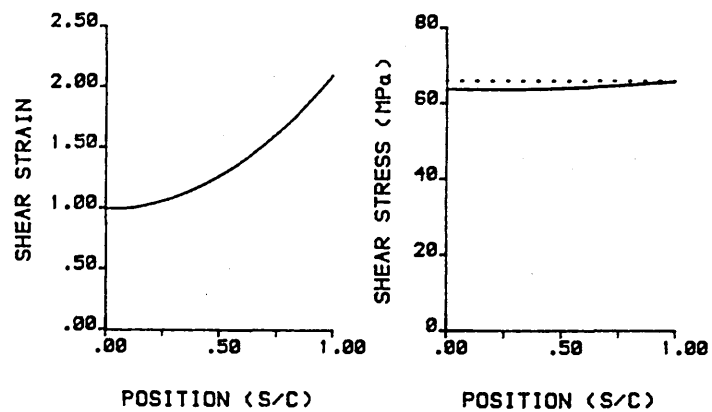


FIGURE 4.8

# PEEL STRESS DISTRIBUTION

UNIDIRECTIONAL APC-2, 20.3mm OVERLAP

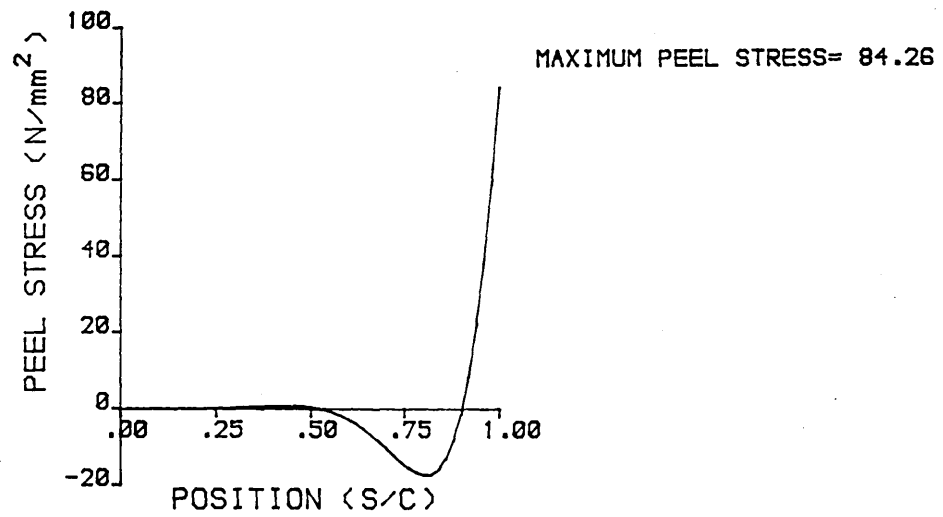


FIGURE 4.9

# ON JOINT STRENGTH

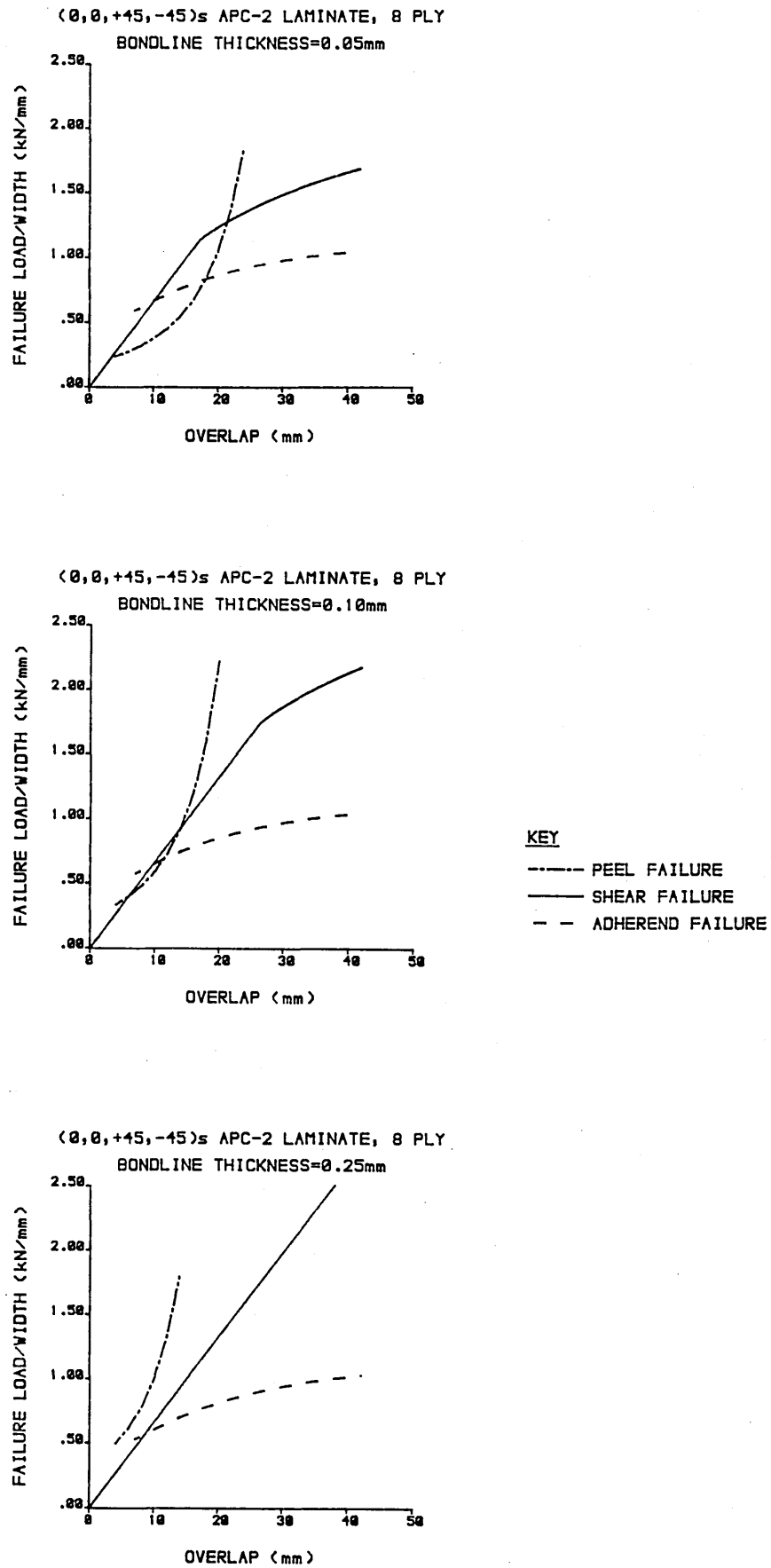


FIGURE 4.10

# INFLUENCE OF ADHEREND THICKNESS ON JOINT STRENGTH

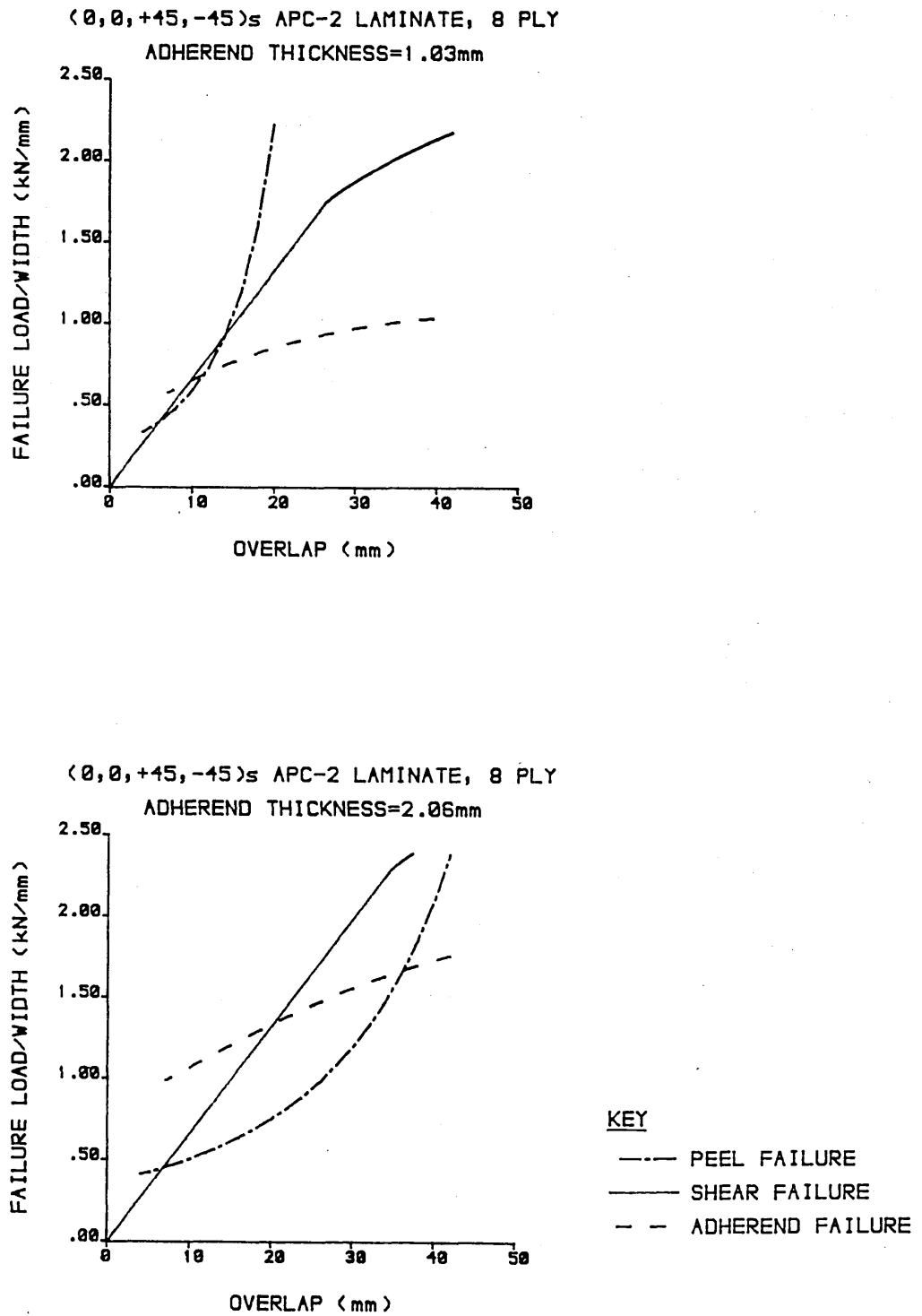


FIGURE 4.11

## EXPERIMENTAL EQUIPMENT

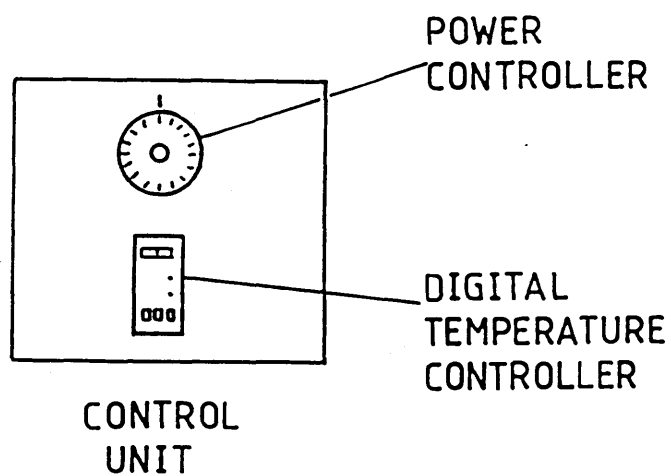
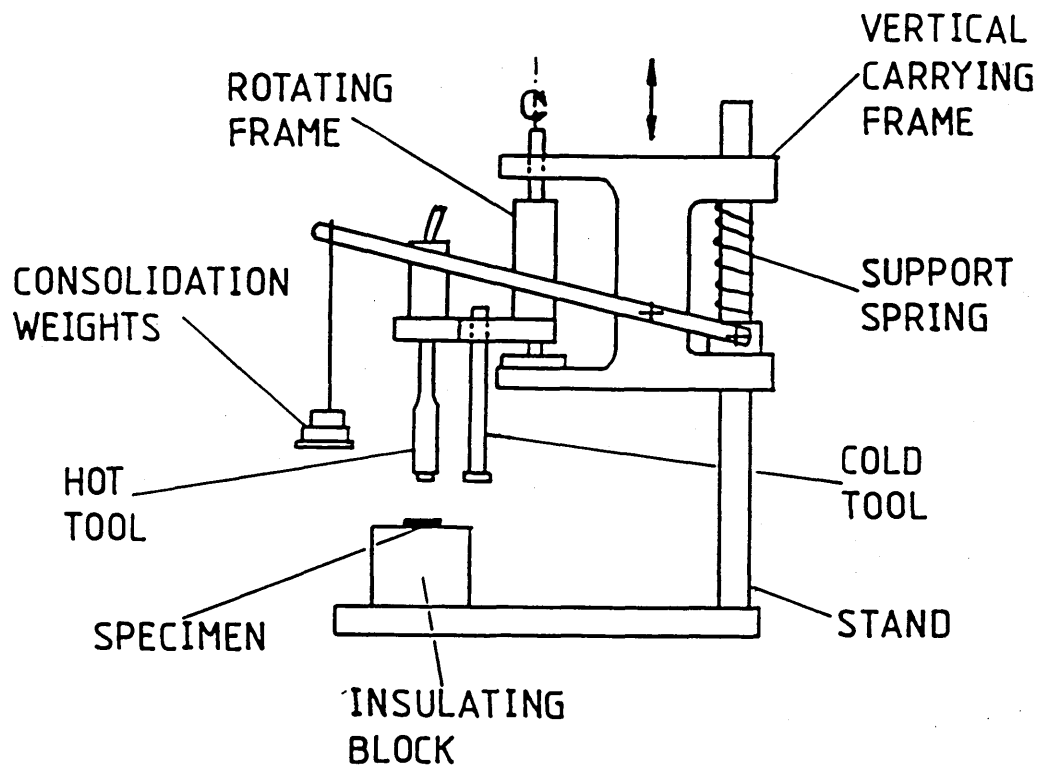


FIGURE 5.1

# SPOT WELDER

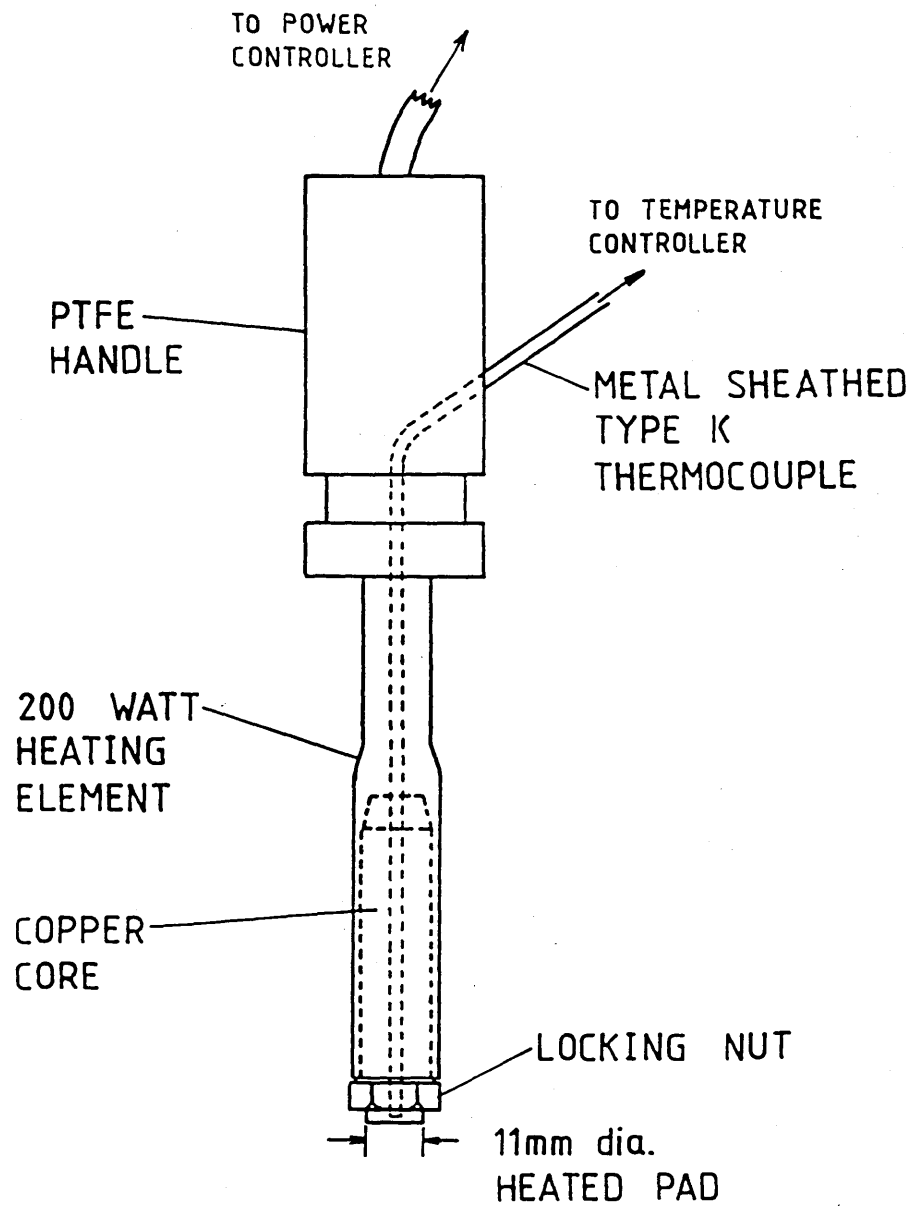


FIGURE 5.2

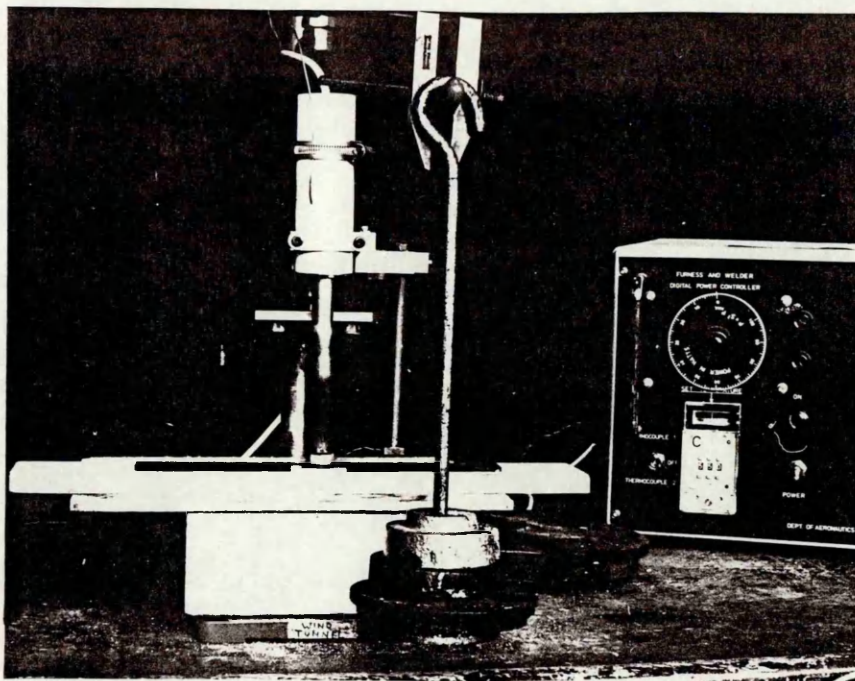


FIGURE 5.3(a) Photograph of Experimental Arrangement

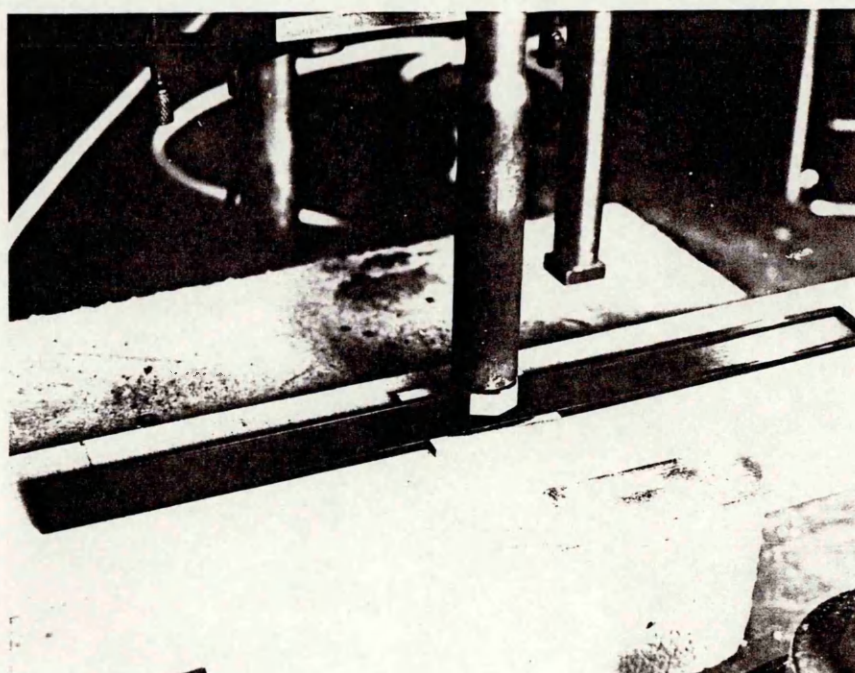


FIGURE 5.3(b) Photograph of Spot Welder SW2

FIGURE 5.3



## SPECIMEN LAYUP

### KEY

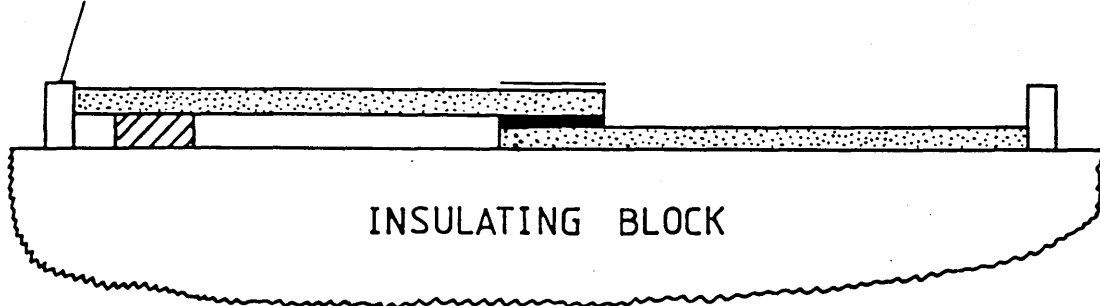
— STAINLESS STEEL

▨ PACKING PIECE

▤ COMPOSITE

■ 0.1mm thick  
STABAR FILM

PICTURE FRAME



### SPECIMEN DIMENSIONS

LENGTH = 250 mm

WIDTH = 16 mm

OVERLAP = 20 mm

FIGURE 5.4

## ARRAY WELD

TOP ADHEREND	<div>+3    +2       +1,6 +4    +5</div>	BOTTOM ADHEREND
-----------------	---	--------------------

Weld Head Position	Time at end of Heating Period (mins,secs)
-	0,00
1	2,00
2	4,10
3	6,20
4	8,30
5	10,40
6	12,50
Cold tool, 1	15,00

FIGURE 5.5

## SPECIMEN TESTING

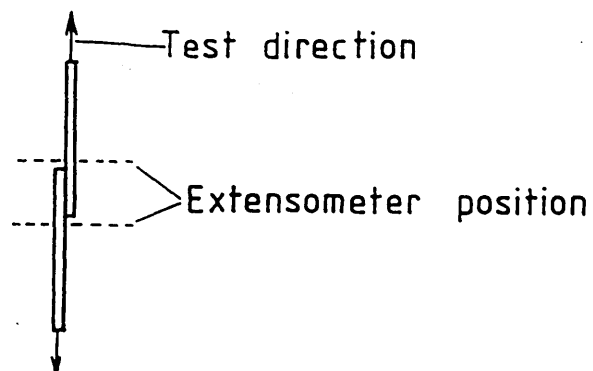
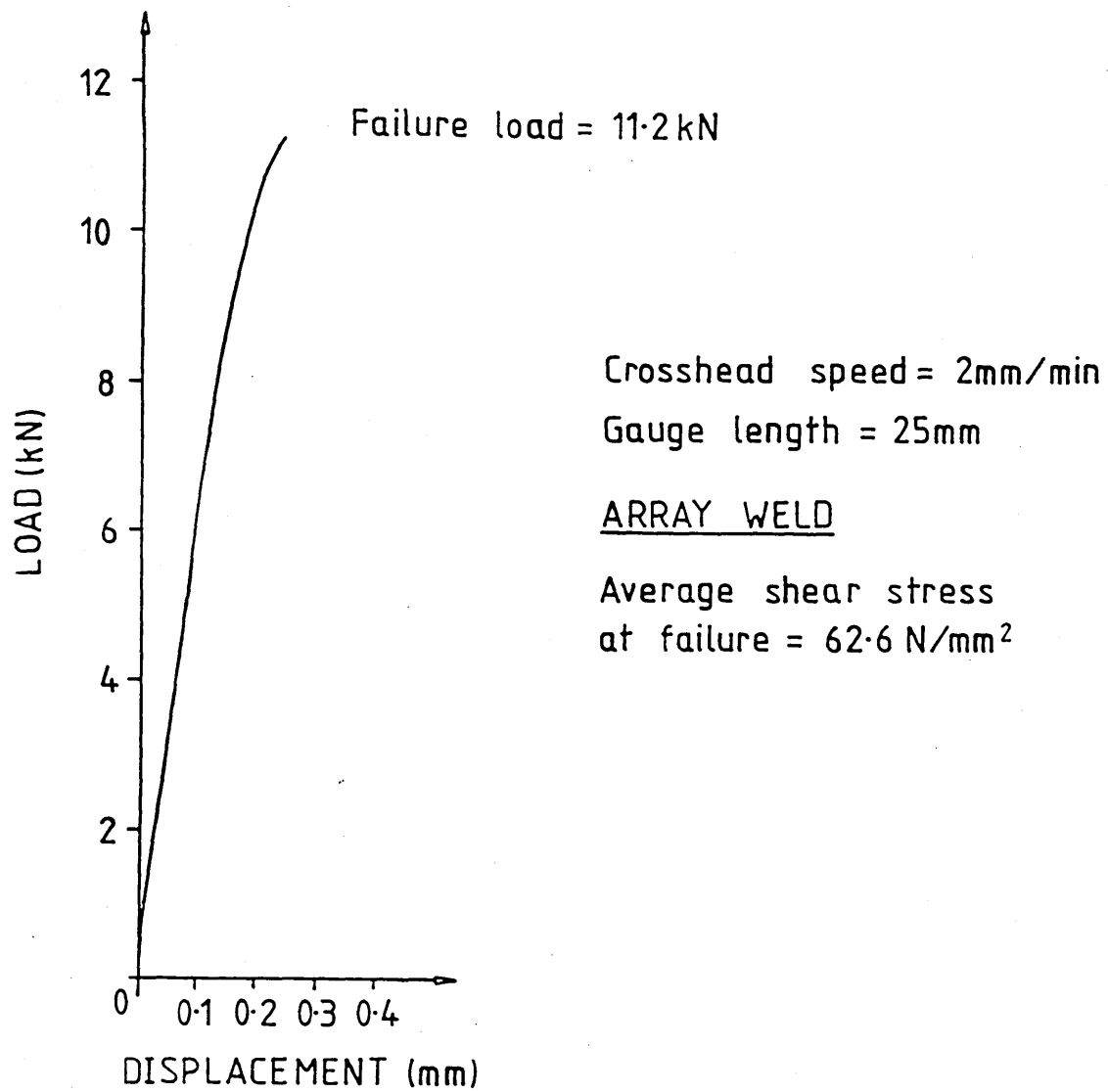
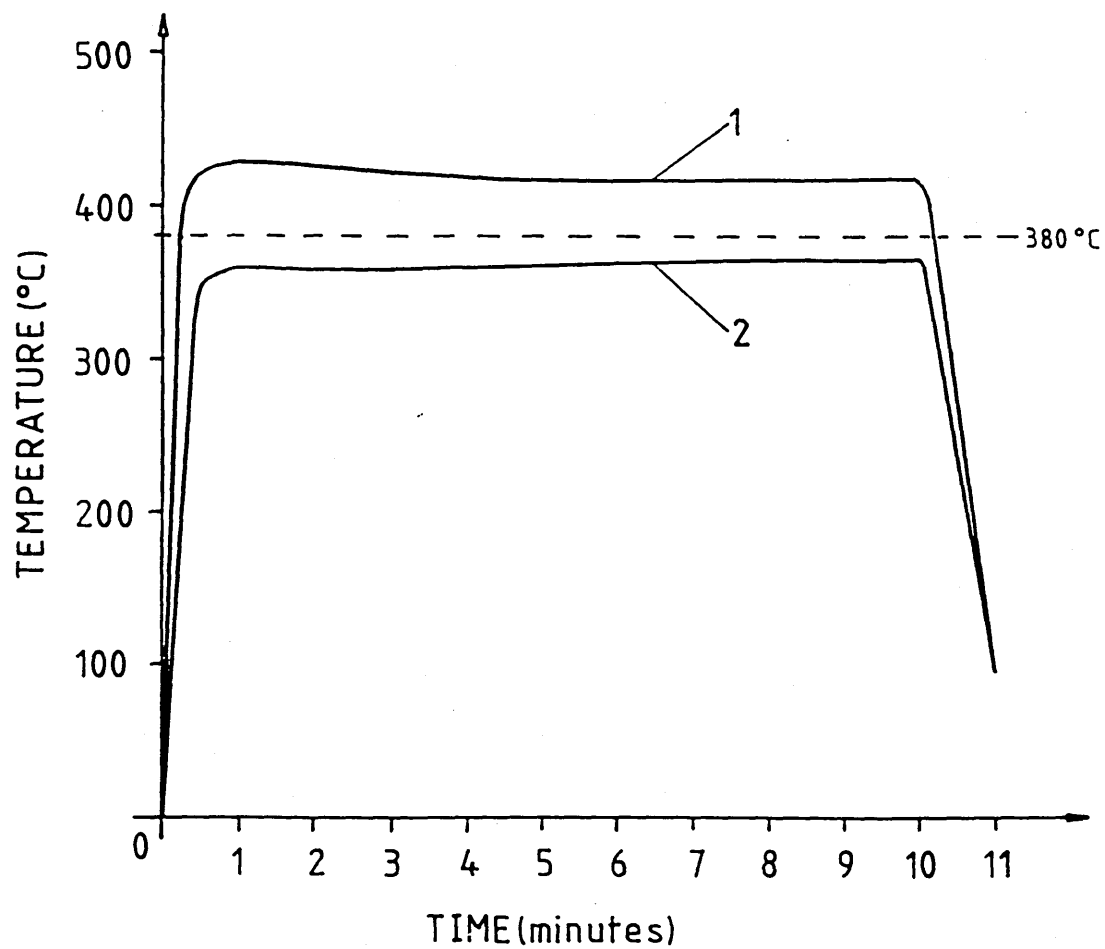


FIGURE 5.6

# HEATING CURVE (SW1)

CURVE 1: Top adherend, top surface temperature

CURVE 2: Bondline temperature



Tool preheat temperature 550 °C

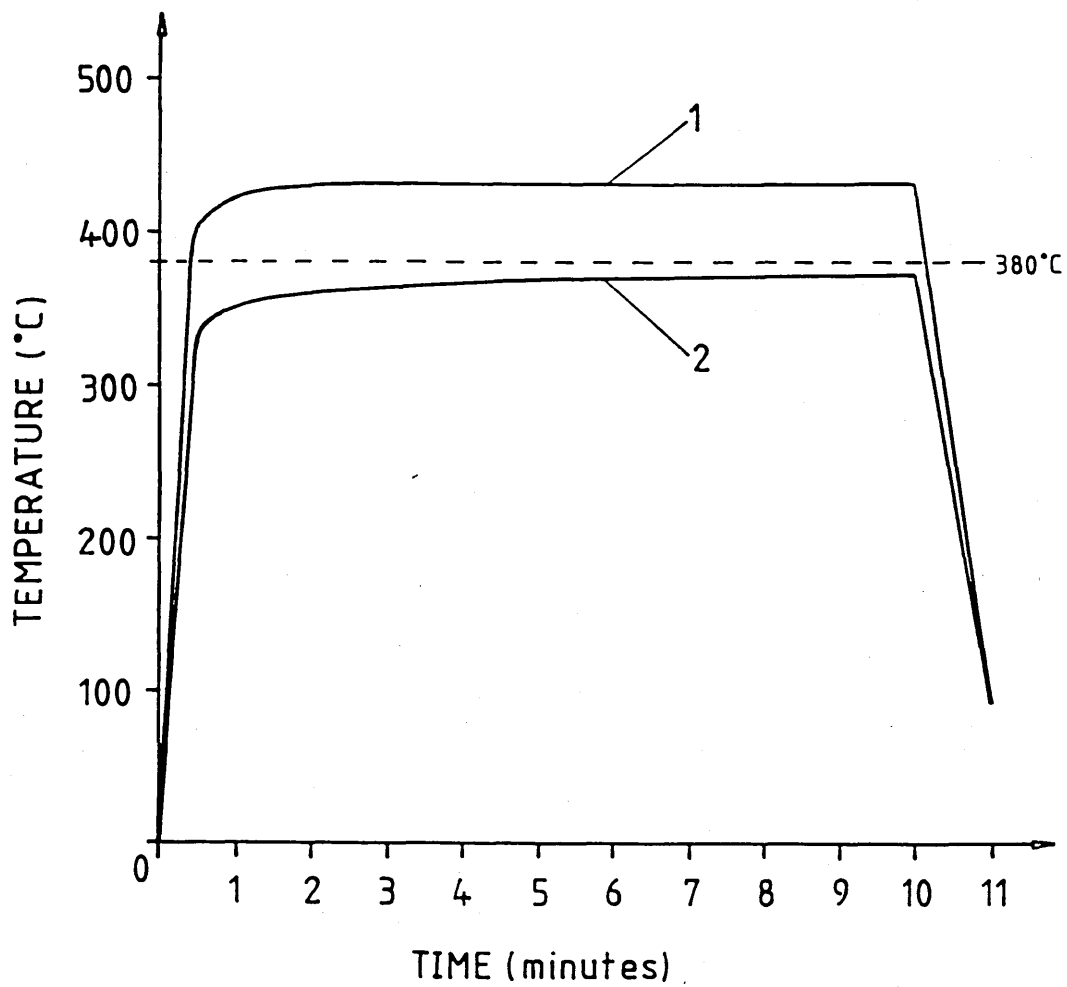
Power output 100 Watts

FIGURE 5.7

# HEATING CURVE (SW 2)

CURVE 1: Top adherend, top surface temperature

CURVE 2: Bondline temperature



Tool preheat temperature 550°C  
Power output 200 Watts

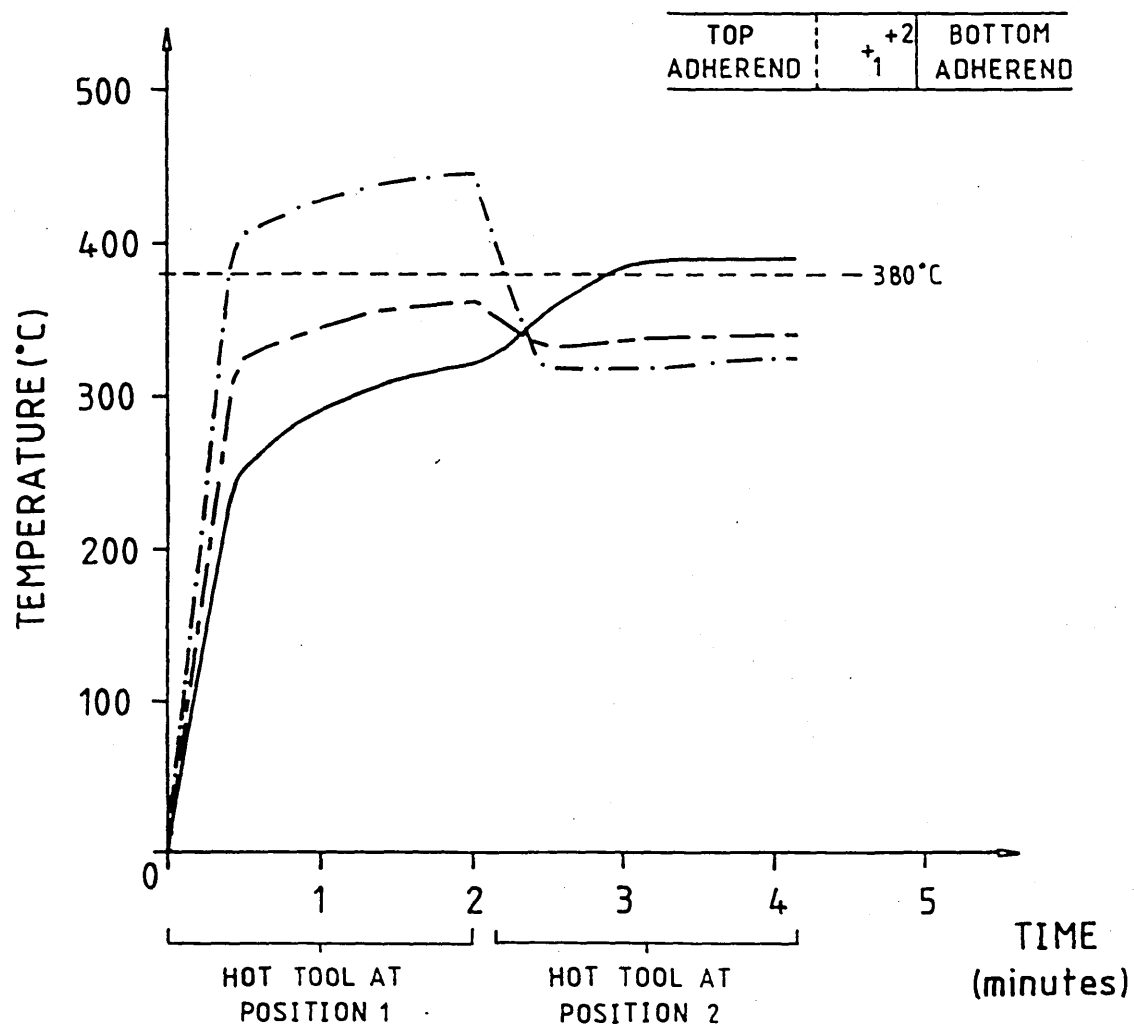
FIGURE 5.8

## HEATING CURVES, ARRAY WELD (SW2)

----- Top adherend, top temperature, position 1

----- Bondline temperature, position 1

----- Bondline temperature, position 2



Tool preheat temperature 550°C

Power output 200 Watts

FIGURE 5.9

INFLUENCE OF PROCESS  
ON JOINT STRENGTH

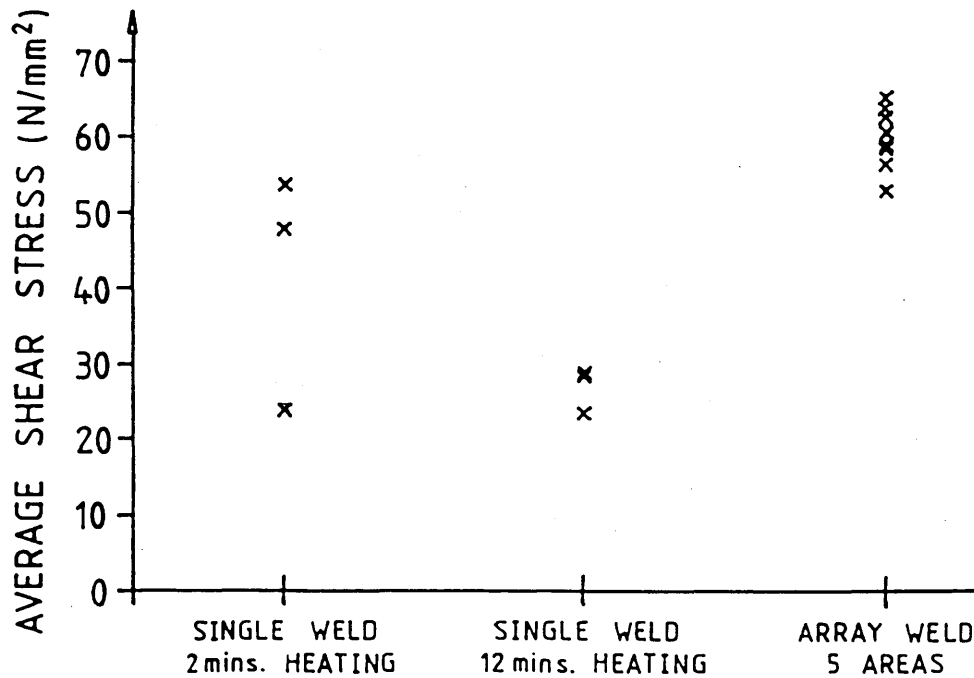
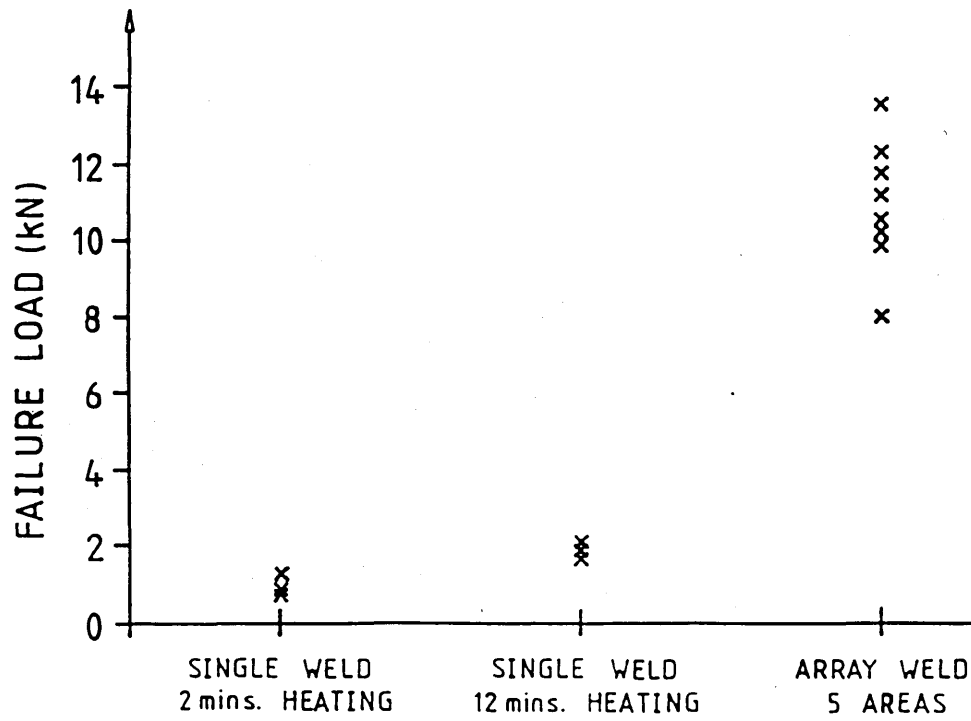


FIGURE 5.10

# INFLUENCE OF PROCESS ON JOINT STRENGTH

Weld Process	Heating Time (mins.)	Weld Area(mm <sup>2</sup> )	Failure Load(kN)	Average Shear Stress(N/mm <sup>2</sup> )
Single	2	24.0	1.30	54.2
Single	2	16.6	0.80	48.0
Single	2	35.6	0.85	23.9
Single	12	72.0	2.10	29.2
Single	12	66.0	1.90	28.8
Single	12	76.0	1.80	23.7
Array	2 mins/weld	208	13.6	65.4
Array	2 mins/weld	160	10.2	63.8
Array	2 mins/weld	179	11.2	62.6
Array	2 mins/weld	132	8.0	60.6
Array	2 mins/weld	200	11.8	59.0
Array	2 mins/weld	168	9.9	58.9
Array	2 mins/weld	217	12.3	56.6
Array	2 mins/weld	198	10.5	53.0

**NOTE:** 0.1mm thick Stabar film used in joint.  
Overlap dimensions 16mmx20mm.  
Surface degreased with Acetone.  
Consolidation pressure 0.28-0.34MPa (40-50psi).  
Crosshead speed during testing, 2mm/min.

TABLE 5.1



ADHEREND SURFACE FINISH

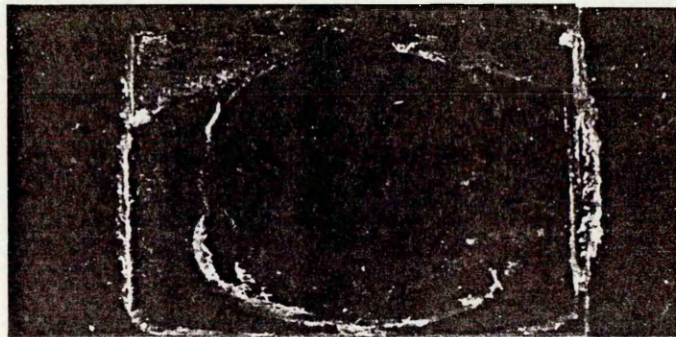
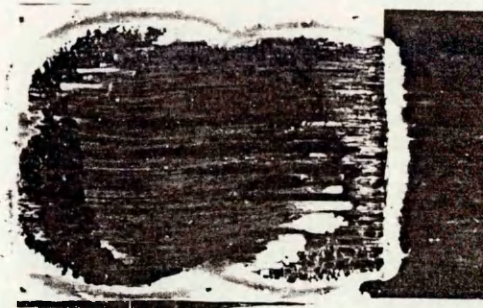


FIGURE 5.11



**FIGURE 5.12(a)** Failure surface of top adherend of spot welded specimen



**FIGURE 5.12(b)** Failure surface of bottom adherend of spot welded specimen

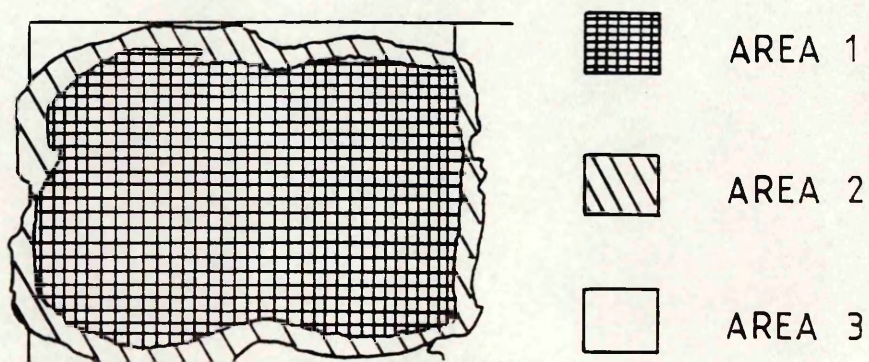


**FIGURE 5.12(c)**



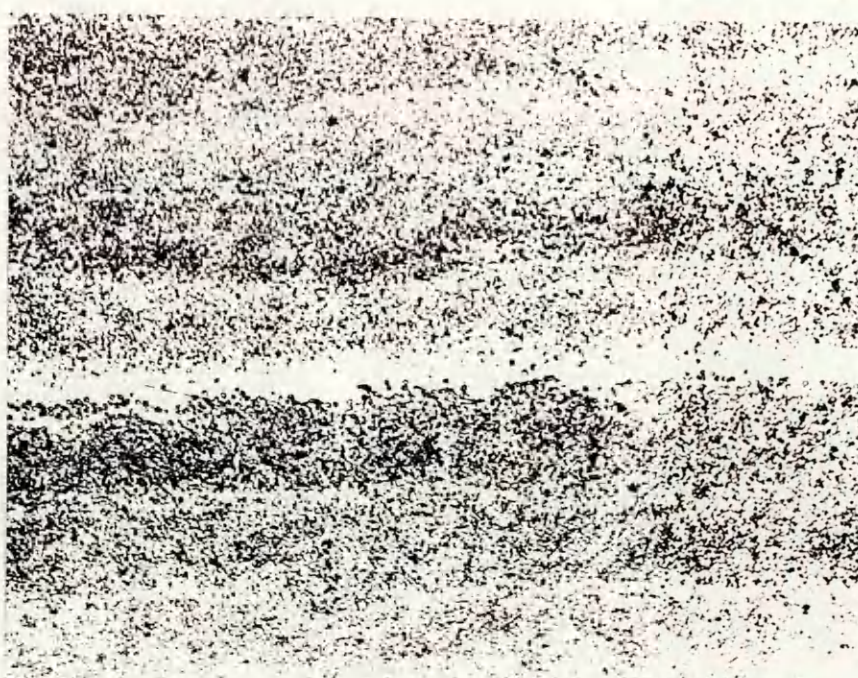


**FIGURE 5.13(a)** Cross-section through middle of spot welded specimen, (array weld)

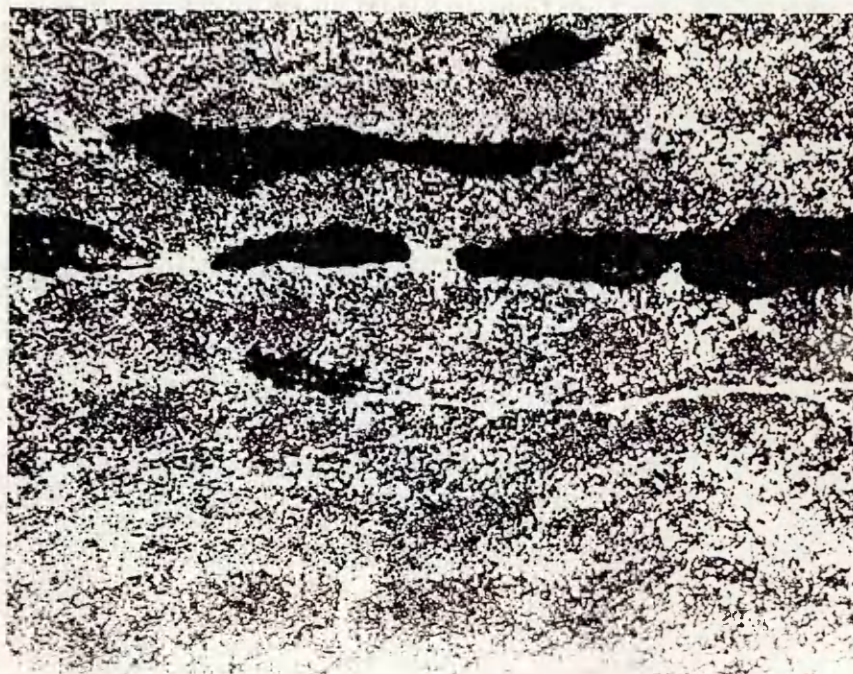


**FIGURE 5.13(b)** Cross-section through end of spot welded specimen, (array weld)

**FIGURE 5.13**